

HETEROGENEITY IN HUMAN NSCLC TUMOR GLUCOSE METABOLISM:
ON THE ORIGINS AND ROLE OF PYRUVATE METABOLISM

APPROVED BY SUPERVISORY COMMITTEE

Ralph J. Deberardinis, MD, PhD

Jerry Shay, PhD

Benjamin Tu, PhD

Hao Zhu, MD

DEDICATION

I would like to dedicate this work to a young man I briefly met at Parkland with osteosarcoma in his hip. When asked who the individual was whose name was prominently tattooed on his skin, he replied it was his ex-wife's. She had left him after he was diagnosed with cancer. I hope he is still alive with something else in his life to give him that amount of happiness.

HETEROGENEITY IN HUMAN NSCLC TUMOR GLUCOSE METABOLISM:
ON THE ORIGINS AND ROLE OF PYRUVATE METABOLISM

by

CHRISTOPHER THOMAS HENSLEY

DISSERTATION

Presented to the Faculty of the Graduate School of Biomedical Sciences

The University of Texas Southwestern Medical Center at Dallas

In Partial Fulfillment of the Requirements

For the Degree of

DOCTOR OF PHILOSOPHY

The University of Texas Southwestern Medical Center at Dallas

Dallas, Texas

August, 2015

Copyright

by

Christopher Thomas Hensley, 2015

All Rights Reserved

HETEROGENEITY IN HUMAN NSCLC TUMOR GLUCOSE METABOLISM:
ON THE ORIGINS AND ROLE OF PYRUVATE METABOLISM

Christopher Thomas Hensley, BS in Biochemistry and Cell Biology

The University of Texas Southwestern Medical Center at Dallas, 2015

Supervising Professor: Ralph J. Deberardinis, MD, PhD

In 1956 Otto Warburg, the most prominent scientist in cancer metabolism, stated that “the problem of cancer is...to discover the differences between cancer cells and normal growing cells” (Warburg, 1956a). Over fifty years later, the field still lacks a valid experimental framework to discover such metabolic differences in human tumors. A major limitation is the inability to faithfully recapitulate the microenvironment of primary human tumors in model systems. As a result, fundamental questions about tumor metabolism, including the suppression of pyruvate oxidation upon transformation proposed by Warburg more than 50 years ago, have only rarely been subjected to direct experimental assessment.

To provide a direct readout of primary human tumor metabolism in vivo, we have used intra-operative ¹³C-glucose infusions in non-small cell lung cancer (NSCLC) patients to compare metabolism between tumors and non-cancerous lung. Pre-surgical imaging, including non-invasive assessment of tissue perfusion using dynamic contrast enhanced magnetic resonance imaging (DCE-MRI), allowed us to select areas of microenvironment-based heterogeneity, to guide sample acquisition. Specifically, this microenvironment-based heterogeneity was assessed relative to the oncogenotype, histological parameters, and metabolism of glucose through glycolysis and the TCA cycle. Diverse tumors displayed enhanced glycolysis and glucose

oxidation. Furthermore, we discovered that due to the low enrichment in acetyl-CoA and other TCA cycle intermediates, all tumors had evidence for oxidation of multiple nutrients. We identified lactate as a carbon source for tumor oxidative metabolism. Additionally, metabolically heterogeneous regions were identified within and between tumors using DCE-MRI. Regions of lesser contrast enhancement demonstrated higher ^{13}C enrichment, likely reflecting contributions of non-glucose nutrients to central carbon metabolism in well-perfused areas, or the cause or consequence of aberrant proliferation of aggressive clones resulting in inadequate perfusion. The data indicate that the heterogeneous metabolism of these tumors is highly and predictably related to the microenvironment.

In summary, we have made novel, significant progress in assaying and analyzing primary human tumor metabolism and its relation to the microenvironment *in vivo*. I close with a separate project for future directions to begin to dissect the cellular origins of the whole tumor fragment signal that is amenable to direct assays in patients.

TABLE OF CONTENTS

Title fly	i
Dedication	ii
Title page	iii
Copyright	iv
Abstract	v
Table of contents	vii
Acknowledgements	xii
Prior publications	xiv
List of figures	xv
List of tables	xvii
List of abbreviations	xviii
Chapter 1: a case for the utility of studying heterogeneity in tumor metabolism using glucose-derived pyruvate oxidation as an example	
1.1 The original debate on the general role of respiration in cancer cells	1
1.2 Evidence in support of microenvironment regulation of cancer cell metabolism	3
1.3 In vivo tracer studies to faithfully report tumor metabolism	4
1.4 Methods to dissect heterogeneity in tumor metabolism are necessary to interpret primary human tumor data	6

Chapter 2: Primary assays of NSCLC patient tumor glucose metabolism in-vivo reveal enhancements of both glycolysis and glucose-derived pyruvate metabolism in the TCA cycle relative to patient matched non-cancerous lung.

2.1 Results	14
2.1.1 Workflow for pre-operative imaging, intra-operative ¹³ C-glucose infusion, and image-informed sample acquisition.	14
2.1.2 Comparison between bolus and continuous infusion routes of [U- ¹³ C]glucose administration for analysis of NSCLC metabolism.	16
2.1.3 Evidence for enhanced anaerobic and aerobic glucose metabolism in NSCLC.....	17
2.2 Methods	20
2.2.1 Clinical Protocol	20
2.2.2 Mass Spectrometry	21
2.2.3 NMR Spectroscopy	22
2.2.4 Modeling	22
2.2.5 Statistics	22
2.3 Discussion	23
2.3.1 There is no in vivo evidence for a suppression of glucose-derive pyruvate oxidation in cancer....	23
2.3.2 Glucose depletion in tumors is likely a combination of decreased supply and increased demand	24

Chapter 3: NSCLC tumors import and oxidize lactate in vivo in both humans and mice

3.1 Results	35
3.1.1 NSCLC patient tumors metabolize lactate in vivo	35
3.1.2 Human NSCLC cell lines xenografted into mice flanks metabolize lactate in vivo.....	36
3.1.3 A modeling based argument for lactate metabolism in mice flank xenografts	36
3.1.4 Extending the modeling to [U- ¹³ C]glucose infusions in mice flank xenografts	38
3.1.5 A re-analysis of the modeling between non-cancerous lung and lung tumors in the NSCLC patients in light of the possibility of lactate as a substrate choice.....	40
3.2 Methods	40
3.2.1 Mouse studies	40
3.3 Discussion	41
3.3.1 Supportive surrogate biomarker evidence of lactate metabolism in NSCLC	41

Chapter 4: Heterogeneity in glucose-derived pyruvate oxidation both within and between NSCLC patient tumors in vivo

4.1 Results.....	48
4.1.1 NSCLC tumors display heterogeneous degrees of glucose metabolism predicted by an MRI marker of tissue perfusion	48
4.1.2 Intratumor regions of NSCLC tumors display heterogeneous degrees of glucose metabolism predicted by an MRI marker of tissue perfusion	49
4.2 Methods.....	50

4.2.1 Multi-parametric Magnetic Resonance Imaging	51
4.3 Discussion.....	52
4.3.1 A substrate diffusion model of cancer cell metabolism predicts microenvironment regulation of oxidative substrate usage	52
4.3.2 Studies of primary tumor heterogeneity can unravel the drivers of tumor metabolic phenotypes in vivo	53
4.3.3. Semi-quantitative vs. quantitative DCE-MRI as a marker of perfusion.....	54
4.3.4. On the stability and reproducibility of DCE-MRI signal in tumors.....	55

Chapter 5: Dissecting metabolic heterogeneity in a mixed population of cells using the cell cycle as a determining phenotype

5.1 Introduction	61
5.1.1 Rationale that the cell cycle likely imposes oscillations in metabolism	61
5.1.2 Available data seem to discredit a possible link between glycolysis and cancer cell proliferation in vitro	62
5.1.3 There is conflicting evidence for a link between glucose-derived pyruvate oxidation and cancer cell proliferation.....	63
5.1.4 On nucleotide biosynthesis and cell proliferation	64
5.1.5 Flawed previous evidence in support of cell cycle stage correlated metabolic activities in cycling cells	64
5.2 Results.....	66

5.2.1 Development of models to sort a population of cells by cell cycle phase	66
5.2.2 [U- ¹³ C]glucose results of cells labeled with DNA dyes.....	67
5.2.3 [U- ¹³ C]glutamine results of cells labeled with DNA dyes or sorted by FUCCI	68
5.2.4 Metabolomics results of cells sorted by Hoechst.....	68
5.3 Methods.....	70
5.3.1 Creating FUCCI vector stably infected cell lines	70
5.3.2 Sorting cells by DNA content	70
5.3.3 Sorting cells by the FUCCI reporter system	71
5.3.4 Cell culture and metabolic experiments.....	71
5.4 Discussion.....	71
5.4.1 A unique form of data on the general concept of glutamine metabolism and cell proliferation ...	71

Chapter 6: Summary and Future Directions

6.1.1 Progress in the analysis of primary human tumor metabolism in vivo	80
6.1.2 Future directions in the analysis of primary human tumor metabolism in vivo	81
6.2.1 Progress in uncovering the connection between the tumor microenvironment and metabolism	85
6.2.2 Future directions in uncovering the connection between the tumor microenvironment and metabolism	85
6.3 Progress and future directions in studying intratumor metabolic heterogeneity at the cellular level ...	88
Bibliography	91

ACKNOWLEDGEMENTS

I would like to first thank my mentor Ralph Deberardinis for all of the time and effort invested not only in the current quality of my science but on my long term career. Through providing multiple chances to practice my scientific writing, to suggesting alternate projects when my original project did not materialize as hoped, I appreciate how his generosity has led to opportunity. My PhD experience has exposed me to a field of career opportunities that I would not have likely discovered on my own.

I would like to thank all of the members of the NSCLC patient tumor metabolism group. I recognize what an extreme privilege it is to have such a large multidisciplinary group investing time and effort in addition to their own individual interests. As for the core members, I thank Dr. Robert Lenkinski for all of the discussion of not only the short term science but also the larger philosophy on how to conduct science. I also thank him for introducing me to the field of imaging and his patience in willingness to co-mentor a complete novice. I thank Dr. Craig Malloy for taking the time to continually discuss metabolic tracer experiments on a deeper level. Many of the major findings stem from such discussion, significantly improving the metabolic analysis of the manuscript. I would also like to thank Dr. Malloy for sponsoring my application for membership into the International Society of Magnetic Resonance in Medicine (ISMRM), and inviting me to speak at the Advanced Imaging Research Center (AIRC) symposium this spring. As with Ralph, I appreciate the generosity of opportunity. Finally, I would like to thank Dr. Kemp Kernstine for his tireless support of the project. From writing the IRB document, to replying with long emails critically assessing the science after what I imagine a long day as a surgeon, I appreciate how extremely lucky I am to work with a surgeon this invested in the project.

I would like to thank Dr. Naama Lev-Cohain and Dr. Qing Yuan for running, and Dr. Lev-Cohain for additionally analyzing, the MRI scans of the patients when this project was at the stage of pilots with no long term funding. The initial connection between the DCE-MRI and ^{13}C tracer data was an opportunity for me to delve into the world of imaging in my project, so I am forever grateful for this. I would like to thank Eunsook Jin for processing and running the NMR scans of the tissue. The NMR significantly strengthened the conclusions of the manuscript. I would like to thank Dr. Jose Torrealba and Dr. Yasmeen Butt for pathological analysis. I would like to thank Dr. John Minna and Dr. Brenda Timmons for taking time out of their busy schedules to talk to me about the project and provide resources, and specifically Dr. Minna for running the Harmon Center WIPS that provided many opportunities for me to practice giving scientific talks. I additionally thank Joan Schiller for her support of the project. Finally, I would like to thank Rachael Skelton and Laurin Loudat for all of their hard work on the project in dealing with the complications of conducting research in patients.

For the cell cycle project, I thank Dr. Sean Morrison for providing an institute where I can walk a short distance from the cell culture hood to state-of-the-art flow cytometers. I thank Nicholas Loof for training me in flow cytometry, and Zeping Hu for running metabolomics pilots for the project. I thank Ajla Wasti for all of her help in the glutamine and cancer review, and for selflessly allowing me to be first author listed in a co-first authorship.

I would like to thank the UTSW MSTP administration for giving me the opportunity in general to be a physician scientist. I thank my thesis committee for their continued advice and feedback on my thesis. Finally, I would like to thank Rolf Brekken for agreeing to be my qualifying re-examination chair, a substantial amount of work to agree to. I think it is clear from above that I have had an immense amount of help and a number of second chances during my training.

PRIOR PUBLICATIONS

- 1) Hensley CT, Deberardinis RJ. In vivo analysis of lung cancer metabolism: nothing like the real thing. *Journal of Clinical Investigation*, 125(2):495-7(2015) PMID: 25607834
- 2) Yang C, Ko B, Hensley CT, Jiang L, Wasti AT, Kim J, Sudderth J, Calvaruso MA, Lumata L, Mitsche M, Rutter J, Merritt ME, Deberardinis RJ. Glutamine Oxidation Maintains the TCA Cycle and Cell Survival during Impaired Mitochondrial Pyruvate Transport. *Molecular Cell*, 56:414-24(2014). PMID: 25458842
- 3) Hensley CT, Wasti AT, Deberardinis RJ. Glutamine and cancer: cell biology, physiology, and clinical opportunities. *Journal of Clinical Investigation*, 123:3678-84(2013). PMID: 23999442
- 4) Wang Y, Zhou K, Huang G, Hensley CT, Huang X, Ma X, DeBerardinis RJ, Sumer BD and Gao J. A nanoparticle-based strategy for the imaging of a broad range of tumours by nonlinear amplification of microenvironment signals. *Nature Materials*, 13:204-12(2013). PMID: 24317187

LIST OF FIGURES

FIGURE 1.1 A depiction of the Warburg Effect.....	8
FIGURE 1.2 Contrasting views on the cellular origin of oxidative metabolism.....	9
1.2a A model of oxidative metabolism originating in the cancer cells.....	9
1.2b A model of oxidative metabolism originating in the stromal cells.....	9
FIGURE 1.3 Oxygen consumption is not a surrogate of oxidative ATP production.....	10
FIGURE 1.4 A tissue fragment assay workflow to understand tumor heterogeneity.....	11
FIGURE 1.5 A sorted subpopulation workflow to understand tumor heterogeneity.....	12
FIGURE 2.1 Pre-operative multimodality image-guided workflow to analyze glucose metabolism in human non-small cell lung cancer.....	26
FIGURE 2.2 Complete isotopologue distribution for metabolites depicted in figure 2.1d.....	28
FIGURE 2.3 A direct comparison between [U ¹³ -C] glucose infusion (patient 1) and bolus-like (patient 2 and 3) data.....	29
FIGURE 2.4 Common NSCLC patient tumor phenotypes in glucose-derived metabolism.....	30
FIGURE 2.5: Perioperative ¹³ C Glucose plasma enrichment curves for all patients in the study.....	32
FIGURE 2.6: NMR evidence in support of GC-MS isotopologue phenotypes and interpretation.....	31
FIGURE 2.7 Metabolite pool size analysis of tumor fragments relative to non-cancerous lung.....	32
FIGURE 3.1: Evidence for import and metabolism of extracellular lactate in NSCLC tumors.....	43
FIGURE 3.2: Comparing modeling results of 3PG vs lactate metabolism in mouse lactate infusions.....	45

FIGURE 3.3: Comparing various scenarios in a series of mice bearing contralateral flank cancer cell line xenografts infused with [U- ¹³ C]glucose.	46
Figure 3.4: Comparing various scenarios in the NSCLC patient data.	47
FIGURE 4.1: Whole tumor contrast enhancement correlated metabolic heterogeneity in NSCLC patient tumors	57
FIGURE 4.2: Intratumor contrast enhancement correlated metabolic heterogeneity in two NSCLC patient tumors	58
FIGURE 4.3: NMR and modeling evidence supportive of intratumor qualitative gcms analysis in patient 8	60
FIGURE 5.1: Description of the FUCCI cell cycle stage reporter system	73
FIGURE 5.2: Example of sorting cells by Hoechst dye	74
FIGURE 5.3: Pilot of sorting k562 cells stained with vybrant dna dye followed by a 2 hour [U- ¹³ C] glucose label	75
FIGURE 5.4: Aggregate results of [U- ¹³ C]glucose labeling experiments in G1 vs SG2M sorted k562 cells stained with DNA dyes	77
FIGURE 5.5: Aggregate results of [U- ¹³ C]glutamine labeling experiments in G1 vs SG2M sorted k562 cells stained with DNA dyes or expressing various combinations of FUCCI reporters	78
FIGURE 5.6: Results of a metabolomics pilot of k562 cells sorted into G1 and SG2M populations with Hoechst dye	79

LIST OF TABLES

TABLE 2. 1 Patient demographics and clinical tumor parameters 27

LIST OF ABBREVIATIONS

[U-¹³C]: Molecule in which all carbons are ¹³C
3PG: 3-Phosphoglycerate
ADC: Apparent Diffusion Coefficient
ALA: Alanine
ASP: Aspartate
ATP: Adenosine Triphosphate
CoA: Coenzyme A
CT: Computed Tomography
D: Doublet
DCE: Dynamic Contrast-Enhanced
DWI: Diffusion Weighted Imaging
FDG: Fluorodeoxyglucose (¹⁸F)
GC: Gas Chromatography
Glc: Glucose
GLN: Glutamine
GLU: Glutamate
GLY: Glycine
iAUC₆₀: Initial area under the gadolinium contrast enhancement curve in 60 seconds.
LAC: Lactate
M+n: full parent ion for a given metabolite with n ¹³C carbons incorporated
Mal: Malate
Min: minutes
MRI: Magnetic Resonance Imaging
MS: Mass spectrometry
NMR: Nuclear magnetic resonance
NSCLC: Non-small cell lung cancer
OAA: Oxaloacetate
PC: Pyruvate Carboxylase
PDH: Pyruvate Dehydrogenase
PET: Positron Emission Tomography
Ppm: parts per million
Pt: Patient
Q: Quartet
S: Singlet
SOC: Standard of Care
SUC: Succinate
TAU: Taurine
TCA: Tricarboxylic acid
^xC: Carbon atom with x atomic mass units.

CHAPTER ONE

Introduction

A CASE FOR THE UTILITY OF STUDYING HETEROGENEITY IN TUMOR METABOLISM USING GLUCOSE-DERIVED PYRUVATE OXIDATION AS AN EXAMPLE

1.1 The original debate on the general role of respiration in cancer cells.

A heated debate in 1956 between leaders of the field with opposing views on oxidative metabolism in cancer serves as a succinct review on the prevailing knowledge and opinions of the time (Burk and Schade, 1956; Warburg, 1956a; Weinhouse, 1956). Otto Warburg had a conviction in summarizing his work that respiratory impairment in the mitochondria of cancer cells was the origin of tumors (Warburg, 1956b). He invoked this impairment to explain his original observation termed the “Warburg Effect”, that tumor tissues continue to convert significant amounts of glucose to lactate in the presence of oxygen, whereas in non-cancerous tissue lactate production is significantly inhibited by oxygen (Figure 1.1). The Warburg Effect is the prototypical, most heavily studied phenotype in cancer metabolism (Gatenby and Gillies, 2004; Kim and Dang, 2006; Vander Heiden et al., 2009). Yet, as demonstrated below, key mechanistic issues concerning the Warburg Effect, and explanations for the effect and its coupled phenotypes, remain inconclusive.

Sidney Weinhouse took issue with Warburg’s conclusion that respiratory impairment was a fundamental property of transformation. He provided multiple lines of evidence to refute Warburg’s

hypothesis. Specifically, he noted that in some instances tumors consume oxygen at equivalent rates to non-cancerous tissue, convert specific nutrients (namely glucose, discerned through radioisotope tracer studies) to carbon dioxide at rates similar to non-cancerous tissue, and display similar responses to uncoupling agents as non-cancerous tissue. Additionally, he noted that some non-neoplastic tissues with high oxygen uptake also display high glycolytic rates (Figure 1.2a). He concluded that “this can mean only that glucose catabolism is so rapid in tumors that the normal channels for disposal of pyruvic acid are overloaded” (Weinhouse, 1956). This explanation for the Warburg Effect, with further evidence from *in vitro* studies, has been invoked in the modern literature (DeBerardinis et al., 2008a).

The crux of Warburg and Burk’s rebuttal lied in distinguishing tumor metabolism, a mixture of cancer and non-cancer (stromal and immune) cells, from cancer cell metabolism (Figure 1.2b) (Burk and Schade, 1956; Warburg, 1956a). Warburg cited his favorite model of mouse ascites tumor, which he claimed as nearly 100% cancer cells, and noted “the more cancer cells a tumor contained, the higher was the fermentation and the lower was the respiration.” He further cited an example of the chorion during embryogenesis, which undergoes rapid growth yet secretes negligible amounts of lactate, to discredit the idea that the Warburg Effect is an overflow of maximized pyruvate oxidation during cell growth (DeBerardinis et al., 2008a; Warburg, 1956a). Burk reiterated Warburg’s cell type argument, and questioned Weinhouse’s methodology of comparing different species’ tissue metabolism. Burk additionally noted that an uncoupling agent’s effect on oxygen consumption cannot be extended to infer about the state of how protons are shuttled across the mitochondrial membrane in cancer, whether through ATP production via ATPases or other means. We now know that there is molecular support for Burk’s statement by the discovery of links between cancer and other methods of recycling protons other than ATPases, such as uncoupling proteins and the nicotinamide

nucleotide transhydrogenase (NNT) protein (Burk and Schade, 1956; Derdak et al., 2008; Gameiro et al., 2013). Assuming oxygen consumption or carbon dioxide formation faithfully report on ATP generation from respiration is a common error in the literature that misinforms to this day (Reitzer et al., 1979; Zu and Guppy, 2004) (Figure 1.3).

Regardless, the standstill in this debate originates in Burk's own argument to Weinhouse, by dismissing some previous data because "simple saline media were employed" as opposed to more trustworthy updated data later acquired in media containing serum. This leads to a slippery slope, as in 2015 there are still no agreed upon standards as to "physiologic" culture conditions. So Weinhouse could claim that cell culture is prone to artifacts that fail to recapitulate the behavior of intact tumors, while the reductionists Otto Warburg and Dean Burk could claim that tumor measurements are prone to contamination of signal from the stroma.

In this thesis I claim that we have made significant progress to address the Weinhouse concern of faithfully recapitulating the microenvironment by furthering our ability to assay and analyze patient tumor metabolism and its connections to the microenvironment *in vivo*. I close with a discussion of a separate project that I undertook to address the Warburg and Burke concern of cell of origin heterogeneity. We were able to prove the principle of a novel method to assay the separate metabolism of subpopulations of cells within a heterogeneous population. This experimental workflow is amenable to assaying primary human tumors *in vivo*.

1.2 Evidence in support of microenvironment regulation of cancer cell metabolism.

Recent work has definitively demonstrated that non-cell-autonomous influences alter tumor cell metabolism to support survival and growth. Compromised tissue perfusion resulting from an abnormal neovasculature is believed to be a major environmental driver of altered tumor metabolism. Inadequate perfusion may lead to cellular hypoxia, which induces a host of alterations in nutrient metabolism, including enhanced glycolysis (Coleman et al., 2002; Guillaumond et al., 2013; Le et al., 2012; Metallo et al., 2012; Sonveaux et al., 2008; Wise et al., 2011). Reduced perfusion also compromises nutrient availability, which activates another set of compensatory metabolic responses to support cell survival (Birsoy et al., 2014; Commisso et al., 2013; Zhang et al., 2014b). Interactions among malignant cells experiencing different conditions within a solid tumor, or between tumor cells and stromal cells, can also impact overall tumor metabolism (Pavrides et al., 2009; Sonveaux et al., 2008). Thus, a full accounting of tumor metabolism will ultimately need to account for these extrinsic influences in addition to the complexity imposed by the oncogenotype. Although cell lines have produced a wealth of information about metabolic regulation, they cannot provide a comprehensive view of tumor metabolism because the effects of stromal components and the tumor microenvironment are difficult if not impossible to recreate *ex vivo*.

1.3 In vivo tracer studies to faithfully report tumor metabolism

Stable isotopes (e.g. ^{13}C) are widely used to investigate metabolism in biological systems, because patterns of ^{13}C enrichment in metabolites downstream of a labeled nutrient encode information about the pathways used to metabolize the nutrient (Buescher et al., 2015). Appropriate choice of the tracer, coupled with assessment of ^{13}C enrichment using nuclear magnetic resonance spectroscopy (NMR) and/or mass spectrometry (ms), enables many pathways to be investigated in a single experiment (DeBerardinis et al.,

2007; Hiller et al., 2010). Furthermore, the safety of ^{13}C makes these studies feasible in human subjects. A few studies have introduced ^{13}C -labeled nutrients into cancer patients prior to surgical resection of the tumor and then extracted metabolites from tissue fragments and used the ^{13}C enrichment patterns to infer metabolic activity. In gliomas and brain metastases, infusions of $[\text{U-}^{13}\text{C}]$ glucose revealed metabolism of glucose through both glycolysis and the tricarboxylic acid (TCA) cycle, with a number of pathways maintaining TCA cycle activity by providing oxaloacetate (OAA) and/or acetyl-CoA (Maher et al., 2012). Co-infusion of labeled glucose and acetate demonstrated that these tumors could also convert acetate to acetyl-CoA to supply oxidative metabolism (Mashimo et al., 2014). In non-small cell lung cancer (NSCLC), introducing a bolus of $[\text{U-}^{13}\text{C}]$ glucose revealed that both glycolysis and oxidative metabolism of pyruvate in the TCA cycle were apparent in the tumor, and that the abundance of metabolites labeled by these pathways was generally higher in the tumors than in the lung (Fan et al., 2009). Pyruvate carboxylase (PC), the enzyme converting pyruvate to OAA, was highly expressed in these tumors and contributed to some of the labeling differences between tumor and surrounding lung (Sellers et al., 2015). Thus, pre-operative and intra-operative metabolic tracing using infused ^{13}C -labeled nutrients in cancer patients provides substantial insights that potentially cannot be achieved through cell culture studies alone. Furthermore, a recent study in non-small cell lung cancer (NSCLC) demonstrated that tissue slices from a primary human tumor labeled in culture gave different general conclusions to the *in vivo* experiment, further validating the necessity for *in vivo* direct assays of tumor metabolism.

1.4 Methods to dissect heterogeneity in tumor metabolism are necessary to interpret primary human tumor data

Recent work in NSCLC patients highlights the difficulty of interpreting tracer data from *in vivo* studies, where the influence of multiple cell types within the microenvironment may influence isotope enrichment in target metabolites. The study authors validate the enhanced glycolysis in NSCLC, and demonstrate additional enhancements in glucose carbon flow through the mitochondrial reactions of pyruvate carboxylase (PC) and pyruvate dehydrogenase (PDH) (Figure 1.4a)(Sellers et al., 2015). Specifically, the authors stress how PC is the anaplerotic source of the TCA cycle, not glutamine carbon as demonstrated in the majority of cancer cell lines (Hensley and DeBerardinis, 2015). A similar conclusion, of glutamate generation from glucose instead of glutamine catabolism, was reached in brain tumors *in vivo* (Maher et al., 2012; Marin-Valencia et al., 2012). However, now we have reached a dilemma that cannot be rectified by whole tumor measurements alone (Sellers et al., 2015). As Warburg and Burk argued, could the majority of the oxidative metabolism and hence ^{13}C enrichment pattern in the tumor be arising from the stroma (Figure 1.4b)? This would rectify the vast literature that clearly establishes the importance of glutamine catabolism in both culture and *in vivo* models of cancer cell metabolism (Hensley et al., 2013).

This is not merely an esoteric exercise, because the relative contributions of various cell types to overall metabolic activity lead to different possible strategies of targeting tumor metabolism and stratification for clinical trials. For instance, glutamine synthetase receives little attention as a cancer drug target in the literature, but may be a valid avenue if intratumor glutamine symbiosis exists (Kung et al., 2011). To address this dilemma, I can conceive of three possible methods to discern the origin of averaged signals in a mixed population of cells within a tumor. First, the most practical and trustworthy method in terms of the quality of the data, one could draw correlations between cell types and signals to infer their origin from various tissue

fragment samples (Figure 1.4). We take this approach in the NSCLC patient tumor metabolism project. Second, one could separate out the various cell types and then test their separate signals (Figure 1.5). This approach was attempted in the cell cycle project, and potentially suffers from the effects of the process of separation before metabolic measurements. Third, one could measure each individual cell within a population and the metabolic signals it contains. This technology is theoretically available, but currently lacks the sensitivity to provide reliable measurements in our metabolites of interest (Walch et al., 2008). For these reasons, we prioritized the first method of retrospective correlations of signal within an intact tumor fragment. However, we were able to make progress in a proof of principle study in the sorting method.

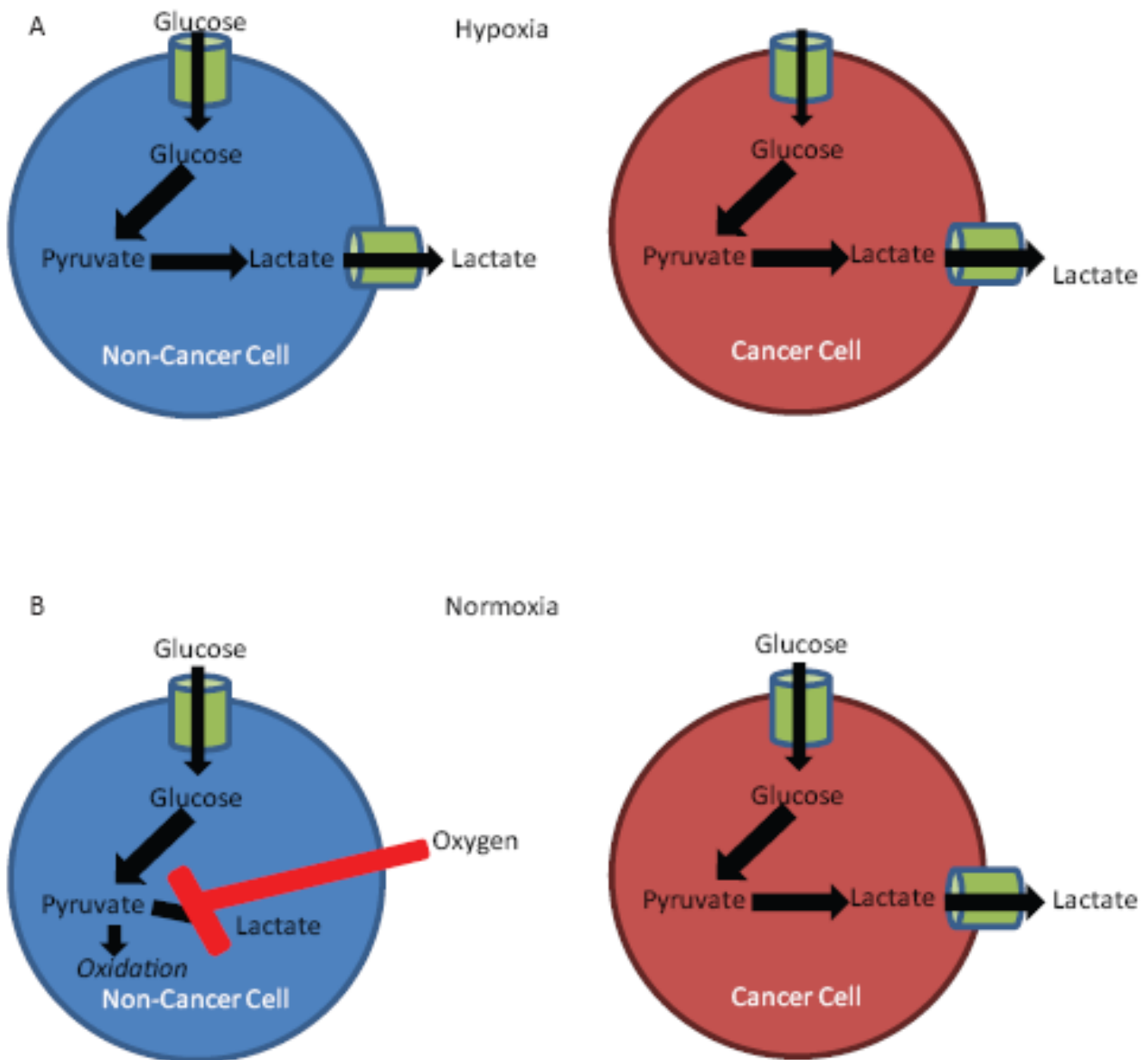


Figure 1.1: A depiction of the Warburg Effect.

(A) In hypoxia, both cancer and non-cancerous cells engage in anaerobic glucose metabolism to lactate to maintain bioenergetics viability.

(B) Upon the addition of oxygen, non-cancerous cells secrete significantly less lactate. This repression of lactate secretion upon the addition of oxygen is known as the Pasteur effect. However, cancer cells continue to secrete significant amounts of lactate upon the addition of oxygen. Hence, the Warburg Effect is essentially a suppressed Pasteur effect.

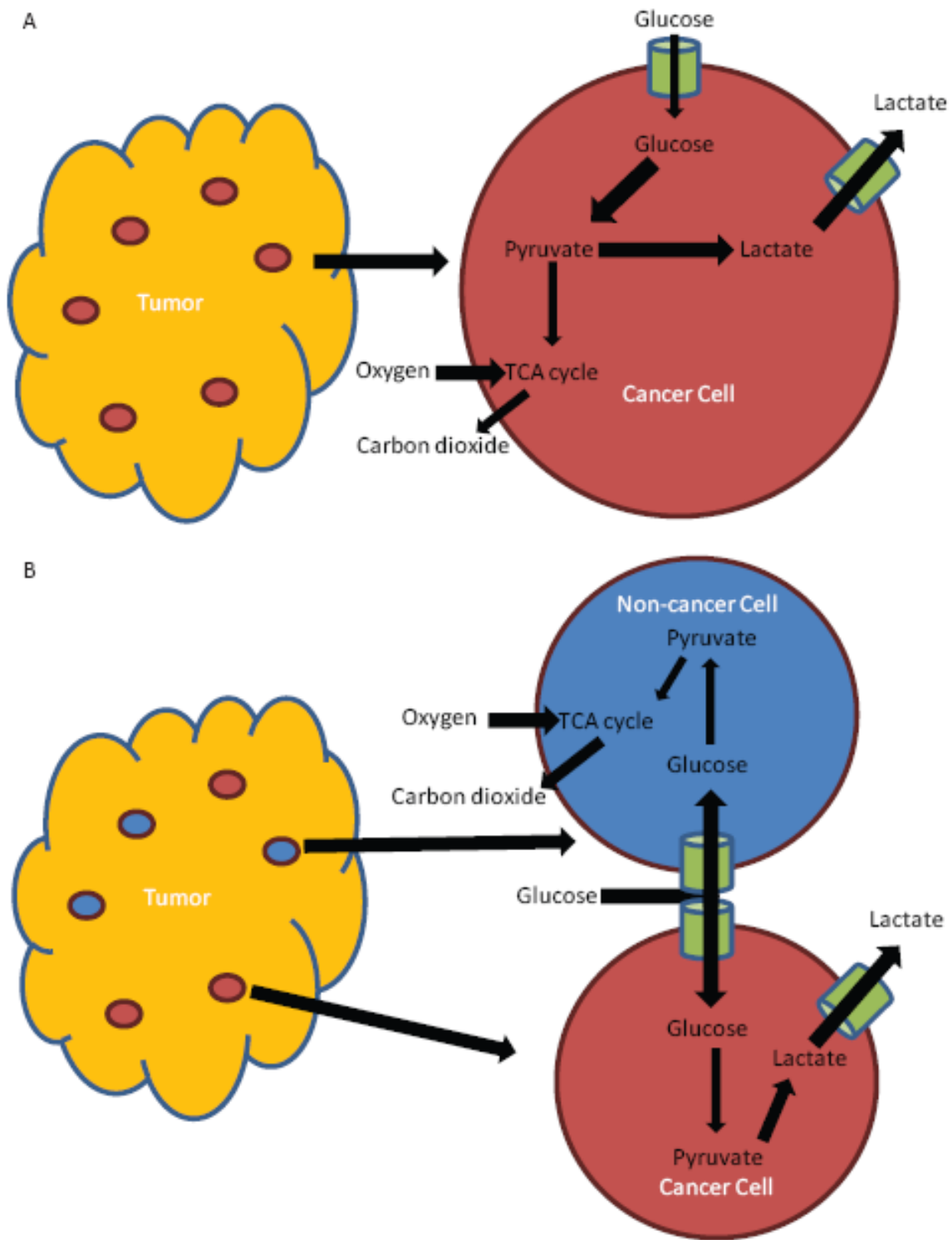


Figure 1.2: Contrasting views on the cellular origin of oxidative metabolism in tumors.
 (A) A model of oxidative metabolism originating in the cancer cells.
 (B) A model of oxidative metabolism originating in the stromal cells.

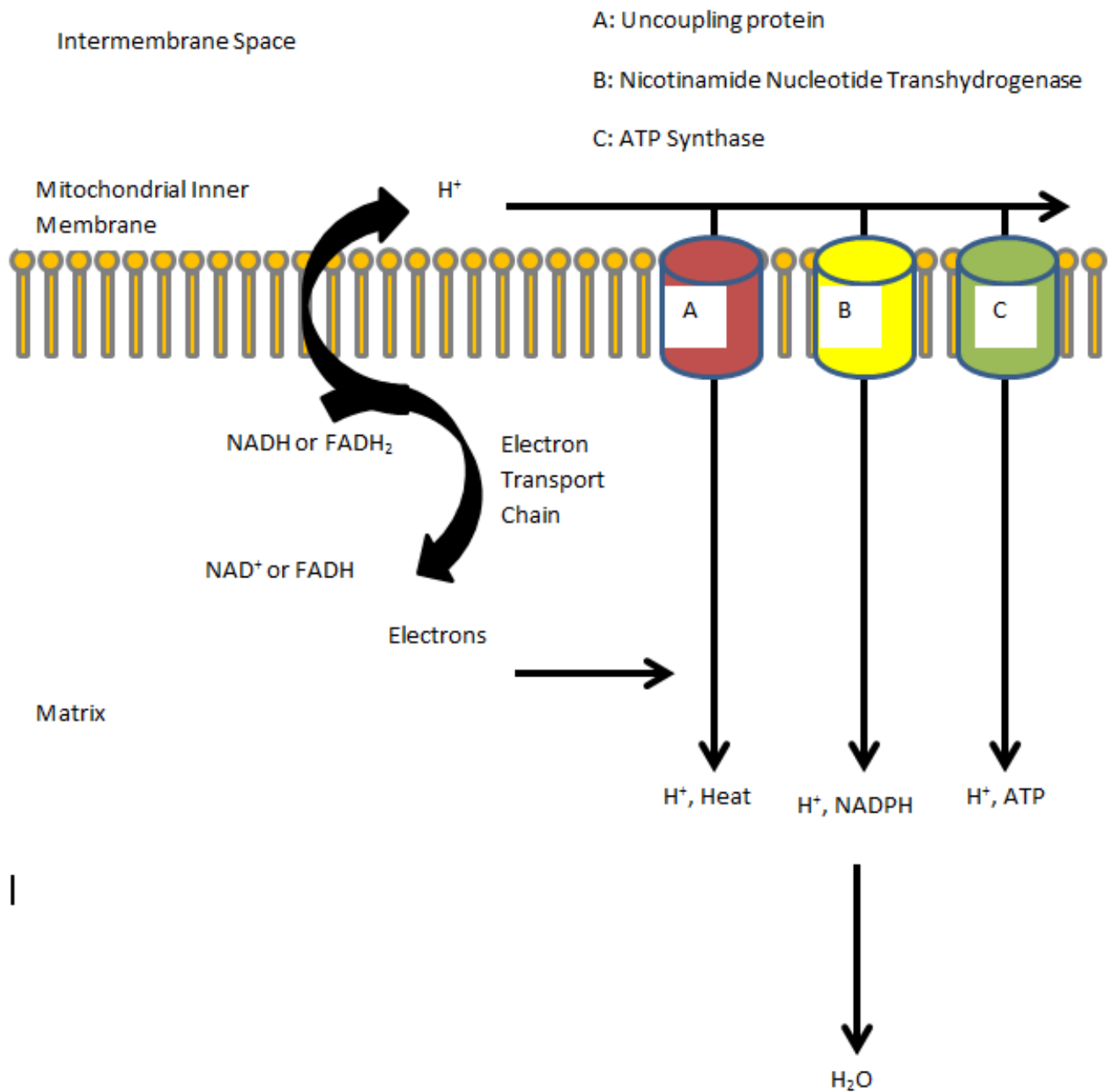


Figure 1.3: Oxygen consumption is not a surrogate of oxidative ATP production. Protons pumped into the intermembrane space can return to the matrix via many routes. Uncoupling proteins, Nicotinamide Nucleotide Transhydrogenase, and ATP Synthase generate heat, NADPH, and ATP as products, respectively, when transferring protons from the intermembrane space back to the matrix.

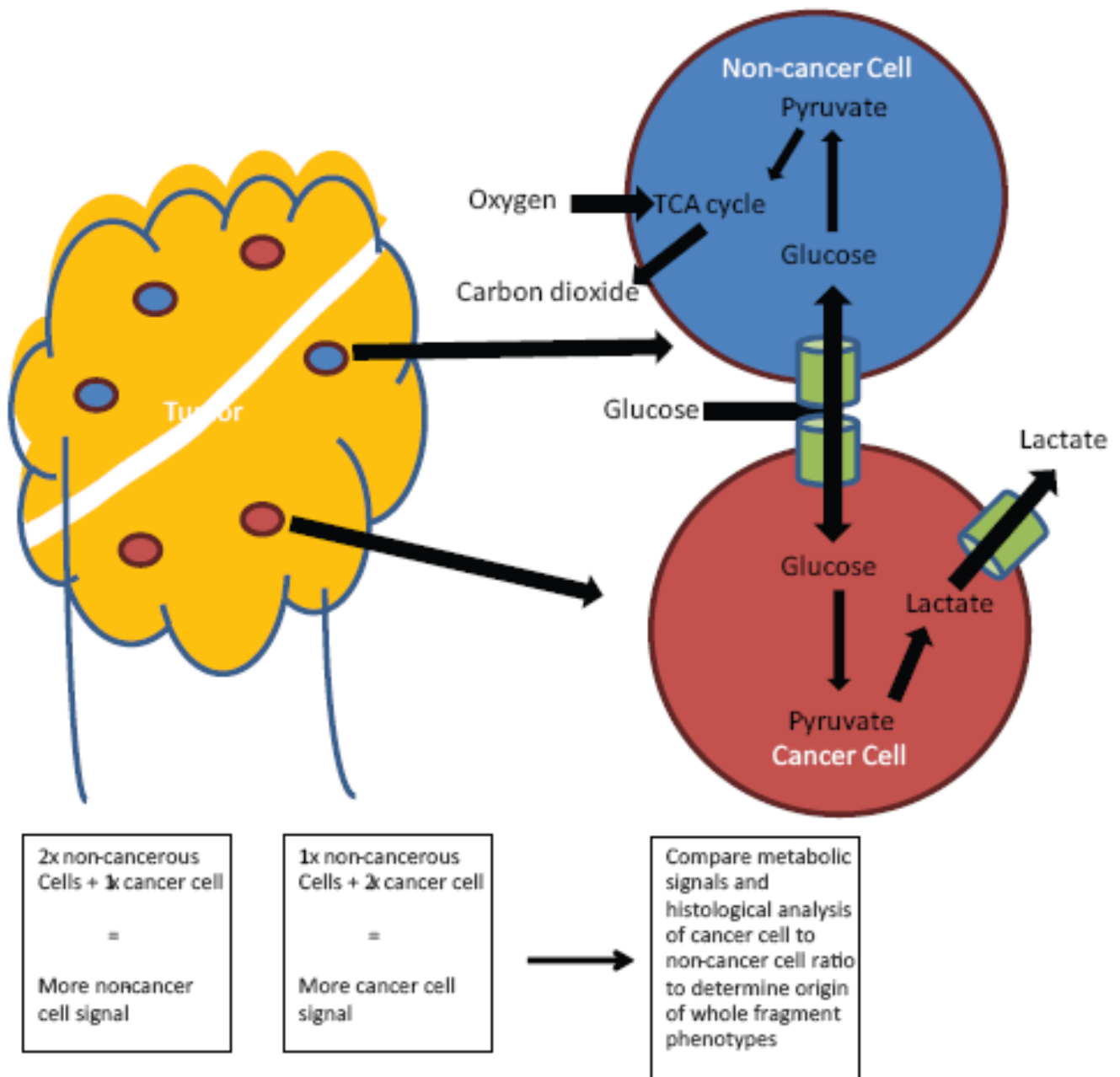


FIGURE 1.4 A tissue fragment assay workflow to understand tumor heterogeneity.

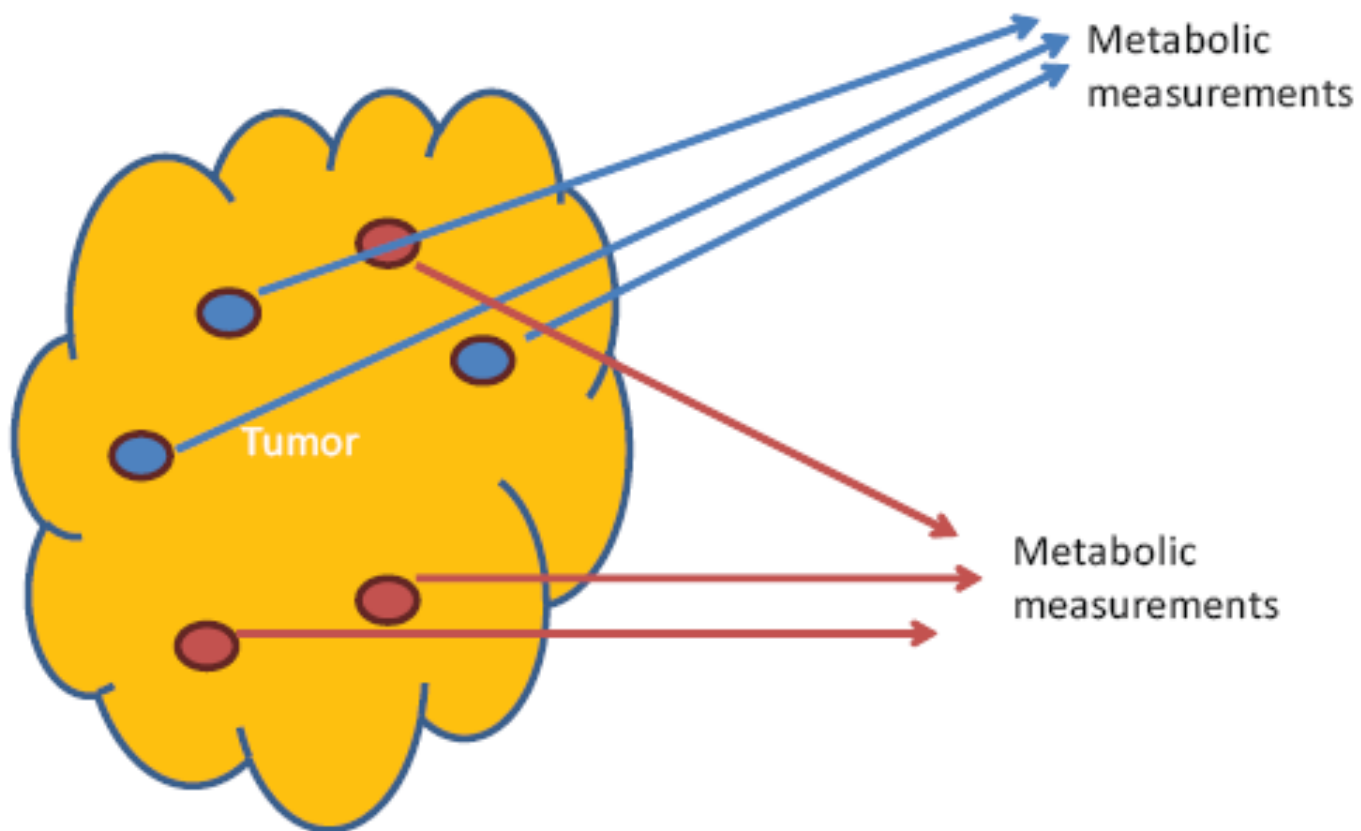


FIGURE 1.6 A sorted subpopulation workflow to understand tumor heterogeneity.

CHAPTER TWO

PRIMARY ASSAYS OF NSCLC PATIENT TUMOR GLUCOSE METABOLISM IN-VIVO REVEAL ENHANCEMENTS OF BOTH GLYCOLYSIS AND GLUCOSE-DERIVED PYRUVATE METABOLISM IN THE TCA CYCLE RELATIVE TO PATIENT MATCHED NON-CANCEROUS LUNG.

2.1 Results

2.1.1 Workflow for pre-operative imaging, intra-operative ¹³C-glucose infusion, and image-informed sample acquisition.

Prior to surgery, tumors were assessed by FDG-PET and multi-parametric magnetic resonance imaging (MRI) (Figure 2.1a). MRI techniques consisted of T2-weighted imaging for anatomic delineation of the mass; diffusion-weighted imaging (DWI) as a surrogate for cellularity and tissue density; and dynamic contrast-enhanced MRI (DCE-MRI), which measures time-dependent entry of a contrast agent into regions of interest and is used to assess tissue perfusion (Koh and Collins, 2007; Yankeelov and Gore, 2009). Multidisciplinary conferences involving the research team, cardiothoracic surgeon and radiologist were held to discuss the images and plan the approach for tissue sampling. On the day of the surgery, the patient had an intravenous catheter placed into each arm. One was used to deliver 8 grams of [U-¹³C] glucose over approximately 10 minutes, followed by a continuous infusion of 8 grams/hour for an average of three hours until the lobectomy

was performed. The other catheter was used to withdraw blood samples periodically for subsequent analysis of ^{13}C enrichment in plasma glucose. This infusion approach was similar to one previously used to analyze glucose metabolism in human gliomas, where the goal was to achieve a persistent state of high enrichment of the plasma glucose pool (Maher et al., 2012). After removal of the affected lobe, the tissue was quickly reoriented according to anatomic landmarks and then dissected to procure specific fragments prioritized according to the pre-surgical imaging. These fragments were briefly rinsed in saline and frozen in liquid nitrogen, within on average 5 minutes of lobe removal. Frozen fragments were used for histological, molecular and metabolic analysis. For metabolic analysis, plasma and tissue samples were extracted and metabolites were analyzed by gas chromatography and in some cases ^{13}C nuclear magnetic resonance spectroscopy.

As an example of the workflow, imaging and ^{13}C data from a 59 year-old female smoker with a grade 3 adenocarcinoma (patient 1) are shown in Figure 2.1b-d. This tumor exceeded 22 cm^3 by MR measurements and was highly FDG-PET avid, demonstrating some heterogeneity of FDG signal but a maximum of greater than 10 (Figure 2.1b, Table 2.1). Plasma glucose exceeded 30% enrichment for 3 hours prior to removal of the diseased lobe (Figure 2.1c). Metabolites were extracted from a fragment of the lung and from an FDG-avid, relatively ADC-low (i.e. highly cellular) fragment of the tumor selected based on pre-surgical imaging. Analysis of ^{13}C enrichment in these fragments revealed that glucose and the glycolytic intermediate 3-phosphoglycerate (3PG) had somewhat lower fractional enrichments in the tumor relative to lung, but that lactate and TCA cycle-related metabolites citrate, glutamate and malate were more enriched in the tumor (Figure 2.1d; full isotopologue distributions of these metabolites are in Figure 2.2). Thus, in this patient's tumor, high FDG uptake correlated with enhanced contribution of glucose carbon to both the lactate pool and to pools of TCA cycle intermediates.

2.1.2 Comparison between bolus and continuous infusion routes of [U-¹³C]glucose administration for analysis of NSCLC metabolism.

Administering ¹³C glucose as a single or multiple boluses rather than a continuous infusion has also been used successfully to characterize tumor metabolism in humans and mice (Fan et al., 2009; Sellers et al., 2015; Xie et al., 2014; Yuneva et al., 2012). Boluses have the advantage of reduced cost and ease of administration, significant considerations for human studies. On the other hand, longer infusions are predicted to lead to improved ¹³C signal, better evaluation of complex pathways requiring persistent exposure to ¹³C, and the possibility of achieving isotopic steady state in the tumor, at which point interpretation of ¹³C labeling patterns is simplified somewhat (Davidson and Vander Heiden, 2012; Marin-Valencia et al., 2012). In particular, analysis of the TCA cycle is complicated by the fact that the number and position of ¹³C depends not only on route of entry into the cycle, but the number of times the cycle has turned over; the latter factor is sensitive to the duration of ¹³C exposure (Cheng et al., 2011). To compare these two methods, we assessed the type of qualitative labeling data obtained from brief vs. prolonged periods of ¹³C exposure. One patient (patient 2) received an 8 g bolus of [U-¹³C] glucose, followed shortly thereafter by surgical resection. This produced a rapid rise in the plasma glucose enrichment, but no steady state in the circulating pool (Figure 2.3a). Another patient (patient 3) received two periods of [U-¹³C] glucose administration: an 8 g bolus prior to induction of anesthesia followed by administration of another 8 g approximately 1 hour before surgery (Figure 2.3b). Metabolites were then extracted from the lung and tumor and analyzed for the extent and distribution of ¹³C label. As in patient 1, enrichment in lactate (m+3 isotopologue) and TCA cycle intermediates (m+2

isotopologues of citrate, glutamate and malate) were higher in the tumor than in the lung of patients 2 and 3 (Figure 2.1d, Figure 2.3c). The relative enrichment of these species was not improved by patient 1's longer infusion. However, the absolute enrichments were somewhat lower in patients 2 and 3, and this resulted in very low signal for some isotopologues, particularly for higher-order labeling (e.g. m+3-4 in citrate and malate, Figure 2.3d-e). The m+1 isotopologues of these metabolites were also better represented in the longer ^{13}C glucose exposure before surgical resection in patients 1 and 3; this form of labeling likely arises after multiple turns of the TCA cycle involving entry of unlabeled acetyl-CoA (Figure 2.3f). Thus, short exposure methods are sufficient to detect abundant isotopologues, and the relative lack of labeling in higher-order isotopologues in single or repeated bolus administrations may heighten the relative differences of first-turn labeling between tumor and lung. Longer infusions appear to generate higher overall enrichment and better representation of some of the less abundant isotopologues. For these reasons, we used the bolus plus infusion method for subsequent patients.

2.1.3 Evidence for enhanced anaerobic and aerobic glucose metabolism in NSCLC.

Data from nine patients, including the three already described, are summarized in Figure 2.4a and shown individually in Figure 2.4f. The evolution of plasma glucose enrichments for all patient infusions is in Figure 2.5. Single samples were divided into multiple smaller fragments for metabolic, genetic, and histological analysis. All lung samples demonstrated enrichment of intermediates from glucose and the TCA cycle, indicating that benign lung tissue uses both of these pathways. Glycolytic intermediates and TCA cycle intermediates were also enriched in all tumors. There was substantial variability in ^{13}C enrichment among

fragments, and the variability between patients far exceeded the variability among fragments from the same tumor, indicating that this technique detects biological variation in human tumor metabolism (Figure 2.4h).

To provide an intuitive view of how ^{13}C labeling compared between the tumor and lung for each patient, the average relative fractional enrichments (i.e. the ratio of fractional enrichments for each isotopologue of tumor to lung) are shown for several informative and abundant metabolites. Despite the fact that all tumors displayed FDG uptake by PET, the fractional enrichment of glucose was significantly lower on average in the tumor than the lung. Lactate, by contrast, was significantly more enriched in the tumor fragments, indicating a greater propensity to convert $[\text{U-}^{13}\text{C}]\text{glucose}$ to $[\text{U-}^{13}\text{C}]\text{lactate}$ than non-cancerous lung. Furthermore, metabolites related to glucose-derived pyruvate entry through pyruvate dehydrogenase and first turn of the TCA cycle, namely modeled acetyl-CoA $m+2$, and measured citrate, glutamate and malate $m+2$ were also significantly more enriched in the tumors than in the lung (Figure 2.4a).

Although $m+2$ enrichments in citrate, glutamate and malate likely reflect entry of label into the TCA cycle via the pyruvate dehydrogenase (PDH) reaction, MS analysis does not provide positional information about ^{13}C enrichment. This potentially confounds the interpretation of labeling data restricted to qualitative assessment of MS isotopologue distributions, and could be particularly problematic when the overall enrichment in metabolites supplying the TCA cycle (e.g. pyruvate and acetyl-CoA) is low in human infusions. The $m+2$ isotopologues in citrate, etc. may therefore reflect PDH-dependent labeling during the first turn of the cycle, multiple turns of the cycle, or the combined effects of PC-dependent entry followed by multiple turns. To limit the assumptions needed to interpret the labeling data, we analyzed several lung and tumor fragments (from patients 2, 3, 4, 5 and 8) by ^{13}C NMR spectroscopy, which definitively assigns the position of ^{13}C (Fig. 2.6). These spectra revealed prominent 4-5 doublets in carbon 4 of glutamate, a pattern specifically

associated with PDH activity in the presence of pyruvate labeled in positions 2 and 3 (or all three carbons). This doublet was much more prominent in tumor than lung, and labeling of the 4-5 doublet relative to the singlet of C4 was highly correlated with the fractional enrichments of m+2 in citrate, glutamate and malate (Fig. 2.6). We interpret these observations to indicate that the enhanced labeling of TCA cycle intermediates in the tumor fragments primarily reflects entry of uniformly labeled pyruvate into the cycle via PDH. Strong correlations between mass isotopologues lactate m+3 and citrate m+2, and between citrate m+2 and malate m+2 also indicate intact PDH and TCA cycle activity in the tumors, supporting this interpretation (Fig. 2.4b-c). To rule out artificial inflation of ^{13}C labeling by metabolite pool depletion, we also analyzed the abundance of relevant metabolites in each fragment (Figure 2.7). Glucose was significantly less abundant in the tumor fragments, lactate was more abundant, and TCA cycle intermediates displayed no clear trend in either direction. There were no differences in the normalization factor of the product of protein abundance and total ion current for the tumor and lung fragments used in the analysis. Thus, qualitative first-pass assessment of the combined MS and NMR data indicate enhanced oxidation of glucose carbon through the pyruvate dehydrogenase reaction and TCA cycling in tumors relative to normal lung.

We next analyzed other aspects of TCA cycle metabolism. Lung tumors contain increased expression of PC and potentially have evidence of enhanced flux through this anaplerotic enzyme as assessed by qualitative assessment of mass isotopologue distributions (Sellers et al., 2015). PC converts $[\text{U-}^{13}\text{C}]$ pyruvate into OAA m+3, which can condense with unlabeled acetyl-CoA to produce citrate m+3 and can equilibrate with malate to produce malate m+3. Fractional enrichments of citrate m+3 and malate m+3 were higher in the tumor than the lung (Figure 2.4d). However, the absolute abundance of these isotopologues was much lower than the PDH-derived isotopologues. Citrate m+5, the condensation product of OAA m+3 and acetyl-CoA m+2, was

barely detectable, likely because of the low absolute enrichment in the OAA and acetyl-CoA pools. TCA cycle turnover was assessed by analyzing the fractional contributions of m+1 isotopologues in citrate and malate (Figure 2.4e). Both of these isotopologues were over-represented in the tumors. Therefore, enhanced fractional abundance of M+2 TCA cycle isotopologues is not an artifact of suppressing multiple turns of the cycle. To validate our qualitative isotopologue analysis, and avoid the potential pitfall of the enhanced tumor relative to lung enrichments in TCA cycle intermediates originating from higher enrichment in lactate, we modeled the isotopologue data with TCASIM. This program can model the fluxes of PDH and PC relative to citrate synthase, and the fractional enrichment of [U-¹³C] acetyl-CoA. Strikingly, the data indicate that the relative anaplerotic flux through PC is higher in the tumors, and that PDH flux, also enhanced in the tumors, accounts for the majority of carbon entry in both tissues (Figure 2.4g).

2.2 Methods

2.2.1 Clinical Protocol

Nine surgically eligible patients with either ¹⁸FDG-PET positive lung masses or biopsy verified lung tumors were enrolled in an IRB-approved clinical protocol after obtaining informed consent. A bolus of 8g over 10 minutes followed by 8g/hr continuous infusion of pyrogen-free [U-¹³C] glucose from Cambridge Isotope Laboratories was administered for each patient through a peripheral intravenous line on the day of the surgery. Standard of care surgical procedures were followed for NSCLC, with the majority of the cases being robotic lobectomies. Based on pre-operative imaging analysis and gross inspection after resection, the

surgeon avoided necrotic tissue for tissue sampling, unless separate analysis of necrotic tissue was planned. Upon removal from the patient, tissue fragments were briefly washed in ice-cold saline and immediately frozen in liquid nitrogen. The average total time between removal of tissue from the patient and freezing in liquid nitrogen was approximately 4 to 5 minutes. All histological analyses were conducted by surgical pathologists blinded to the results of the study.

2.2.2 Mass Spectrometry

Blood was obtained prior to and approximately every 30 minutes during infusion of [U-¹³C] glucose until affected lung tissue was removed from the patient. Obtained blood was chilled on ice and subsequently centrifuged to separate and freeze the plasma. 50-100µl of plasma was added to 80:20 methanol:water. 50-100mg of frozen tissue fragments were added to 50:50 methanol:water. Samples were freeze thawed three times and subsequently centrifuged at 16,000 relative centrifugal force for 15 minutes to precipitate macromolecules. Protein concentrations for relative pool size analysis were assayed from the pellets via Pierce BCA Protein Assay kit. The supernatants, with 10µl of sodium oxybutyrate added as an internal control, were evaporated, derivitized in 150µl of a trimethylsilyl donor (TriSil, Pierce), and analyzed using either an Agilent 6890 or 7890 gas chromatograph coupled to an Agilent 5973N or 5975C Mass Selective Detector, respectively. Measurements of mass isotopologue distributions were corrected for natural abundance using Metran. Parent ions monitored were 445-441 for glucose, 459-462 for 3-phosphoglycerate, 219-222 for lactate, 465-471 for citrate, 363-368 for glutamate, and 335-339 for malate.

2.2.3 NMR Spectroscopy

Sample preparation was as previously described (Maher et al., 2012). NMR spectroscopy was performed on a Varian ANOVA 14.1 T spectrometer (Agilent, Santa Clara, CA) equipped with a 3-mm broadband probe with the “observe” coil tuned to ^{13}C (150 MHz). Proton decoupling was performed using a standard WALTZ-16 pulse sequence. Carbon spectra were acquired under the following conditions: pulse flip angle 45° , repetition time 1.5 s, spectral width 35 kHz, number of data points 104,986, and number of scans $\sim 23,000$ – $30,000$, requiring 20–25 h. Free induction decays were zero filled to 131,072 points and apodized with exponential multiplication. Relevant peak areas were determined using ACDLabs SpecManager (Advanced Chemistry Development).

2.2.4 Modeling

Simulations of tcasim were run using the 3PG M+3 fractional enrichment in the lactate input of tcaSIM, which is modeled as interchangeable with pyruvate fractional enrichment. Relative to citrate synthase, the PDH, PC and YS fluxes, with YS defined as an additional anaplerotic source entering as succinate, were simulated in a stepwise fashion of 0.05 from 0 to 1. The cycles function that models turns of label in the TCA cycle was run from 1 to 6 turns, for a total of 55,566 simulations per tissue fragment. In a simulation using the average tumor 3PG enrichments, 6 turns in tcaSIM reached similar values to steady state (modeled as 35 turns) within reason given the significant figures of the raw data. The 55,556 simulations were imported into excel, and the simulated citrate m0-m1, glutamate m0-m5, and malate m0-m4 were compared to the

experimental data. The absolute difference between each isotopologue's experimental and simulated data was summed for each simulation, yielding a total delta. The simulations were ranked by total delta, and the simulation with the lowest total delta value was used for PDH and PC relative flux values.

2.2.4 Statistics

Patient-matched tumor and non-cancerous lung samples, as well as intratumor samples processed on the same day, were analyzed by a paired student's t test. Correlation plots were analyzed for significance with Pearson's product-moment correlations coefficients of the trend lines. All data was considered significant if $p < 0.05$.

2.3 Discussion

2.3.1 There is no in vivo evidence for a suppression of glucose-derive pyruvate oxidation in primary non-small cell lung cancer in humans.

The conceptual foundation for the imaging use of fluorodeoxyglucose positron emission tomography (FDG-PET) in NSCLC diagnosis, staging and detection of metastases arose from a primary observation that cancer cells have higher rates of glycolysis, defined as the conversion of glucose into lactate, than their differentiated counterparts *ex vivo* (Fletcher et al., 2008; Vander Heiden et al., 2009; Warburg, 1925; Weinhouse, 1955). However, empirical evidence validating the Warburg Effect *in vivo* in spontaneously-

formed human tumors, and exploring the relationship between tumor glycolysis and other aspects of metabolism or tumor biology, is fairly sparse compared to conclusions drawn from indirect assays (Higashi et al., 2000; Hori et al., 2011; Hu et al., 2013). One well accepted facet of the Warburg Effect is an accompanying cancer cell-autonomous decrease in glucose-derived pyruvate oxidation coupled to its increased conversion to excreted lactate (Kim and Dang, 2006). To date, all *in vivo* attempts to assay this decreased glucose oxidation within a tumor fragment have demonstrated robust TCA cycle oxidation of glucose carbon, and we further demonstrate no suppression in this study by comparing to non-cancerous lung (Maher et al., 2012; Marin-Valencia et al., 2012; Sellers et al., 2015).

2.3.2 Glucose depletion in tumors is likely a heterogeneous combination of decreased supply and increased demand.

One determinant of tumor metabolism that may significantly change between cell culture and *in vivo* assays is the well-documented, drastically different microenvironment in tumors *in vivo* compared to the standard practice of nutrient-replete, normoxic cell culture (McKnight, 2010). The phenomenon of glucose scarcity in tumor tissues has been noted as a general property of many tumor types, yet the most widely used culture media are formulated with diabetic concentrations of glucose (Birsoy et al., 2014; Hirayama et al., 2009; Urasaki et al., 2012). As the NSCLC patient tumors additionally demonstrated consistently less fractional enrichment of their glucose pools with [U-¹³C] glucose, this argues against the simplest explanation of tumor enhancements of glucose uptake and metabolism being the sole factor contributing to both glucose depletion and increases in enrichment in downstream metabolites, some factor downstream of glucose uptake must be

enhanced in the tumors (Figure 2.4a, Figure 2.6). There are two possible causes for this lower fractional enrichment in glucose in the tumors. First, compromised tumor perfusion could lead to slower kinetics of glucose delivery or areas of the tumor that are inaccessible to glucose originating in the plasma. In partial support of this idea, we observed an insignificant direct trend ($r^2 = 0.07$) between relative glucose fractional enrichment and the DCE semi-quantitative parameter of initial area under the curve in 60 seconds (iAUC60) (data not shown). Compensatory increases in glucose uptake and trapping in response to decreases in perfusion is likely weakening this correlation (van Baardwijk et al., 2007). In agreement with this compensatory increase possibility, a recent study in NSCLC patient tumors observed an inverse correlation between FDG-PET SUVmax and SUVmean and DCE-MRI parameters of perfusion in lung adenocarcinomas, which accounted for seven of the nine patients in this study (Zhang et al., 2014a). The second possible determinant of the lower glucose fractional enrichments in the tumors is cycling of glucose through cellular glycogen pools (Favaro et al., 2012; Yano et al., 1996; Zois et al., 2014).

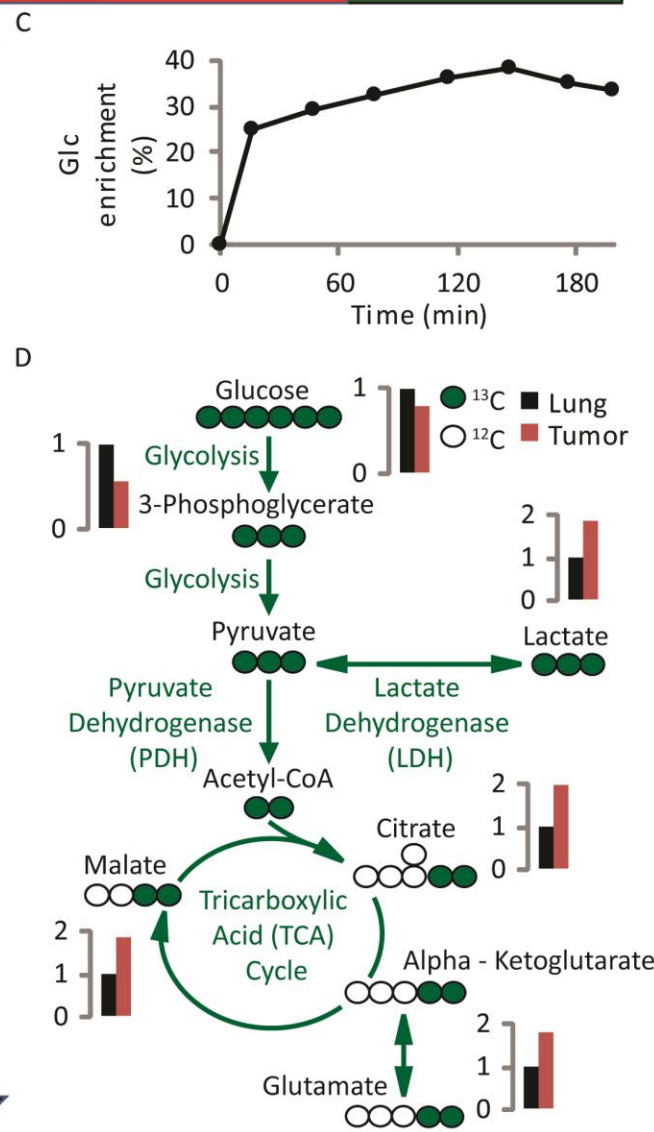
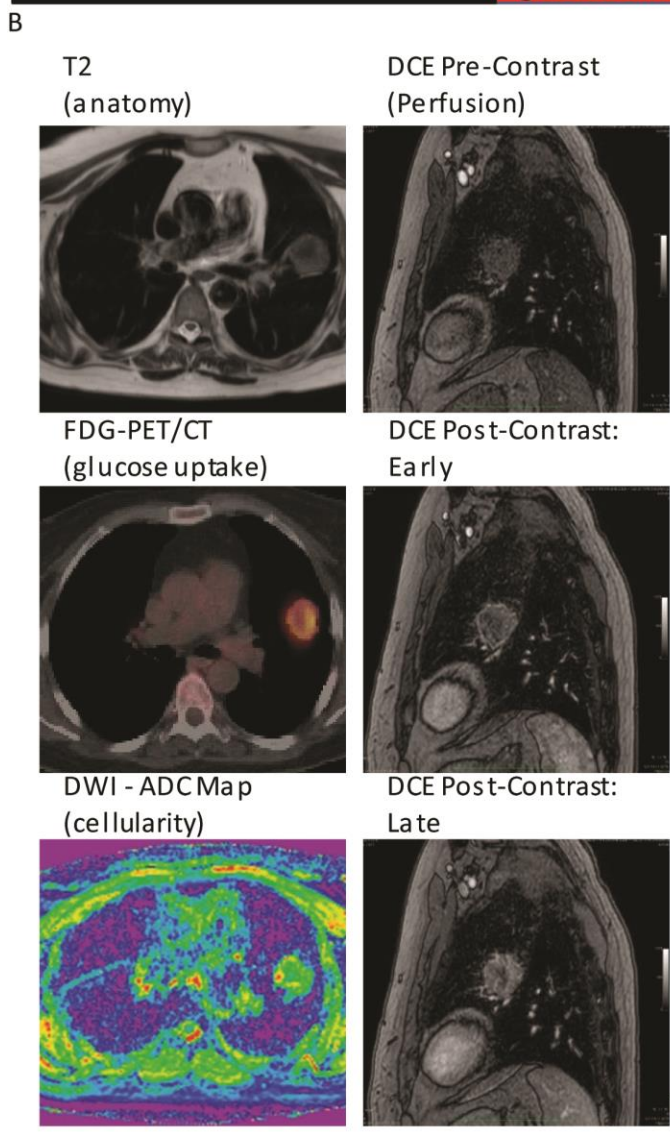
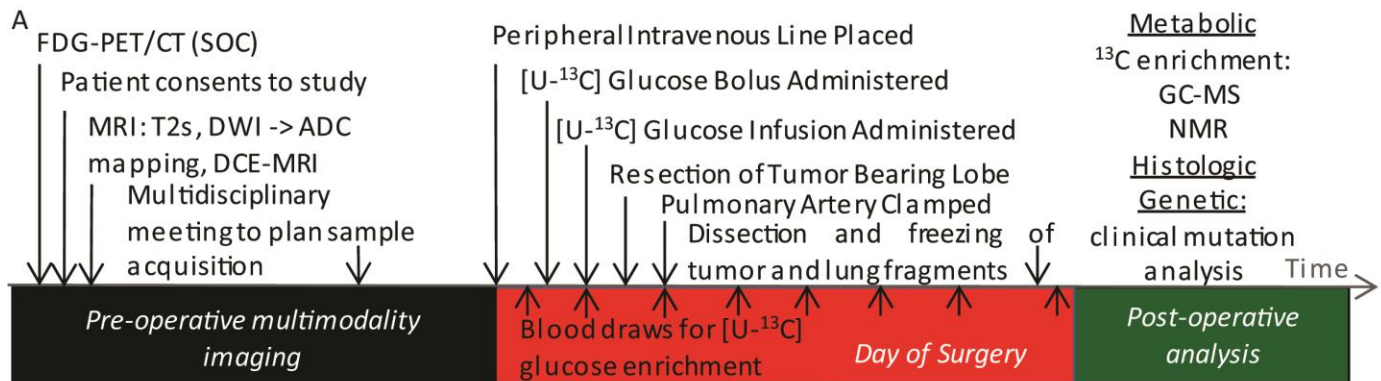


Figure 2.1: Pre-operative multimodality image-guided workflow to analyze glucose metabolism in human non-small cell lung cancer.

(A) Diagram of standard workflow of a patient enrolled in the study.

(B) Pre-operative multimodality imaging of patient 1. All images are from a single session of magnetic resonance imaging, except for the prior standard of care FDG-PET/CT.

(C) Plasma glucose enrichment time-course of perioperative ¹³C glucose infusion of patient 1.

(D) Relative fractional enrichment of the depicted ¹³C enriched glycolytic and TCA cycle metabolites.

Tumor values were normalized to patient matched lung values.

Abbreviations: FDG-PET/CT, Fluorodeoxyglucose-Positron Emission Tomography, Computed Tomography; SOC, standard of care; MRI, magnetic resonance imaging; DWI, diffusion weighted imaging; DCE, dynamic contrast-enhanced; GC-MS, Gas Chromatography-Mass Spectrometry; NMR, Nuclear Magnetic Resonance; ADC, Apparent Diffusion Coefficient.

Patient	Age	Sex	Smoking History	Tumor Size (cm ³)	Histological Type	TNM stage	Grade	MIB-1 (KI-67)	EGFR mutation	BRAF mutation	KRAS mutation	ALK mutation	SUVmax
1	59	F	20 pack-years	10.2	ADC, 90% solid, 10% ac	pT2aN0MX	G3						10.2
2	74	F	45 pack-years	0.6	ADC (invasive), ac type	pT1apN0MX	G1	0.2	N	N	Y	N	Not tested
3	55	F	10 pack-years	4.9	LCNEC	pT1bpN0pMX	G4	0.8	Not tested	Not tested	Not tested	Not tested	8.9
4	73	F	None	5.4	ADC (invasive), pap predominant	pT2aN0MX	G2		Y	N	N	N	4.7
5	63	M	None	10.1	ADC (invasive), ac predominant	pT2aN0MX	G2		Y	N	N		5.1
6	81	M	120 pack-years	15.5	ADC, pap 60%, lep 20%	pT2aN0MX	G2						32
7	82	M	30 pack-years	22.2	SQCC	cT1bN0M0	G3						8.3
8	66	F	None	16.1	ADC, Ac and Pap (predominant) Type	pT2aNpN1MX	G2		Y	N	N	N	13.3
9	43	M	None	3.8	ADC (ac 50%, pap 40%, mpap (5%) and lep 5%)	pt1bN0MX	G2		N	N	N	N	2.5

Table 2.1.

Patient demographics and clinical tumor parameters.

Tumor size assessed by T2 weighted magnetic resonance imaging. NSCLC TNM staging: T1a – Tumor greatest dimension ≤ 2cm. T1b – Tumor greatest dimension > 2cm but ≤ 3cm. T2a – Tumor greatest dimension > 3cm but ≤ 5cm. N0 – regional node metastases not present. N1 – Ipsilateral peribronchial and/or ipsilateral hilar lymph nodes metastases present. MX – Distant metastasis unknown. M0 – Distant metastases not present. G1 - well differentiated. G2 - moderately differentiated. G3 – poorly differentiated. G4 – undifferentiated. Abbreviations: ADC = Adenocarcinoma, ac = acinar, pap = papillary, mpap = micropapillary, lep = lepidic. LCNEC = Large Cell Neuroendocrine Tumor. SQCC = Squamous Cell Carcinoma.

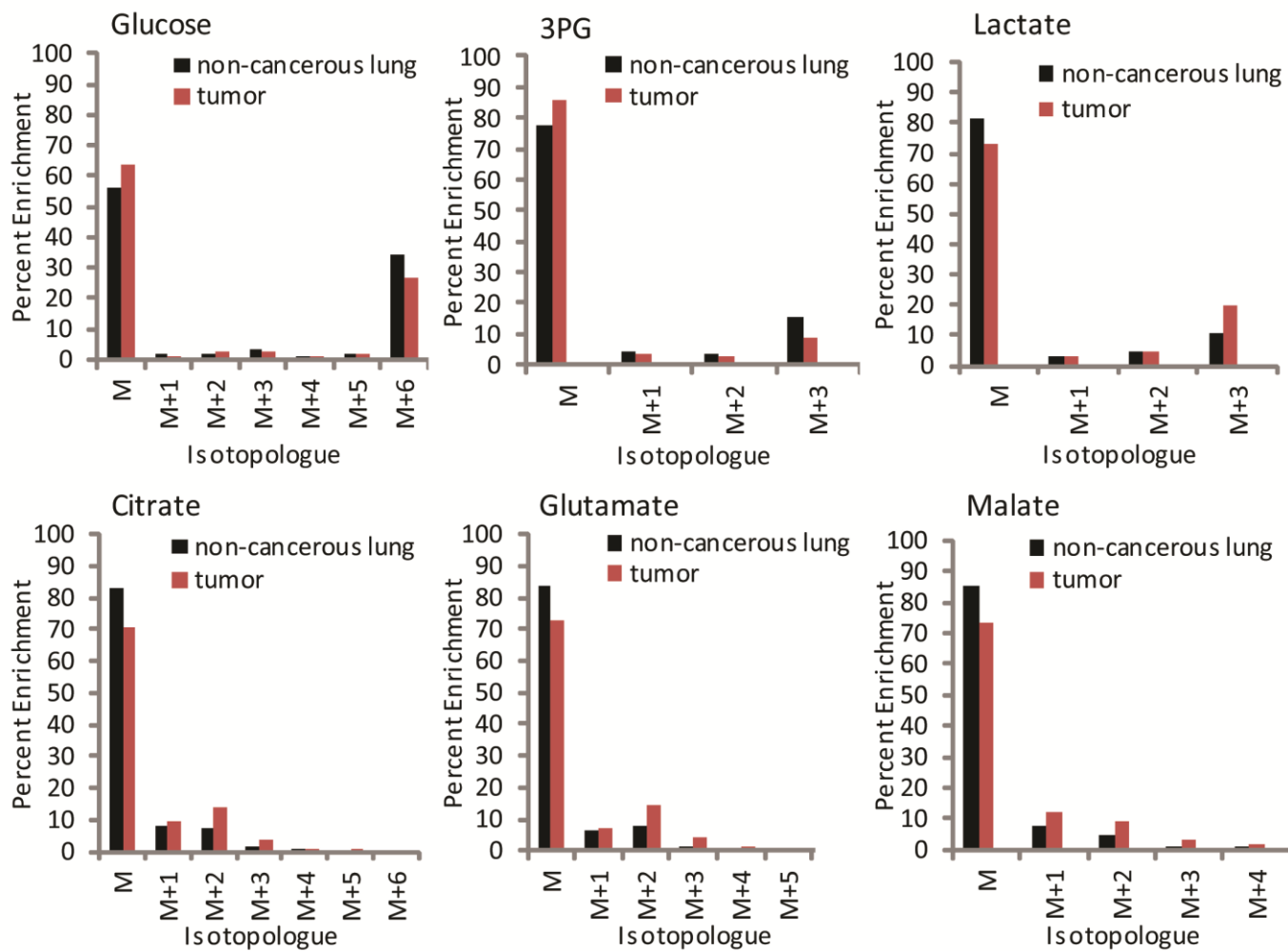


Figure 2.2

Complete isotopologue distribution for metabolites depicted in figure 2.1d.

Abbreviations: M+n, full parent ion for a given metabolite with n ¹³C carbons incorporated; 3PG, 3-Phosphoglycerate.

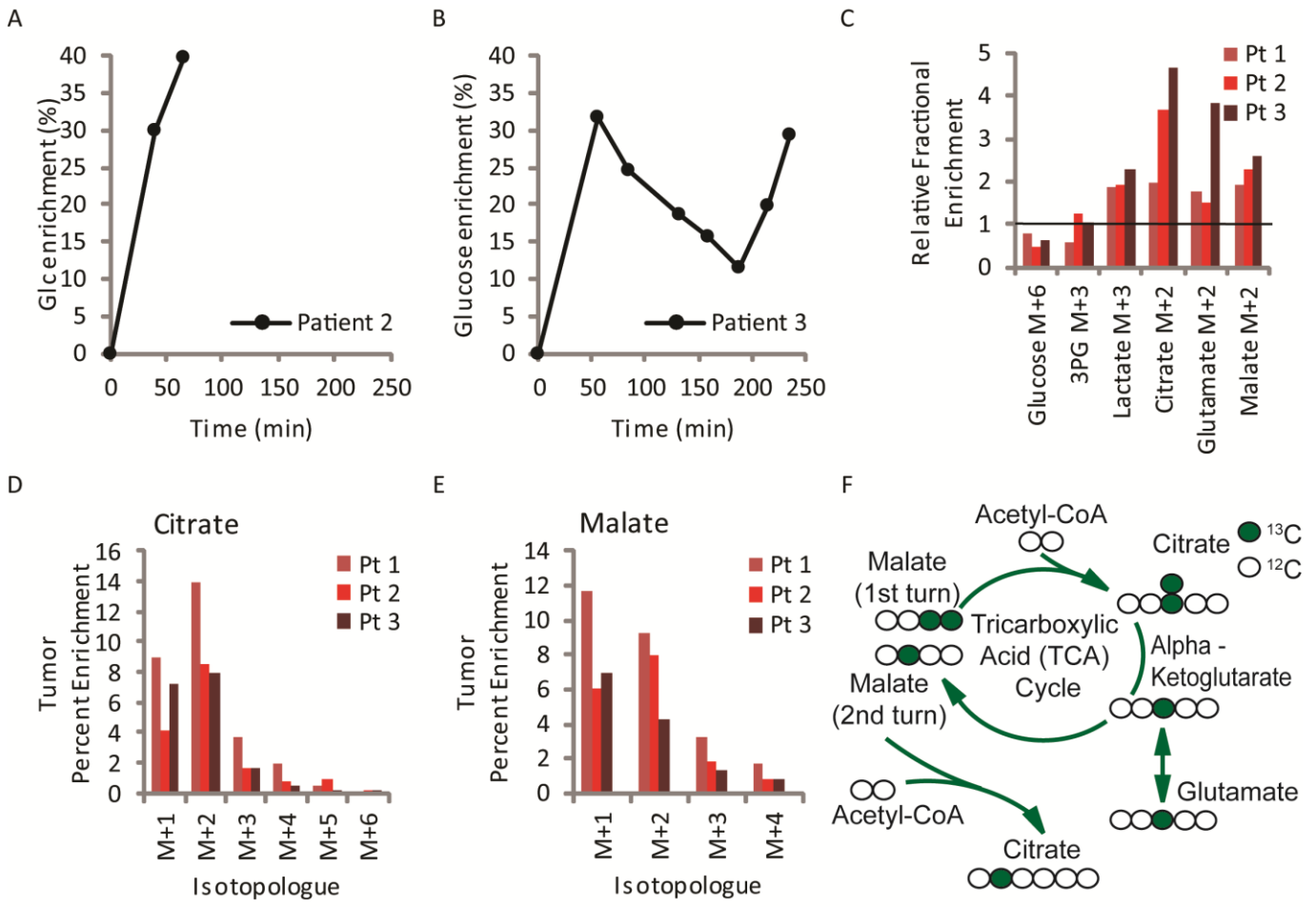


Figure 2.3

A direct comparison between [U- ^{13}C] glucose infusion (patient 1) and bolus-like (patient 2 and 3) data.

(A) Enrichment time-course of perioperative ^{13}C glucose infusion of patient 2.

(B) Enrichment time-course of perioperative ^{13}C glucose infusion of patient 3.

(C) Relative fractional enrichment of ^{13}C to ^{12}C of the depicted glycolytic and TCA cycle metabolites depicted in figure 1D of patient 1, 2 and 3. Tumor values were normalized to patient matched lung values of 1.

(D) Full isotopologue distribution of citrate in the tumors of patients 1, 2, and 3.

(E) Full isotopologue distribution of malate in the tumors of patients 1, 2, and 3.

(F) Proposed tracer scheme for the origin of M+1 isotopologue during [U- ^{13}C] glucose administration.

Abbreviations: Glc, Glucose; min, minutes; M+n, full parent ion for a given metabolite with n ^{13}C carbons incorporated; Pt, Patient; CoA, Coenzyme A; ^xC , carbon with x atomic mass units.

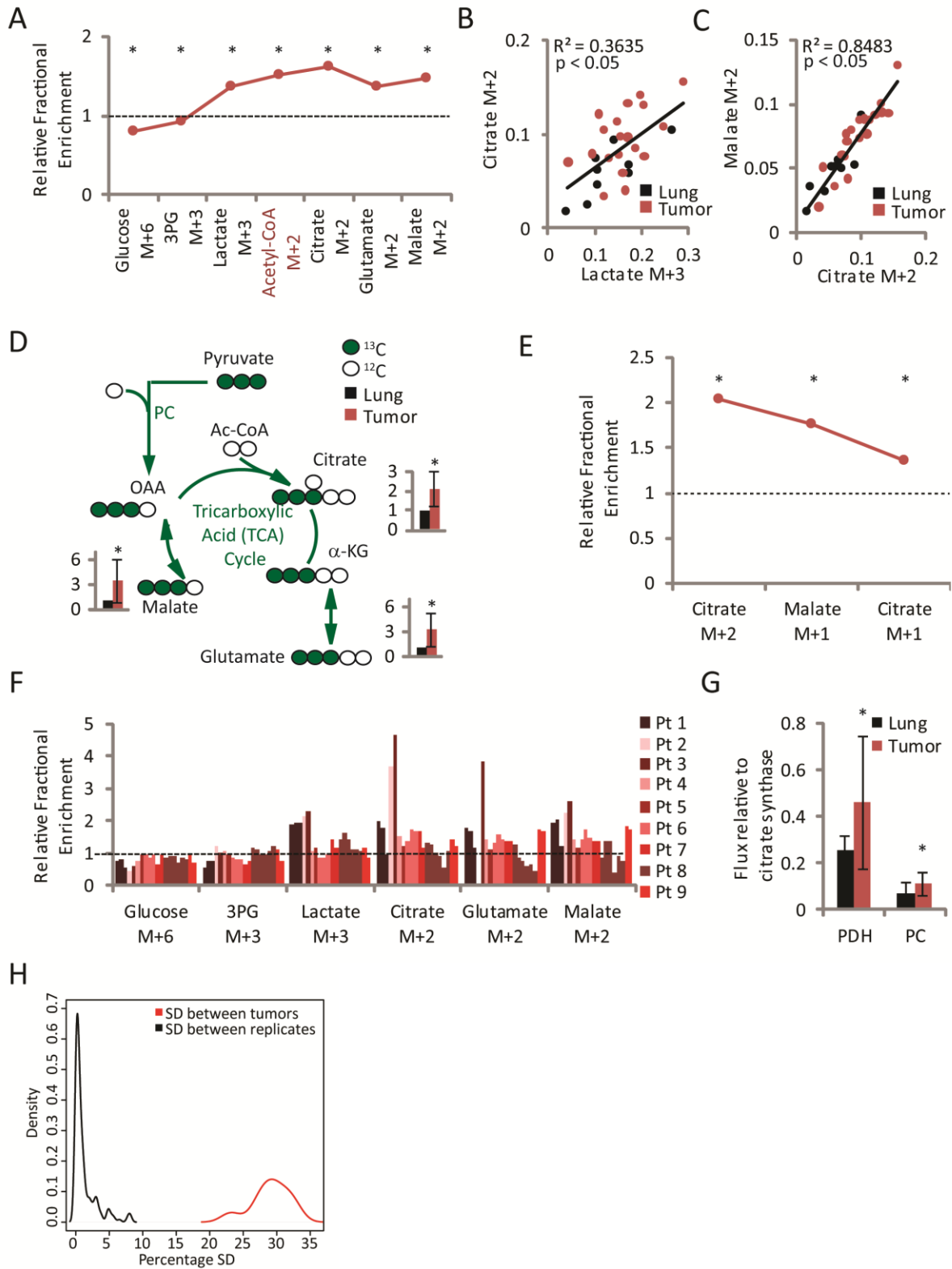


Figure 2.4

Common NSCLC patient tumor phenotypes in glucose-derived metabolism.

(A) Average relative fractional enrichments, tumor to lung, in the metabolic pathways of figure 1d.

Acetyl-CoA was not directly measured but modeled from the data with TCASIM.

(B) Fractional enrichment correlation plot between glycolysis (lactate M+3) and initial entry into the TCA cycle via PDH (citrate M+2). Shown are all fragments, non-cancerous lung and tumor, studied.

(C) Fractional enrichment correlation plot between initial entry via PDH (citrate M+2) and first turn of the TCA cycle (malate M+2). Shown are all fragments, non-cancerous lung and tumor, studied.

(D) Tracer scheme for the origin of M+3 species during [U-¹³C] glucose administration. Shown are the average and standard deviation of the relative fractional enrichments, tumor to lung, of all nine patients.

(E) Average relative fractional enrichments, tumor to lung, in the metabolic pathway of figure 2f.

(F) Individual patient relative fractional enrichments, tumor to lung, in the metabolic pathways of figure 1d. Shown are all fragments, non-cancerous lung and tumor, studied.

(G) TCASIM modeled fluxes relative to citrate synthase flux from the fragments of (F).

(H) Plasma glucose M+6 normalized standard deviations for all isotopomers measured in Table S2.

* = $p < 0.05$ by student's paired t-test or Pearson's product moment correlation coefficient in (A), (D), (E) and (G), or (B) and (C), respectively.

Abbreviations: M+n, full parent ion for a given metabolite with n ¹³C carbons incorporated; CoA, Coenzyme A; ^xC, Carbon of x atomic mass units; Pt, Patient; PC, Pyruvate Carboxylase; PDH, Pyruvate Dehydrogenase.

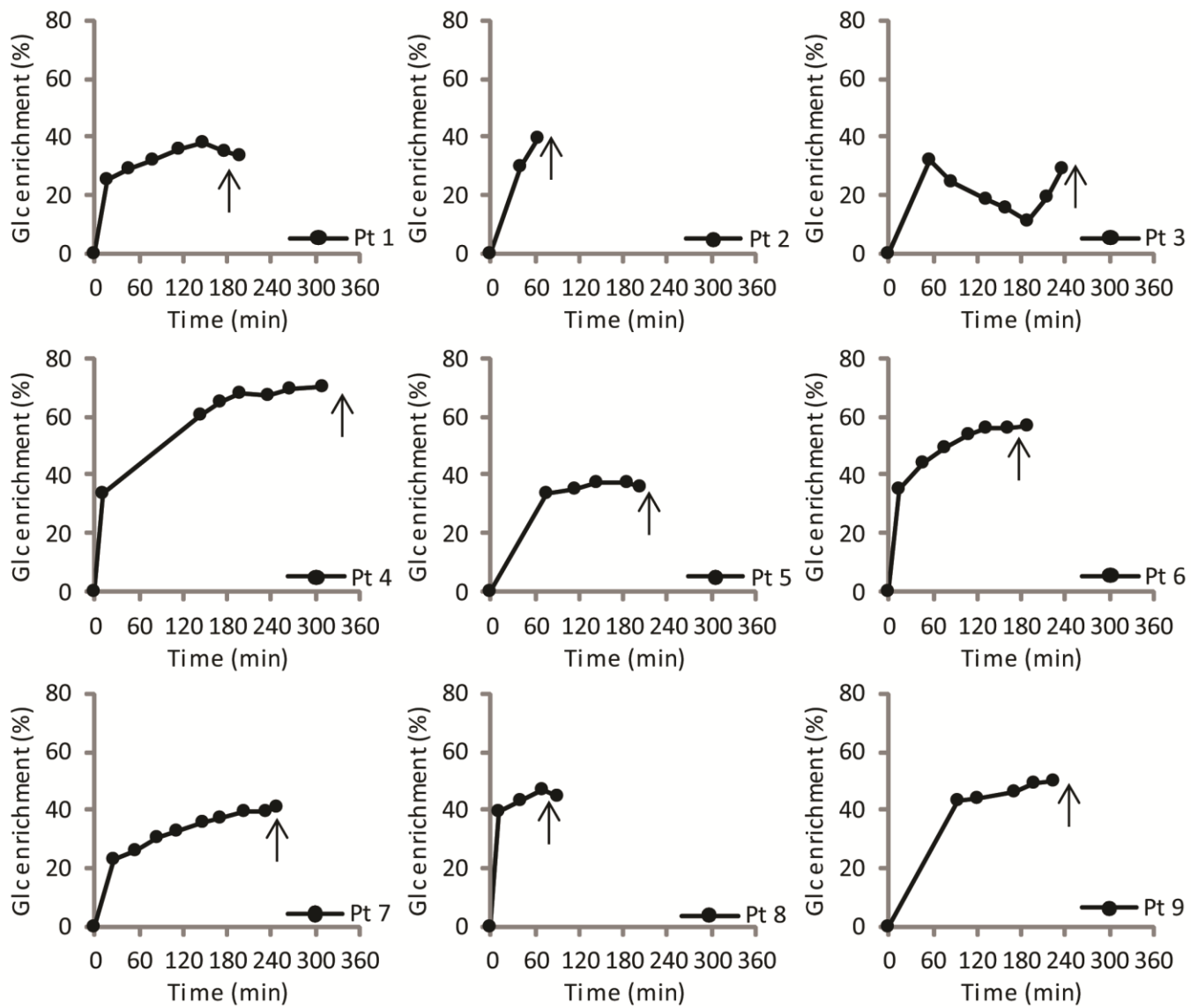


Figure 2.5: Perioperative ^{13}C Glucose plasma enrichment curves for all patients in the study. A bolus of ^{13}C Glucose is administered over a ten minute period, followed by steady infusion until tumor resection. Patient 3 is an exception. Arrows denote point of tumor resection, either before or after the last blood draw.

Abbreviations: Glc, Glucose; Pt, Patient; min, minutes.

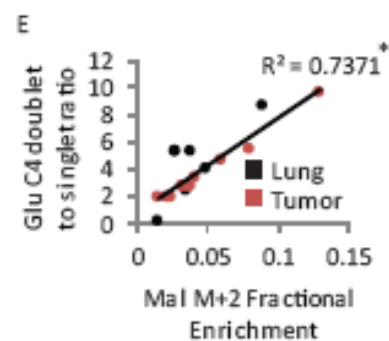
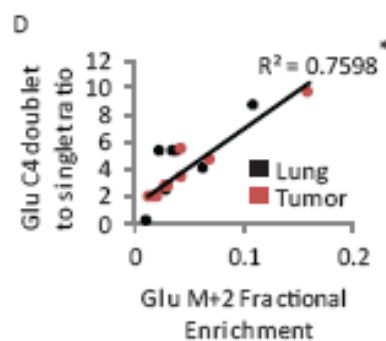
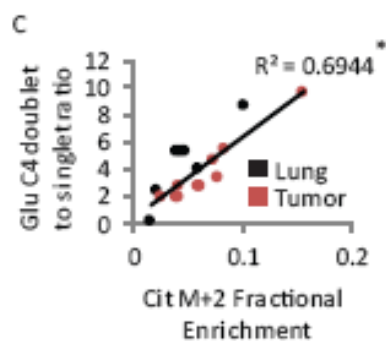
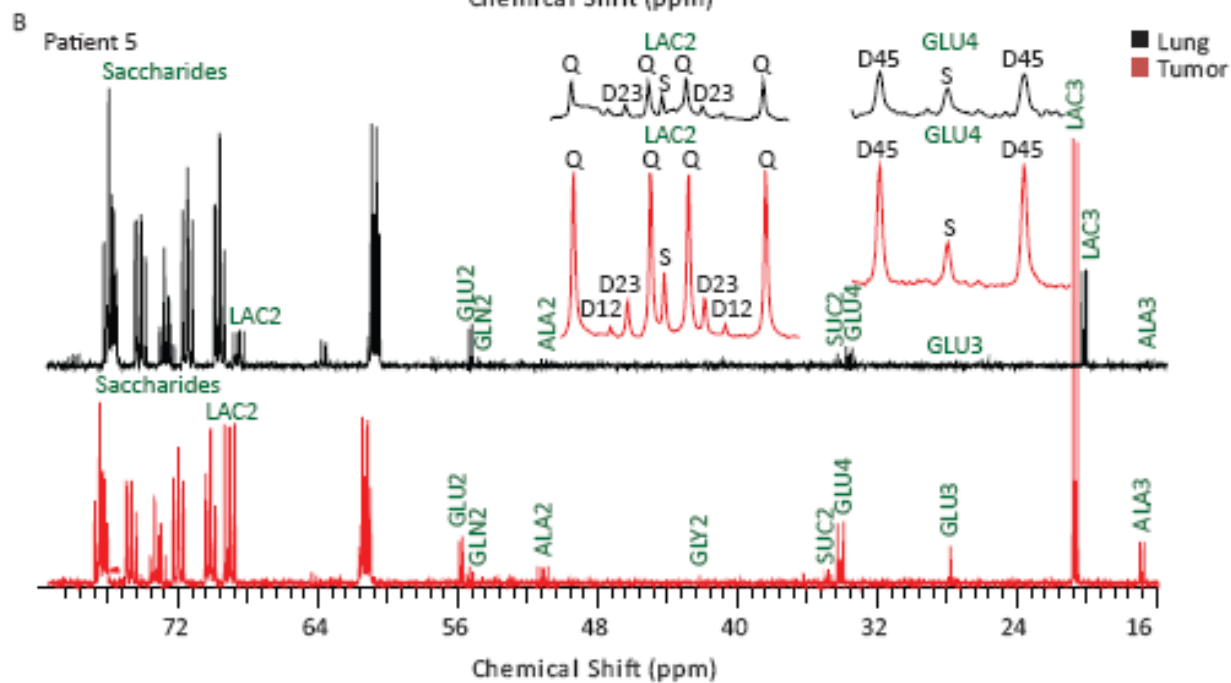
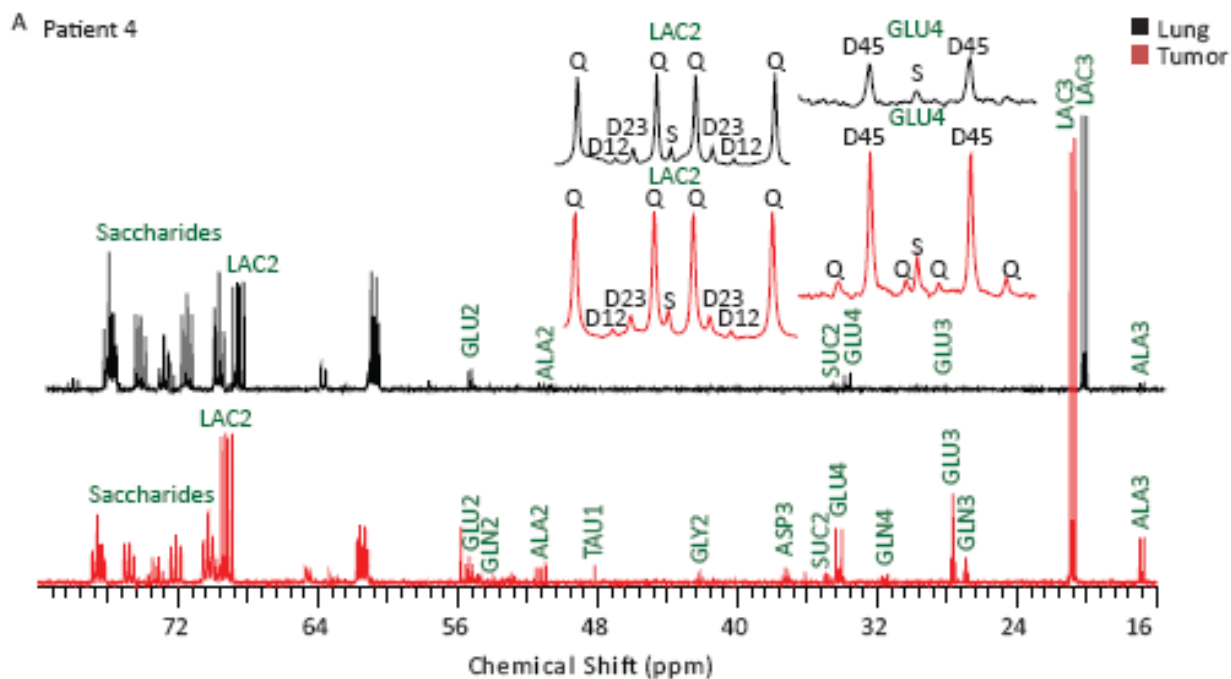


Figure 2.6: NMR evidence in support of GC-MS isotopologue phenotypes and interpretation.

(A) Truncated tumor and lung spectra of patient 4. Equal weights of tissue were submitted. Shown in the magnified inserts are tumor spectra enhancements in the lactate C2 quartet to singlet ratio (similar to lactate M+3 isotopologue) and the glutamate C4 4,5 doublet isotopomer assumed to be the major contributor to the M+2 TCA cycle intermediate isotopologues.

(B) As in (A) for patient 5.

(C) Correlation plot between the glutamate C4 doublet to singlet ratio and citrate M+2 fractional enrichments of all tissue samples submitted for NMR with accompanying regional tissue fragments submitted for GC-MS analysis. NMR analysis was conducted in five patients, with two tumor fragments of one patient.

(D) As in (C), a correlation plot between glutamate C4 doublet to singlet ratio and glutamate M+2 fractional enrichment.

(E) As in (C), a correlation plot between glutamate C4 doublet to singlet ratio and malate M+2 fractional enrichment.

Abbreviations: ppm, parts per million; S, singlet; D, doublet; Q, quartet; LAC, Lactate; GLU, Glutamate; ALA, Alanine; SUC, Succinate; GLN, Glutamine; TAU, Taurine; GLY, Glycine; ASP, Aspartate; Mal, Malate.

* = $p < 0.05$ by Pearson's product moment correlation coefficient.

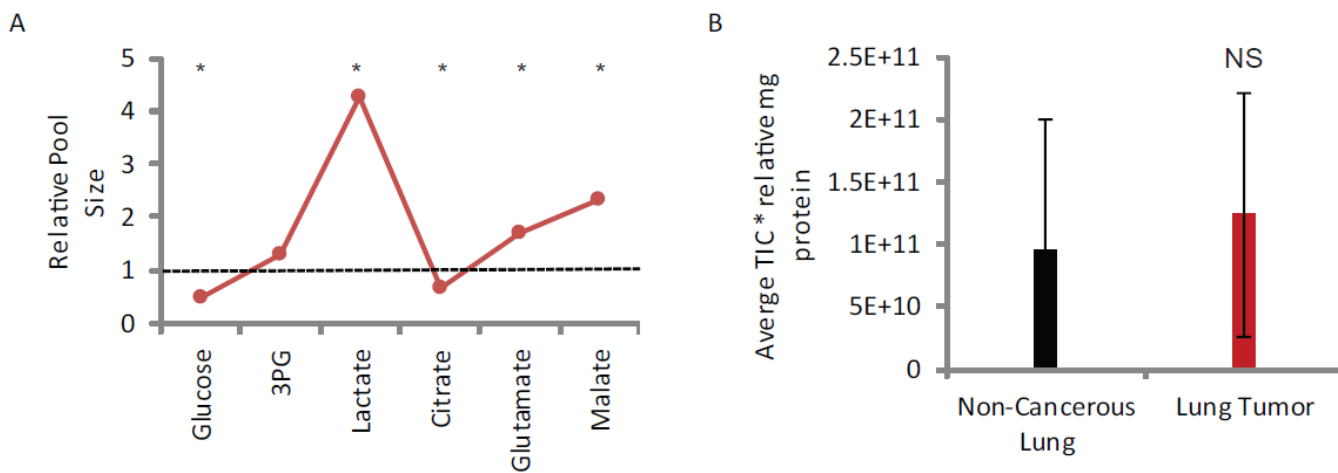


Figure 2.7: Metabolite pool size analysis of tumor fragments relative to non-cancerous lung.

(A) Average tumor fragment metabolite pool sizes relative to non-cancerous lung.

(B) Demonstration of no significant trend in the product of TIC and mg protein input, which was used for relative pool size comparisons.

* = $p < 0.05$ by paired student's t-test

Abbreviations: 3PG, 3-Phosphoglycerate; mg, milligram; NS, Not Significant; TIC, Total Ion Current.

CHAPTER THREE

NSCLC TUMORS IMPORT AND OXIDIZE LACTATE IN VIVO IN BOTH HUMANS AND MICE

3.1 Results

3.1.1 NSCLC patient tumors metabolize lactate in vivo

The low fractional enrichment of the tumor acetyl-CoA pool stimulated analysis of other blood-borne metabolites that might contribute to central carbon metabolism. Lactate circulates at levels of 1-2 mM in humans, and has been demonstrated to be a metabolic fuel for cancer cells under some conditions (Guillaumond et al., 2013; Sauer and Dauchy, 1983; Sonveaux et al., 2008). To examine the impact of circulating lactate on tumor metabolism, we first compared fractional enrichments between 3-PG and lactate in tumor and lung fragments from all nine patients. In the majority of lung fragments, 3PG enrichment was the same or modestly higher than lactate enrichment. This is the expected pattern if lactate arises from glycolysis in the lung, with modest contributions from unlabeled substrates between 3PG and lactate to reduce enrichment of the lactate pool. In striking contrast, lactate enrichment in most of the tumors exceeded 3PG enrichment, implying contribution of an additional substrate to labeled lactate (Figure 3.1a). The most obvious candidate is lactate itself, because lactate imported from the plasma would feed the tumor lactate pool and could also serve as a carbon source for pyruvate-derived TCA cycle metabolism (Figure 3.1c). Indeed, infusion of [U-¹³C] glucose led to measurable amounts of circulating [U-¹³C] lactate (Figure 3.1d), and the lactate

enrichment in the plasma pool sometimes exceeded that of the tumor (Figure 3.1b). Given our confirmation by NMR that m+2 isotopologues primarily reflect entry and passage of [U-¹³C]acetyl-CoA through the TCA cycle, if fractional m+2 enrichment of TCA cycle intermediates exceeds m+3 in 3PG, this would indicate contribution of lactate to TCA cycle metabolism. This relationship was observed in several patients, including patient 1 (Figure 3.1d). Others, including patient 5, demonstrated a more conventional pattern of progressive decline in labeling from glucose to all downstream intermediates (Figure 3.1d). Thus, the data indicate that some human lung tumors use lactate as a carbon source for central metabolism.

3.1.2 Human NSCLC cell lines xenografted into mice flanks metabolize lactate in vivo

To examine lactate metabolism more directly in a mouse model, several mice bearing subcutaneous xenografts derived from A549 human non-small cell lung cancer cells were infused with [2-¹³C] lactate in a manner analogous to the [U-¹³C] glucose infusions. This led to rapid and persistent enrichment of the circulating lactate pool (Figure 3.1f), and a lower level of enrichment in glucose as lactate was used as a gluconeogenic precursor. Similar to the findings from the patients, lactate within these tumors was highly labeled (Figure 3.1g). Enrichment in citrate exceeded the enrichment of 3PG (3.1g), indicating that this citrate likely arose from contribution of imported lactate to the TCA cycle, rather than contribution of labeled glucose from the circulation. Thus, lactate is a substrate for oxidative metabolism in these tumors.

3.1.3 A modeling based argument for lactate metabolism in mice flank xenografts

A problem has been introduced by the realization of the possibility of multiple substrate inputs converging on a metabolic node feeding the TCA cycle, such as extracellular lactate and intracellular 3PG converging on pyruvate. Is there a way that we can distinguish between a higher enrichment coupled to a lower flux through an enzyme, such as lactate through PDH, and a lower enrichment coupled to a higher flux through an enzyme, such as 3PG and PDH in our example? I attempted to turn to modeling the GC-MS data to answer this question. I believe the short answer is yes, but there must be a significant difference in enrichment between the two options and a significant amount of labeling in the relevant downstream TCA intermediates.

The mouse flank xenograft lactate infusions provide an example for this problem (figure 3.2). Using the methodology of modeling described in chapter 2, one can compare the “total delta” between the tcaSIM best-fit simulation and the experimental data when using lactate or 3PG as the enriched input. The results yield all of the predictable outcomes of how the program would try to compensate for the decreased enrichment in 3PG in an attempt to improve the fit between the simulation and the data. Entry of label into the TCA cycle is significantly enhanced via PDH and PC in the 3PG series. Additionally, on average the number of turns has increased to build up label in the cycle. However, notice that in some mice the fluxes relative to citrate synthase of PC and PDH have maxed out at 1 in the 3PG condition. I interpret this as the program not being able to get a reasonable fit with a plausible amount of PDH and PC flux relative to citrate synthase to fit the data, indicative of lactate being the more likely substrate than 3PG. If one looks at the individual data, it appears that when both PC and PDH max out at 1 the total delta values become very high, clearly indicating inadequate fits. Note that these are the two infusions with greater fractional enrichment of lactate in the plasma. This data reiterates the theme of balancing infusing enough ^{13}C to maximize signal to noise and the

other issue of trying to keep the conditions as close to normal physiology as possible without overloading substrate. A future experiment would be to repeat the lactate infusions with [U-¹³C]lactate. I predict this would give greater separating power as there would be more ¹³C signal in the TCA cycle.

3.1.4 Extending the modeling to [U-¹³C]glucose infusions in mice flank xenografts

Observations of mice infused with glucose provide an example of the same general pattern with less separation between 3PG and lactate enrichment (figure 3.3). This series compared A549 cells xenografted in the flank of a mouse to an A549 xenograft on the opposite flank with LKB1 added back (A549 cells are mutant for LKB1). It highlights an issue to revisit in the NSCLC patients in the comparisons between tumor to non-cancerous lung (Chapter 2), between different tumors (Chapter 4), or between various regions within a tumor (Chapter 4). Now we have two variables, change in flux and choice of substrate. Specifically, did only the flux increase or decrease into PDH? Or did choice of substrate also change? Or, likely, is it a mixture of these two effects? To prioritize between scenarios, short of alternative experiments, I would turn to the total delta. The most likely situation should have the best fit from the model according to the data.

So given this series, we can systematically assess each scenario and what the resulting consequences and total delta would be. If we assume that both conditions, A549 and the LKB1 add back, draw their TCA cycle signal from glycolysis-derived pyruvate as assessed from modeling using the 3PG data, we see that there are insignificant trends towards less PDH and PC, and more YS flux relative to citrate synthase upon LKB1 add back (Figure 3.3a). Yet clearly, the increase in an additional anaplerotic source upon LKB1 add back looks promising. This analysis essentially validates the necessity for modeling all TCA cycle tracer data, as if one

simply used a first turn analysis and observed the higher m+2 species in the LKB1 add back condition, one would have assumed more entry through PDH in the LKB1 situation. However, upon looking at the enrichment data in 3PG, it becomes apparent that the LKB1 group has significantly more signal in the upstream metabolite 3PG. Thus, to reiterate, more signal does not necessarily imply more carbon flow, it must be normalized to the enrichment of the entering upstream substrate (Figure 3.3b). The average total delta under this scenario is 0.30 for the A549 group and 0.21 for the LKB1 group.

We can repeat this analysis with lactate, assuming that both groups primarily metabolize extracellular lactate over intracellular glycolysis-derived pyruvate (Figure 3.3c). Under this scenario, now PDH and PC flux relative to citrate synthase have gone up in the LKB1 add back group relative to A549, yet these changes are insignificant. Interestingly, again under this scenario the YS flux relative to citrate synthase continues to be greater, still insignificant, in the LKB1 group. At this point I would conclude that the YS change is more stable than PDH and YPC, which depend on the assumption made. Finally, this gives total deltas of 0.30 and 0.21 for A549 and the LKB1 group, respectively. This is the same as the previous scenario, so it is impossible to distinguish the source of ^{13}C label no matter which scenario we use.

Now we can turn the last two, more complex scenarios. We can start with the scenario that the A549 group utilized glycolysis-derived 3PG and the LKB1 group used extracellular lactate as pyruvate sources. Essentially this is no different than previous scenarios (data not shown). Finally, we can assess if the A549 group utilized lactate and the LKB1 group utilized intracellular glycolysis for pyruvate metabolized in the TCA cycle (data not shown). This gives the same pattern as well. In summary, perhaps surprisingly, no claim can be made as to choice of substrate, glucose or extracellular lactate-derived pyruvate in these models.

However, this exercise did demonstrate that no matter the assumption, an increase of an anaplerotic source was observed upon LKB1 add back.

3.1.5 A re-analysis of the modeling between non-cancerous lung and lung tumors in the NSCLC patients in light of the possibility of lactate as a substrate choice.

As in the exercise in 3.3.4 above, what would happen if we revisit the modeling in figure 2.3g in light of the possibility of lactate import and metabolism in either the non-cancerous lung tissues or tumors? Again, we can start with the simplest alternative, that both tissues ubiquitously metabolized extracellular lactate as a mitochondrial substrate (figure 3.b). This maintains the trends, and PC stays significant, but blunts the effects to where the observed enhancement in PDH in the tumors is no longer significant. Like the mouse experiments, what if we empirically let the total delta be the deciding factor of whether to use the 3PG or lactate data? This scenario is similar to the previous all lactate scenario, with similar trends but PC being the more robust difference and maintaining significance (figure 5.3c).

3.2 Methods

3.2.1 Mouse studies

1×10^6 A549 cells were injected into the flank of male athymic Ncr nude mice purchased from Taconic. Before infusions, mice were fasted for an average of 12 hours. Mice were anesthetized with isoflurane, and catheters were placed in the tail vein. A 20% weight:weight aqueous solution of [2- ^{13}C] lactate purchased from Cambridge Isotopes was infused via an infusion pump for 150 to 180 minutes, at a rate of 100 μl per minute for the first minute, 24 microliters for 10 minutes, and 2 microliters per minute until the end of the infusion. Blood draws of roughly 50 μl were sampled via retro-orbital procurement. At the end of the infusion, tumors were harvested, rinsed briefly in ice cold saline, and frozen in liquid nitrogen.

3.3 Discussion

3.3.1 Supportive surrogate biomarker evidence of lactate metabolism in NSCLC

Integral to this discussion of oxidized TCA cycle substrates, the modeling of the fractional enrichment data in acetyl-CoA uncovered the surprising result that there were other significant contributors to the tumor acetyl-CoA pool. We provide evidence that one of these substrates is acetyl-CoA derived from lactate import and metabolism (Figure 3). Lactate is transported across the cell membrane by facilitated diffusion by monocarboxylate transporters (Halestrap and Price, 1999; Kennedy and Dewhirst, 2010). Additionally, the lactate dehydrogenase enzyme interconverts pyruvate and lactate, with the ratio of isoforms contributing to the directionality of conversion (Dawson et al., 1964; Doherty and Cleveland, 2013). As *in vitro* studies of lung adenocarcinoma have implicated functional significance for LDHB, which favors the conversion of lactate to

pyruvate, it is plausible that lactate import and metabolism could be a significant metabolic substrate for NSCLC patient tumor metabolism *in vivo* (McClelland et al., 2013).

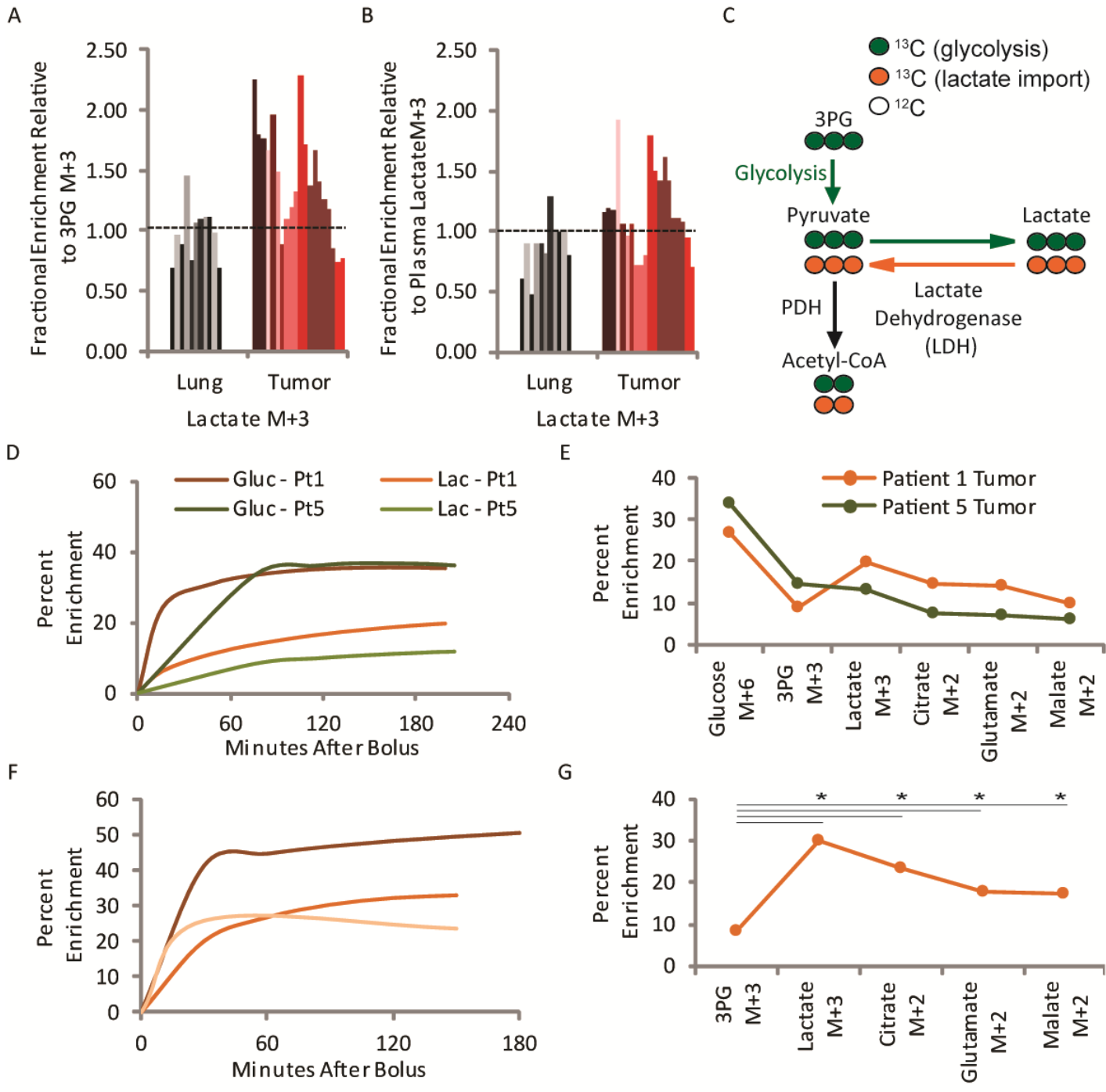


Figure 3.1: Evidence for import and metabolism of extracellular lactate in NSCLC tumors.

(A) Lactate M+3 isotopologue fractional enrichments relative to 3PG M+3 in all patient tissue fragments. Shown are matched tumor and non-cancerous lung series.

(B) Lactate M+3 isotopologue fractional enrichments relative to plasma lactate M+3 in all patient tissue fragments. Shown are matched tumor and non-cancerous lung series.

(C) Tracer scheme for glycolysis-derived pyruvate in green and lactate import and exchange in orange.

(D) Gamma variate curve-fitted plasma enrichment curves of u-labeled isotopologues (glucose M+6 and lactate M+3) for the infusions of patients 1 and 5.

(E) Percent enrichments in tumor fragments of patient 1 and 5 of the isotopologues of the tracer scheme of Figure 1D, with the proposed color schemes of (B).

(F) Gamma variate curve fitted plasma enrichment curves of lactate M+3 isotopologue during ^{13}C lactate infusions in A549 cell line tumor xenograft bearing mice. Shown are three separate experiments.

(G) Results of tumor fragment analysis of the mice of (E). Shown are the averages of fragments from two tumors in contralateral flanks in each mouse, for a total of six fragments.

* = $p < 0.05$ by paired student's t-test.

Abbreviations: M+n, full parent ion for a given metabolite with n ^{13}C carbons incorporated; 3PG, 3-Phosphoglycerate; Gluc, Glucose; Lac, Lactate; PDH, Pyruvate Dehydrogenase; CoA, Coenzyme A.

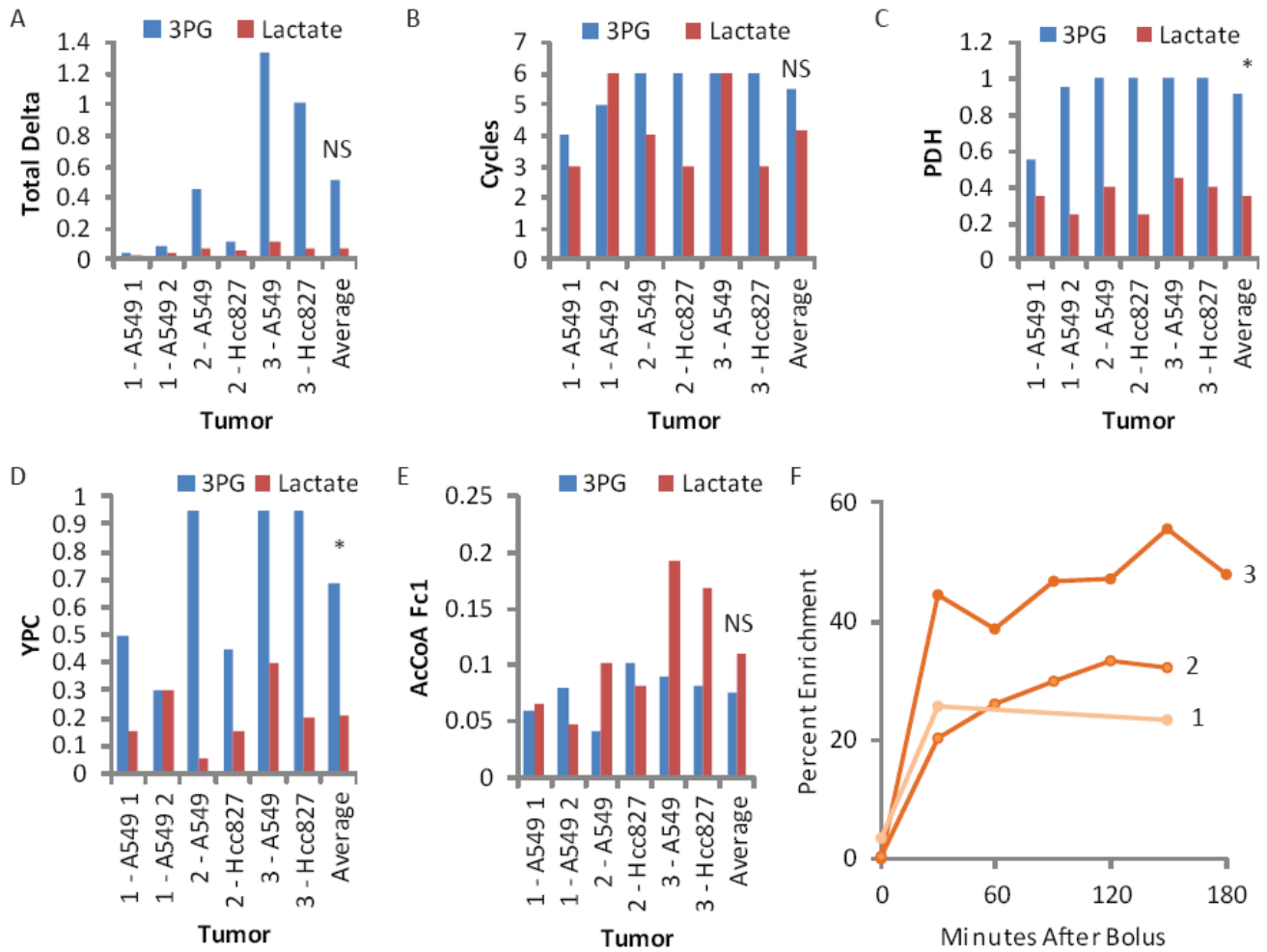


Figure 3.2: Comparing modeling results of 3PG vs lactate metabolism in mouse lactate infusions. The results from the methodology of modeling with tcaSIM in chapter 2 are shown directly comparing 3PG to lactate results in each mouse. Displayed are the results for (a) total delta, (b) cycles, (c) PDH, (d) YPC, (e) AcCoA Fc1 (acetyl-CoA M+1). The tumors are named by the mouse number, followed by the cell line. The infusion curves for these three mice are shown in (f). * = $p < 0.05$. NS = not significant.

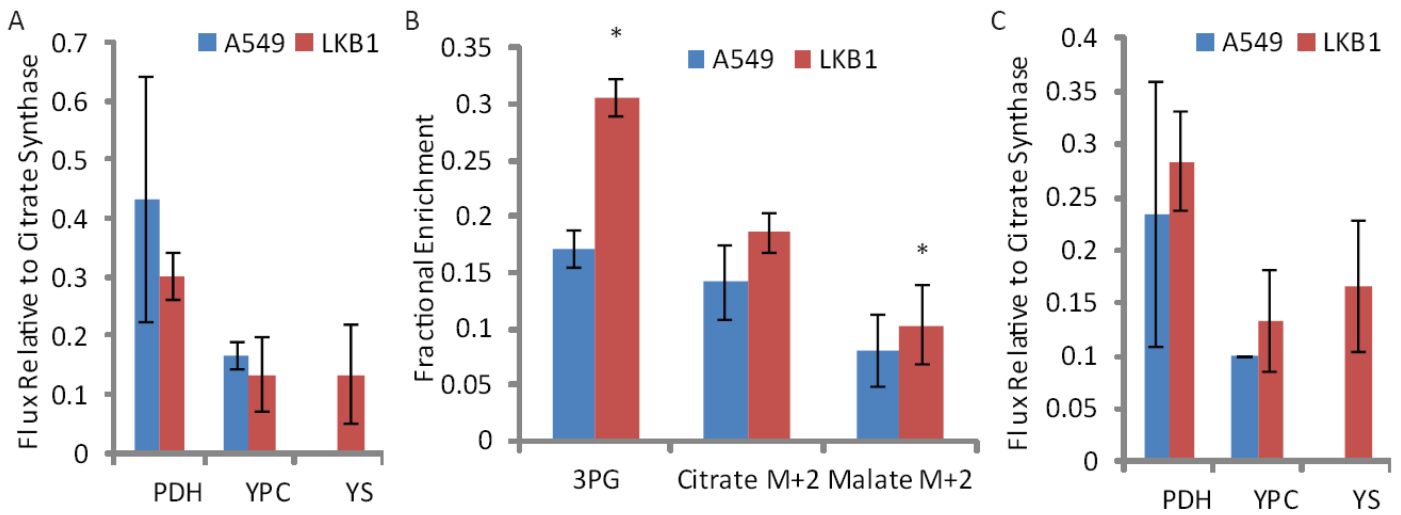


Figure 3.3: Comparing various scenarios in a series of mice bearing contralateral flank cancer cell line xenografts infused with [U-¹³C]glucose.

The cell lines are A549 compared to A549 with functional LKB1 add back (LKB1).

(A) Scenario where both xenografts metabolize glycolysis derived 3PG as a mitochondrial substrate.

(B) Fractional enrichments of metabolites in two groups

(C) Scenario where both xenografts metabolize extracellular lactate as a mitochondrial substrate.

N = 3 mice, infused on separate days.

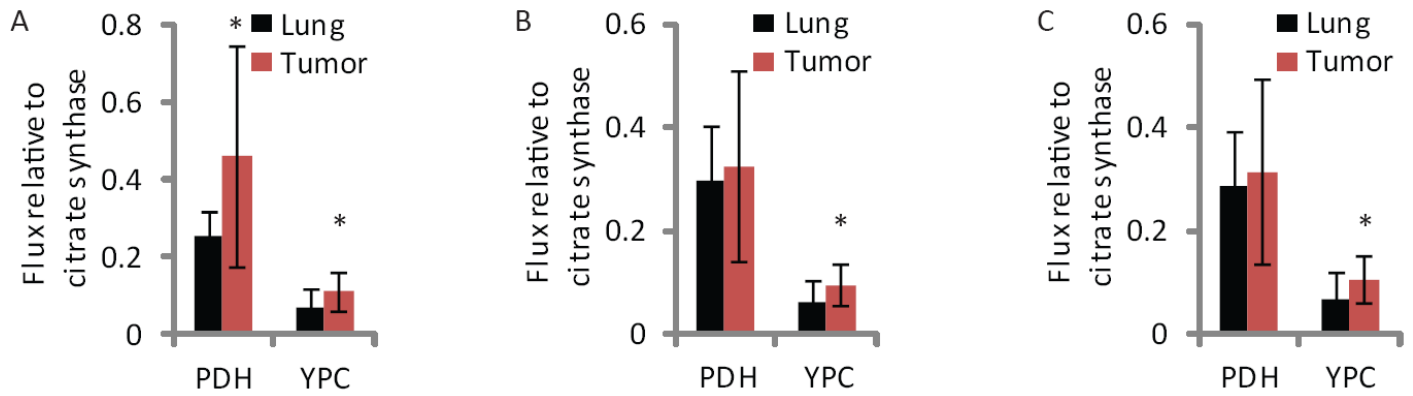


Figure 3.4: Comparing various scenarios in the NSCLC patient data.

(A) Scenario where all tissues TCA cycle signal arises from intracellular glycolysis derived pyruvate (3pg).

(B) Scenario where all tissues TCA cycle signal arises from lactate import derived pyruvate.

(C) A mixture of the two scenarios, with each data point dictated by the total delta as to whether the lactate or 3pg data is utilized.

* = $p < 0.05$ by paired student's t-test.

CHAPTER FOUR

HETEROGENEITY IN GLUCOSE-DERIVED PYRUVATE OXIDATION BOTH WITHIN AND BETWEEN NSCLC PATIENT TUMORS IN VIVO

4.1 Results

4.1.1 NSCLC tumors display heterogeneous degrees of glucose metabolism predicted by an MRI marker of tissue perfusion.

Although transforming mutations may impart tumor cells with the ability to engage in autonomous glucose metabolism, extrinsic factors also influence the metabolism of tumor cells (Birsoy et al., 2014; Commisso et al., 2013; Guillaumond et al., 2013; Zhang et al., 2014b). The extensive metabolic heterogeneity among tumors in our study prompted an examination of the factors that predict ^{13}C enrichment in various metabolites.

The availability of DCE MRI data in all patients provided an opportunity to examine the influence of perfusion on the metabolic phenotype (Yankeelov and Gore, 2009). We first assessed whole tumor DCE data by region of interest (ROI) mean signal intensity of a slice chosen for largest surface area. Patients in our cohort were easily dichotomized based on qualitative assessment of their DCE curves, with several more perfused tumors and several tumors displaying poorer entry of the gadolinium contrast agent (Figure 4.1a). DCE data were then analyzed as the initial area under the curve over 60 seconds after administration of the

contrast agent (iAUC60), a semi-quantitative parameter used as an indicator of tumor perfusion (Figure 4.1c) (Barnes et al., 2012). This feature also enabled the tumors to be separated into two groups, with high and low perfusion. Analysis of fractional enrichment data revealed that metabolites from the well-perfused tumors were nearly indistinguishable from the surrounding lung, whereas the tumors with lower iAUC60 values had, on average, larger enhancements of enrichment over benign tissue (Figure 4.1b). Additionally, as the iAUC60 is a quantitative parameter, significant direct or inverse correlations could be observed between iAUC60 and 3PG M+3 or malate M+2 relative fractional enrichments, respectively (Figure 4.1d). Lastly, the modeling results demonstrated enhancements in PDH flux in the tumors displaying less contrast enhancement (Figure 4.1e). These findings are consistent with the inverse relationship between FDG-PET signal and contrast enhancement assessed by DCE-MRI (Zhang et al., 2014a). The FDG-PET examinations in our study were conducted at various oncology centers without a standardized approach to measuring SUV parameters, prohibiting similar intertumor assessment of correlation between FDG-PET and either DCE-MRI or ^{13}C enrichment.

4.1.2 Intratumor regions of NSCLC tumors display heterogeneous degrees of glucose metabolism predicted by an MRI marker of tissue perfusion.

Individual solid tumors display substantial molecular heterogeneity. Although metabolic heterogeneity within individual human tumors has not been widely studied, areas of high FDG uptake within large masses were found to be less perfused, as assessed by dynamic FDG-PET, in one series (Vriens et al., 2012). To test whether regions of metabolic heterogeneity existed in the tumors of our NSCLC patients, we first used DCE

MRI to identify anatomic regions of differential contrast enhancement, then selected regions of high and low contrast from the same tumor for metabolite extraction and ^{13}C enrichment analysis. Patient 8 was a non-smoker with an EGFR-mutated adenocarcinoma measuring 16.1 cm³ and a high SUVmax (Figure 4.2a, Table 2.1). Although analysis of DCE MRI signal of the tumor as a whole identified this as a well-perfused mass with high iAUC60 (Figure 4.1a-b), DCE characteristics were dramatically different between the superior and inferior regions of the tumor (Figure 4.2c). A fragment was chosen from the superior and inferior aspect of the tumor and subsequently sectioned into three smaller fragments, extracted, and analyzed for ^{13}C enrichment. Enrichments in the poorly perfused, inferior aspect of the tumor were significantly higher than those in the superior aspect (Figure 4.2e). We further support these results with adjacent fragments analyzed by NMR, as well as modeling of the MS results (Figure 4.3). Patient 9 had a 3.8 cm³ EGFR-wild type adenocarcinoma with a low SUVmax (Figure 4.2b, Table 2.1) and relatively poor DCE MRI signal throughout (Figure 4.1a). Again, however, subtle differences could be detected by DCE MRI, indicating modestly enhanced signal in the posterior compared to the medial region of the tumor (Figure 4.2d). As in the patient 8's larger and more FDG-avid tumor, fragments isolated from these two regions displayed similar albeit more subtle differences in ^{13}C enrichment, with the region of higher DCE signal demonstrating lower ^{13}C enrichment in lactate, citrate and other metabolites. Thus, DCE-based assessment of tissue perfusion predicts the extent of glucose's contribution to both anaerobic and aerobic metabolism. In the small cohort reported here, this relationship is observed in tumors whose overall perfusion and SUVmax are either high or low.

4.2 Methods

4.2.1 Multi-parametric Magnetic Resonance Imaging

Magnetic Resonance Imaging was performed within eight days of the surgery. MRI studies were performed on either a 3T dual-transmit Achieva MR scanner (Philips Healthcare, Best, The Netherlands) with a 16-channel SENSE-XL Torso Coil or a 3T Philips Ingenia scanner with a 28-channel dStream Anterior-Posterior coil. Coronal and axial T2-weighted half-Fourier single-shot turbo spin-echo images were acquired for anatomic reference for localizing the lesion. Dynamic contrast enhanced (DCE) MRI was performed using a 2D or 3D T1-weighted spoiled gradient-echo sequence before, during, and after the administration of a bolus of 0.01 mmol/kg gadobutrol (Gadavist; Bayer Healthcare Pharmaceuticals, Wayne, NJ) using a power injector at a rate of 2 cc/sec followed by a 20 cc saline flush at the same rate. DCE images were acquired with free-breathing for at least 4 minutes using the following parameters: TE/TR = 1.14-1.65/2.5-4.5 ms, flip angle = 10°, field of view = 200-300 x 200-300 mm², in-plane resolution = 0.8-1.7 x 0.8-1.7 mm², and temporal resolution = 0.5-5.2 sec. One or more imaging slices were acquired from the lesion with careful planning to avoid possible imaging artifacts from the heart and major blood vessel(s) depending on the size and location of the lesion.

Tumor volume measurements were based on T2 weighted images by ROI segmentation in Osirix. Dynamic contrast-enhanced MRI was analyzed by manually drawn regions of interest (ROIs) in Osirix. For whole-tumor DCE analysis, ROIs were drawn around the whole tumor of a slice chosen to maximize surface area. For intra-tumor DCE analysis, ROIs of the same size were placed on regions of tumor dictated by anatomical descriptors of tissue procurement. ROIs were automatically propagated throughout the whole time series of a given scan. Average ROI values were plotted using every available time point, and the baseline subtracted by using the value immediately before contrast enhancement, which was given the time point of 0

seconds. Figure curves were generated by using excel solver to generate constants of a gamma variate function that satisfy a minimum between all data points of a DCE scan and the points of a gamma variate function. Initial area under the curve measurements were approximated with the trapezoidal rule.

4.3 Discussion

4.3.1 A substrate diffusion model of cancer cell metabolism predicts microenvironment regulation of oxidative substrate usage.

We propose that the results in aggregate suggest a model of preferential oxidation of less abundant labeled acetyl-CoA generating TCA cycle substrates in both well perfused tumors and regions of tumors, with subsequent oxidation of the more abundantly available glucose-derived pyruvate in the more poorly perfused tumors and regions of tumors once the less abundant substrates are depleted. We propose that the glucose deprivation observed in tumor tissues is symptomatic of a more general nutrient depletion, with other acetyl-CoA generating metabolites among these depleted nutrients. This general concept of upregulating glucose metabolism in response to compromised perfusion has been demonstrated in a larger NSCLC patient cohort by an inverse correlation between FDG-PET SUVmax and SUVmean and DCE-MRI pharmacokinetic parameters of perfusion (Zhang et al., 2014a). However, as elaborated above with current paradigms of the Warburg Effect, the tumor microenvironment regulation of TCA cycle acetyl-CoA substrate usage is relatively unexplored *in vivo*. As we demonstrate enhancements in oxidation of glucose-derived carbon, this raises the possibility of discovering tumor dependencies on acetyl-CoA substrates for survival or growth that may be

more dispensable for non-cancerous cell survival or growth in a microenvironment with more diverse substrate choices.

4.3.2 Studies of primary tumor heterogeneity can unravel the drivers of tumor metabolic phenotypes *in vivo*.

Aside from its relevance to translational efforts, we propose that intratumor heterogeneity can serve as an avenue to conducting *in vivo* studies in cancer metabolism with greater precision as the assay conditions are significantly more controlled within a given patient than between patients. Additionally, we propose intratumor heterogeneity can uncover drivers behind whole tumor phenotypes. For example, based solely on intertumor analysis, no claim can be made as of whether the perturbations in tumor glucose metabolism are a cause or effect of altered perfusion. A cell-autonomous, “aerobic glycolysis” model would predict that a rapidly growing, highly glycolytic tumor could outpace its blood supply as well as be less dependent on it (Levine and Puzio-Kuter, 2010). Indeed, we find that one of the tumors in the “less perfused” group was Kras mutant, which has been linked to upregulated glycolysis and glucose-dependent anabolic pathways for cell growth (Table 2.1, Figure 4.1) (Racker et al., 1985; Ying et al., 2012). In congruence with this cell autonomous proliferation explanation of glycolysis, whole tumor measurements have found direct correlations between Ki67 and FDG-PET in NSCLC patient tumors (Vesselle et al., 2000). However, an alternative microenvironment driven model of metabolic reprogramming of glucose metabolic pathways in tumors would predict that the poor perfusion induced by aberrant tumor growth induces hypoxia or metabolite depletion, which induces an evolutionary selection pressure for enhanced “anaerobic” glycolysis (Gatenby and Gillies, 2004). Indeed, glucose depletion has been shown to increase the prevalence of Kras mutations in culture (Yun et al., 2009).

In congruence with this model, a study of an adenocarcinoma cell line in vitro failed to demonstrate a correlation between FDG-PET uptake and proliferation rate (Higashi et al., 1993).

However, correlation studies between whole tumor measurements of FDG-PET and markers of hypoxia (F-MISO, ^{60}Cu , HIF-1 α levels) have been contradictory in NSCLC (Dierckx and Van de Wiele, 2008; van Baardwijk et al., 2007). A recent study suggests that these discrepancies may be rectified by intratumor measurements. In a mouse xenograft model of NSCLC, evidence has been presented in support of the concept that it is the hypoxic, and not proliferative cell populations, where the majority of FDG-PET signal is originating (Huang et al., 2012). Similarly, we report that it is the less-well perfused regions of tumors, not the regions with greater perfusion harboring a greater fraction of cycling cells, which has greater upregulations in glucose metabolism. We propose intratumor correlations between metabolism and tumor biology as a general framework to begin to categorize and rank the drivers of metabolic phenotypes in cancer cells *in vivo*.

Overall, we propose that a workflow of pre-operative advanced imaging guided sampling followed by coupled analyses of tumor histology, genetics and metabolism will fill a sorely needed gap of assaying in patients the numerous cancer metabolic phenotypes that are being submitted as therapeutic targets in model systems. We demonstrate that such a workflow can be informative of not only how to move forward with a given cancer metabolic phenotype, but may additionally be informative on decisions of how to create a model that faithfully recapitulates the desired phenotype – patient tumor metabolism. Specifically, the results of this study suggest that tumor metabolism may be significantly and predictably regulated by the microenvironment.

4.3.3. Semi-quantitative vs. quantitative DCE-MRI as a marker of perfusion

The logic of the analysis of the DCE data is that the raw contrast enhancement data is a valid surrogate of perfusion. The reality is that due to the chaotic tumor vasculature, higher contrast enhancement may be a marker of vessel permeability or leakiness and not necessarily perfusion that can efficiently transfer oxygen and nutrients. Furthermore, shunting through larger vessels without flow through the capillary beds can actually lead to contrast enhancement that is too fast for meaningful nutrient extraction.

There is no established gold standard for perfusion. Our interest in perfusion lies in the downstream consequence of either hypoxia or nutrient depletion. As there is no gold standard, validation studies of DCE-MRI rely on assessing the correlation of its results to some desired physiological parameter. Semi-quantitative analysis has mainly been assessed in the changes in readout after administration of anti-angiogenic treatments in clinical trials. The initial area under the curve, used in this study, has been shown to have a direct correlation to agents targeting the tumor vasculature (Barnes et al., 2012). Presumably, the connection can be made that the iAUC signal correlates to underlying flow. But as discussed above, it is possible that the vessels have actually become less leaky and “normalized” with better perfusion.

Quantitative analysis has more validation literature. Yet the majority of studies validate to changes after tumor treatment with anti-angiogenics (Barnes et al., 2012). Additionally, many validation studies comparing quantitative to semi-quantitative DCE-MRI have demonstrated their good correlation and concluded either is valid (Chih-Feng et al., 2012; Jackson et al., 2014; Zahra et al., 2009).

4.3.4. On the stability and reproducibility of DCE-MRI signal in tumors

As the MRI scans were performed up to eight days before the surgeries, one important question is how reproducible is DCE-MRI, and at what time scale. Our median time between scan and surgery was four days. A study of tumors within the lung with a median time between scans of 2 days demonstrated within patient coefficients of variance of approximately 20% when assessing the DCE-MRI data with initial AUC (Ng et al., 2010). A separate study of reproducibility of initial AUC in non-lung tumors scanned twice within one week demonstrated a similar range, with essentially all tumors' repeat scans falling within 20% of the original value (Galbraith et al., 2002). As our clustering of contrast enhancements between the low and high groups is over two fold, it is highly probable that the signal is due to underlying biology and not noise of the assay. These reproducibility studies are used to calculate if a change in contrast enhancement is likely due to an underlying change in biology or likely noise of the assay. This is dependent on the patient population, techniques employed and stability of the MRI scans, all of which are ideally performed at the same institution using the same personnel and equipment.

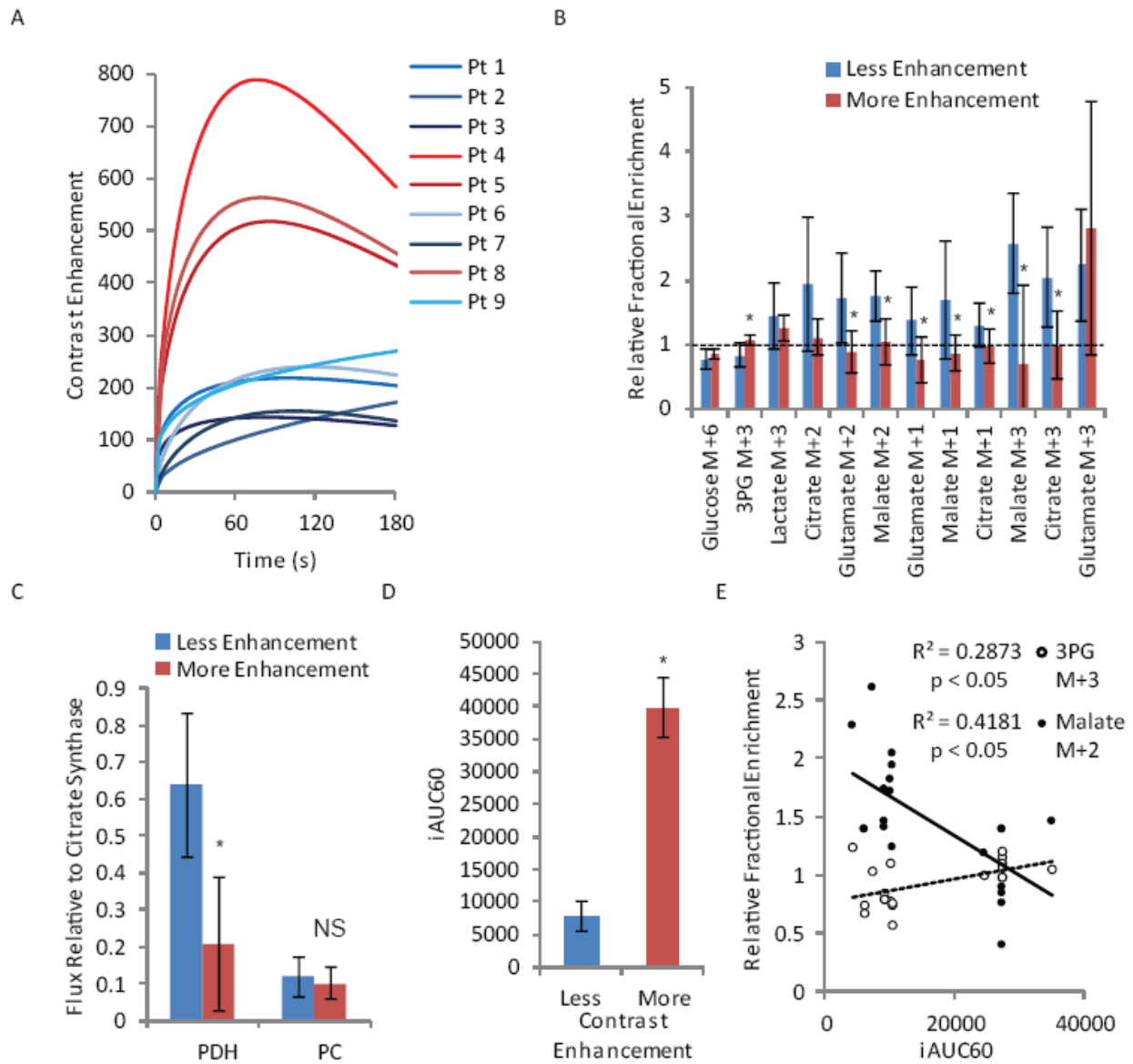


Figure 4.1: Whole tumor contrast enhancement correlated metabolic heterogeneity in NSCLC patient tumors.

- (A) Whole-tumor region of interest contrast enhancement post injection in the NSCLC patient cohort, segregated into “more contrast enhancement” in red shades and “less contrast enhancement” in blue shades. Curves are gamma variate functions of the data.
- (B) Tumor fractional enrichment relative to patient-matched non-cancerous lung of the two clustered groups of (A). The isotopologues depicted are in reference to the tracer scheme of figure 1d, 2f, and 3d.
- (C) Modeling results of figure 3G segregated into the two clustered groups of contrast enhancement.
- (D) Quantified initial area under the curve in 60 seconds of the fitted curves for the two clustered groups of (A).
- (E) Pearson’s correlation between iAUC60 and relative fractional enrichment in 3PG M+3 and malate m+2.

Abbreviations: Pt, patient; iAUC60, initial area under the curve in 60 seconds; NS, Not Significant.

* = $p < 0.05$, student’s unpaired t test.

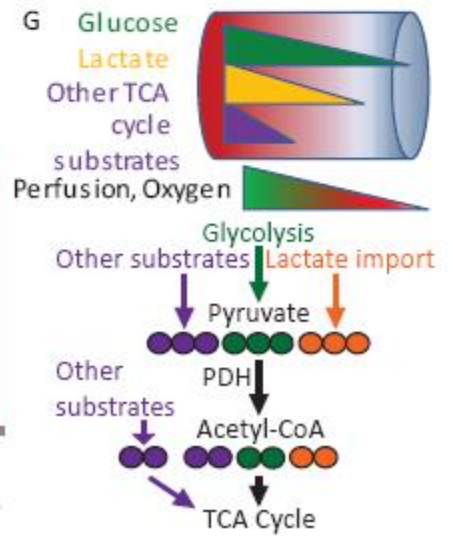
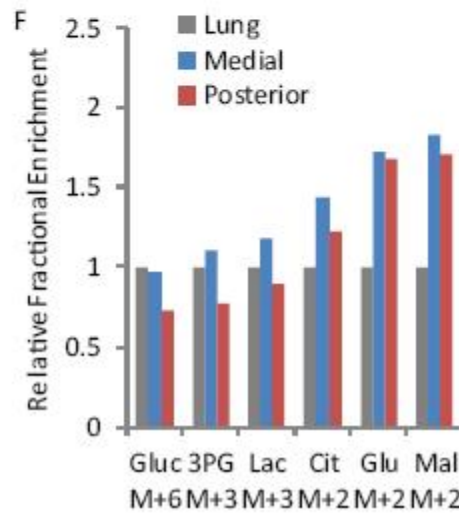
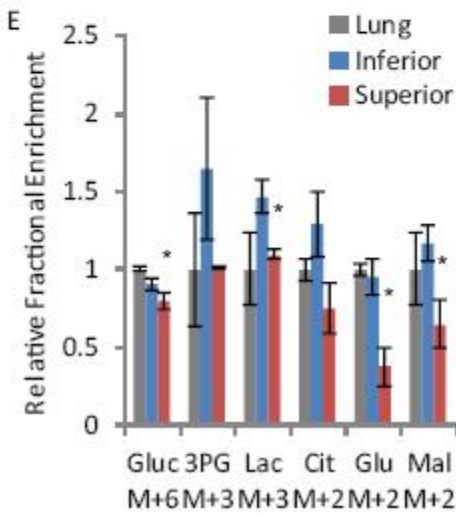
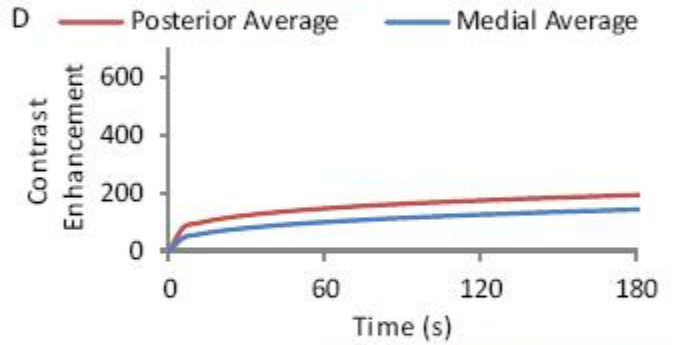
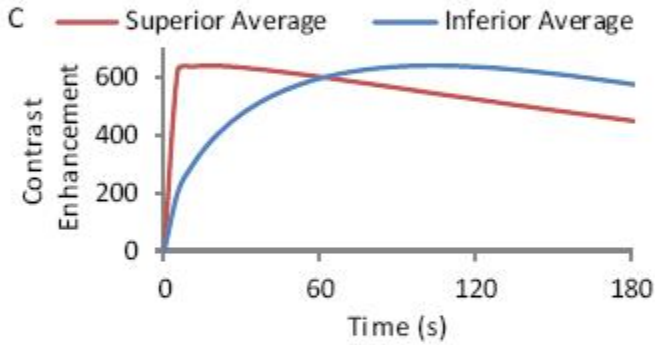
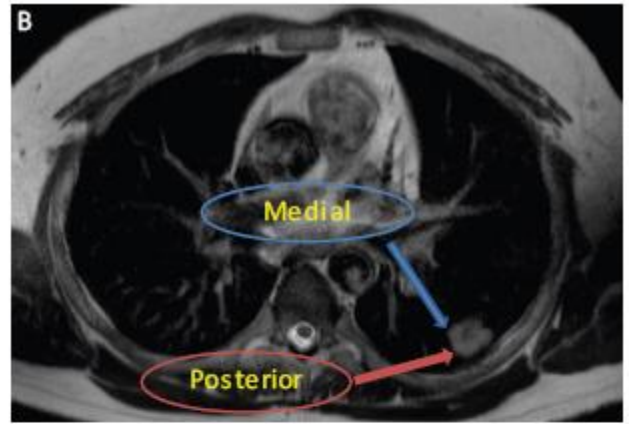
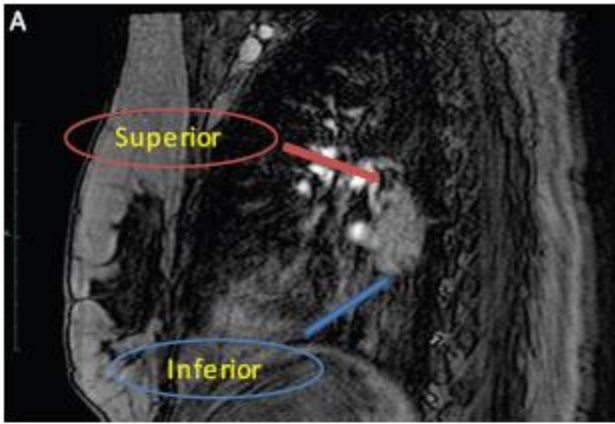


Figure 4.2: Intratumor contrast enhancement correlated metabolic heterogeneity in two NSCLC patient tumors.

(A) Saggital pre-contrast image of a slice through the central region of the tumor of patient eight. Shown are the color schemes and areas of intratumor metabolic sampling.

(B) Axial T2 weighted image of a slice through the central region of the tumor of patient nine. Shown are the color schemes and areas of intratumor metabolic sampling.

(C) Intratumor region of interest contrast enhancement of the regions depicted in (A) of patient eight. Shown are the average curves of gamma variate functions fit to three slices of a given ROI.

(D) Intratumor region of interest contrast enhancement of the regions depicted in (B) of patient nine. Shown are the average curves of gamma variate functions fit to three slices of a given ROI.

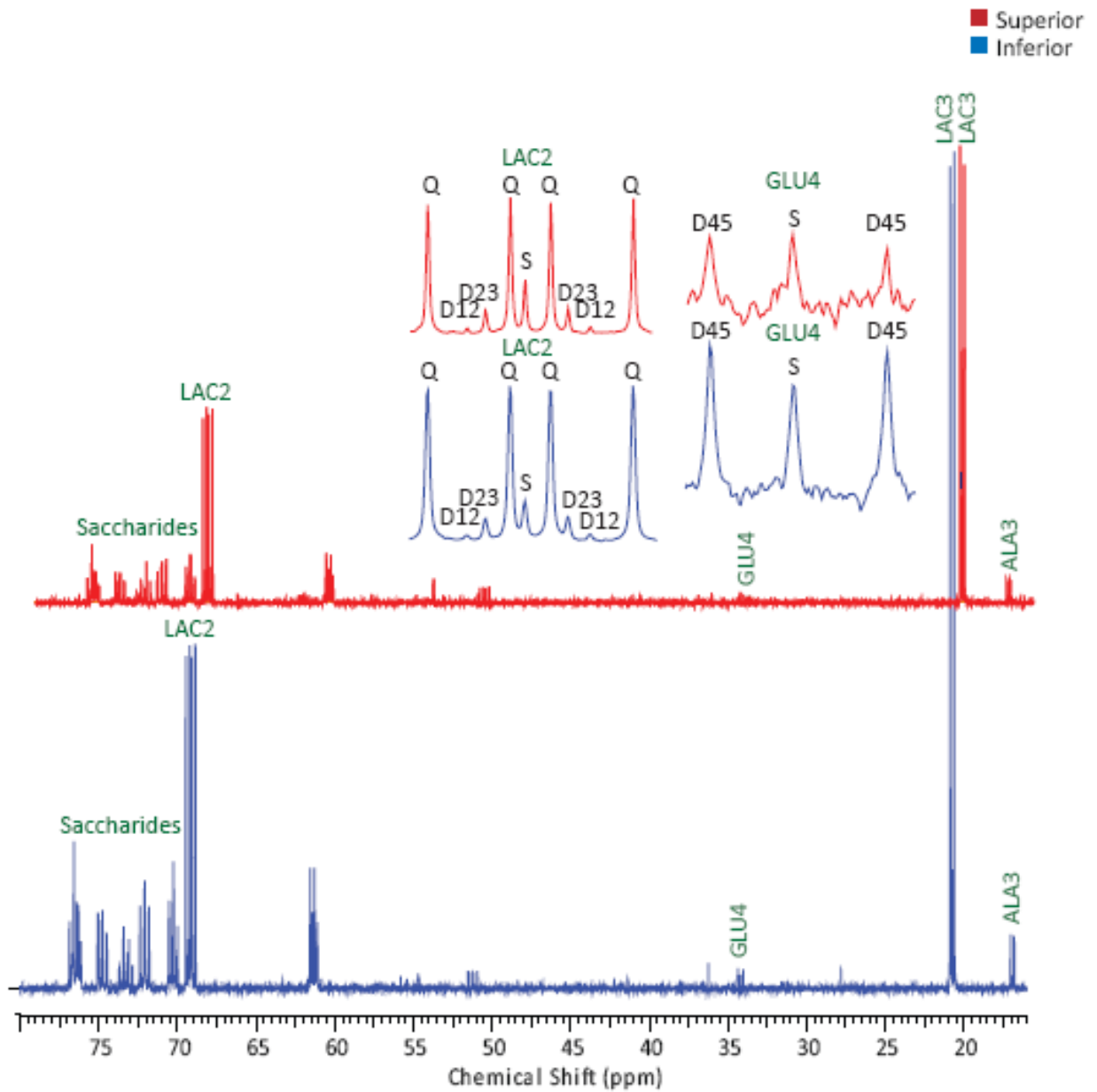
(E) Intratumor metabolic analysis of patient eight of ^{13}C glucose derived metabolites through the first-pass pathways depicted in figure 1D. Shown are the averages and standard deviations of regional triplicate tissue fragments sampled from the areas depicted in (A).

(F) Intratumor metabolic analysis of patient nine of ^{13}C glucose derived metabolites through the first-pass pathways depicted in figure 1D. Shown are the results of single fragments sampled from the regions of (B).

(G) Model of substrate diffusion regulation of NSCLC tumor metabolism.

Abbreviations: Gluc, Glucose; 3PG, 3-Phosphoglycerate; Lac, Lactate; Cit, Citrate; Glu, Glutamate; Mal, Malate; PDH, Pyruvate Dehydrogenase; CoA, Coenzyme A; TCA, Tricarboxylic Acid.

A



B

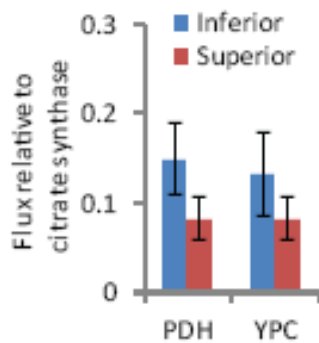


Figure 4.3: NMR and modeling evidence supportive of intratumor qualitative gcms analysis in patient 8. (A) NMR spectra of tissue fragments from the respective regions. (B) Modeling of the qualitative gc-ms data supportive of the conclusions and intertumor trends.

CHAPTER FIVE

DISSECTING METABOLIC HETEROGENEITY IN A MIXED POPULATION OF CELLS USING THE CELL CYCLE AS A DETERMINING PHENOTYPE

5.1 Introduction

5.1.1 Rationale that the cell cycle likely imposes oscillations in metabolism

The cell cycle is an ordered sequence of events in a cell duplicating its biomass and partitioning into two cells. The logic that this would be a valid phenotype to attempt a novel experimental design of sorting cells and subsequently assaying their metabolism lied in the defined portion of DNA replication of the cell cycle, S phase. During this defined period, the cell creates daughter strands of DNA complimentary to the original parent strand. My hypothesis was that this increased demand for nucleotides during this phase would have to impose some change on metabolism relative to the other phases of the cell cycle, G1, G2 and M. Specifically, two scenarios were envisioned. One scenario would be that the pathways of nucleotide biosynthesis or salvage are upregulated in S phase to meet the increased demand. The second scenario would be that these pathways are constant, but that the intracellular nucleotide pools oscillate relative to cell cycle phase, likely rising in G1 to G1/S, falling in S phase, and then rising again during G2/M.

For this logic to be valid, the demand for nucleotides in DNA would have needed to be significantly greater than the demand for nucleotides in RNA. This varies by cell type, but in general the RNA content is

similar to the DNA dry weight of a cell. Or, the biosynthesis of RNA would have to oscillate in a complementary fashion of DNA synthesis during the cell cycle. In intestinal crypts *in vivo*, RNA synthesis has been demonstrated to peak in S phase (Salem et al., 1998). However in Ehrlich ascites tumor cells the RNA synthesis rate appears to peak earlier in G1 (Skog and Tribukait, 1985). This implies that the macromolecular precursor synthesis rates during the various phases of the cell cycle are more regulated by signaling specific to that cell type than an intrinsic property of cell cycle stage.

In retrospect, this was a highly ambitious question that perhaps exceeded the tools available to answer the question. Nonetheless, to potentially build a case for cell cycle stage regulating central metabolism, perhaps a baseline would be to assess whether cell growth and division are related to central metabolism in general.

5.1.2 Available data seem to discredit a possible link between glycolysis and cancer cell proliferation in vitro

A predominant view of the cause for the Warburg Effect is to support the demand for biosynthetic pathways necessary for the aberrant proliferation of cancer cells (Kim and Dang, 2006; Vander Heiden et al., 2009). This idea is weighted on evidence in mitogen-stimulated lymphocytes demonstrating robust inductions of lactate secretion upon exit from quiescence (Karlsson et al., 1997). These results can be replicated with genetic induction of exit from quiescence via inducible expression of Myc in fibroblasts (Morrish et al., 2009). However, conceptually conflicting results suggest that while induced by growth factor signaling, enhanced glycolytic rates may not be necessarily coupled to downstream proliferation. Primary fibroblasts induced into quiescence through contact inhibition maintain their glycolytic rates (Lemons et al., 2010). Additionally, a

negative correlation between lactate secretion rates and cancer cell proliferation rates has been observed in the NCI-60 panel of cancer cell lines (Feizi and Bordel, 2013).

5.1.3 There is conflicting evidence for a link between glucose-derived pyruvate oxidation and cancer cell proliferation

If PDH flux is correlated to the *de novo* fatty acid synthetic rate, this metabolic activity may be under cell cycle stage control if lipid synthesis oscillates relative to cell cycle stage. There is abundant evidence linking *de novo* fatty acid synthesis to proliferation in various cancerous and non-cancerous cell lines (Kuhajda, 2000). However, as PDH flux could be linked to TCA cycle turnover or *de novo* fatty acid synthesis, assuming that PDH flux is correlated to growth rate may be problematic. Accordingly, the literature on PDH flux and cell proliferation is conflicting. Lymphocytes demonstrate no change in PDH flux, yet an increase in PC, upon mitogen stimulation (Curi et al., 1988). This suggests against hypotheses of the Warburg Effect as an overflow pathway for increased PDH flux necessary for the *de novo* lipogenesis for cell growth (DeBerardinis et al., 2008a). However Myc stimulated primary fibroblasts demonstrate an increase in PDH flux, yet a counterintuitive decrease in PC flux (Morrish et al., 2009). To extend the confusion, contact-inhibited fibroblasts demonstrate an increase in PC flux and a decrease in PDH flux (Lemons et al., 2010). This underscores that various forms of the TCA cycle may support cell growth, and that cellular models may differ substantially from each other.

Detachment from the extracellular matrix suppresses glucose uptake in breast cancer cells, which leads to a significant decrease in PDH flux. Of interest, overexpression of the ErbB2 oncogene induces PDH flux in

these cells, buffering the extracellular matrix detachment induced decrease in PDH flux. This model that may mimic the glucose deprived microenvironment of tumors. This overexpression of PDH by ErbB2 increases *de novo* lipogenesis, increases the rate of cell proliferation, and alters the distribution of cell cycle phases, with an increase in the SG2M fraction (Grassian et al., 2011). Thus, there is evidence for a connection between glucose-derived pyruvate oxidation through the PDH enzyme and cancer cell proliferation. However, in colon cancer cells xenografted in the flanks of mice or grown in soft agar to induce colony growth, overexpression of the mitochondrial pyruvate carrier, which was demonstrated to increase the flux through PDH, decreased cell proliferation (Schell et al., 2014). Thus, even in cancer cell lines, there is no common theme of PDH flux and cell proliferation.

5.1.4 On nucleotide biosynthesis and cell proliferation

As the logic of this project was predicated on nucleotide biosynthesis, this is the focus whereas discussions of glycolysis and PDH, interesting as they may be due to recited dogma in the field, are secondary. Detection of nucleotides by GC-MS was not attempted in this project. However, aspartate, which is routinely assayed by the lab, links nucleotide biosynthesis to the TCA cycle. Contact inhibited fibroblasts demonstrate no change in aspartate biosynthesis relative to proliferating fibroblasts (Lemons et al., 2010).

5.1.5 Flawed previous evidence in support of cell cycle stage correlated metabolic activities in cycling cells

Given all of the evidence above, the foundation for specific metabolic pathway alterations of central metabolism that universally distinguish cell proliferation from quiescence was weak. The finding of such a metabolic activity would have been supportive of where to look for first. Regardless, this is a different question than comparing different cell cycle stages within a population that is proliferating. Therefore, consideration was given to supportive evidence of a link between cell cycle stage and central metabolism.

The majority of evidence of a link between cell cycle stage and metabolism employed synchronization methods. I was only able to find one example of sorting cells and assessing changes in mitochondrial membrane potential relative to cell cycle stage. However, whether the cells in this study claimed as G1 were actually G1 cells and not quiescent G0 cells was not established, again begging the question of whether the phenotype was cell cycle stage dependent or associated with whether the cell was quiescent or not (Schieke et al., 2008). In assessing the literature using synchronization methods, I concluded that extrapolating evidence from a population of cells synchronized by only one method to the biology of an unperturbed asynchronous cycling population is invalid. Thymidine block has been demonstrated to alter cell-cycle dependent enzyme activities relative to cells undergoing mitotic shake-off, a sorting method with far lesser perturbation than overwhelming a cell with millimolar concentrations of a nucleotide (Churchill and Studzinski, 1970). This concept has been reiterated for all cell cycle arrest methods of synchronization (Cooper, 2004; Mitchison, 1971). However, a practical solution to this issue is to employ two different synchronization methods and to observe that a particular phenotype is cell cycle stage dependent rather than synchronization method dependent. This strategy has been successfully utilized (Mitra et al., 2009).

This discussion of synchronization methods is important to critique the most relevant study to the issue of a connection between central metabolism and cell cycle stage. A group claimed differential rates of

glucose and glutamine by using different synchronization methods to study different sections of the cell cycle (Colombo et al., 2011). Given the ability and necessity to use two different methods to study a whole passage through the cell cycle, the data of differential use of glucose and glutamine relative to cell cycle stage cannot be interpreted (Colombo et al., 2011; Mitra et al., 2009). Aside from this evidence, there are reports of altering metabolism and observing a cell cycle arrest (Bloom, 1997). However, it is difficult to interpret these studies as to whether there is a connection between metabolism and cell cycle stage in an unperturbed state, or whether loss of a major metabolic activity may affect cell cycle progression by compromising regulatory networks. To use the cited example, there may be a link between redox state and cell cycle stage, or perturbing redox balance may alter the redox state of proteins necessary for cell cycle progression and thereby inhibit their function (Bloom, 1997). In conclusion, the previous literature assessing the interplay between mammalian cell cycle stage and metabolism within a proliferating population was of low quality. However, there is robust evidence for a connection between cell cycle stage and metabolism in yeast grown under glucose limited conditions (Tu et al., 2007). This is actually what had led to my interest in this question in mammalian cells.

5.2. Results

5.2.1 Development of models to sort a population of cells by cell cycle phase

I utilized two general methods to sort cells by cell cycle stage in this project, both using a sorting flow cytometer. One, the fluorescent ubiquitination-based cell cycle indicator (FUCCI) vectors, label cells in various

phases of the cell cycle different colors based on a ubiquitin ligase system that regulates the levels of two reporters at opposing phases of the cell cycle (figure 5.1) (Sakaue-Sawano et al., 2008). I stably infected K562 cells, a suspension leukemia cell line, with this reporter system. I conducted experiments in cells with only one reporter, or both, at various levels of expression (figure 5.1e). The other method I used was to briefly incubate cells in dyes that label DNA content. Shown is an example using Hoechst dye (figure 5.2).

5.2.2 [$U\text{-}^{13}\text{C}$]glucose results of cells labeled with DNA dyes

The Vybrant dye labels cells by DNA content. This was used at a time before the CRI had a sorting cytometer with a UV laser to sort cells with Hoechst. Shown are the results of a pilot sort followed by a two hour label in media containing [$U\text{-}^{13}\text{C}$]glucose (figure 5.3). As shown, the dye worked well in sorting cells of different cell cycle stage (figure 5.3a-b). However, the results of the experiment were underwhelming from a raw data standpoint of the fractional enrichment in metabolites after the two-hour label (figure 5.3c-f).

This general experiment was repeated four times, twice with the Vybrant dye and twice with Hoechst. The period of incubation in labeled media varied after the sort between 30 to 120 minutes per experiment. The results in aggregate are shown in figure 5.3. Modeling of the data in aggregate suggested a significant decrease in PC flux relative to citrate synthase in sg2m cells relative to g1 (figure 5.4a). A qualitative analysis of the raw TCA cycle intermediate data is difficult due to the reproducible differences in lactate fractional enrichment (figure 5.4b). As discussed in previous chapters, this confounds downstream labeling as now we have differences in the upstream substrate. Regardless, the decrease in PC flux is seemingly counterintuitive given the logic of the project that an anaplerotic flux would be increased in S phase. However, what would

justify this is if there was a switch to an alternative anaplerotic source in S phase. Specifically, glutamine would make conceptual sense as a nitrogen donor for nucleotide synthesis in S phase, which could increase glutamine-derived glutamate flux, and potentially push this glutamine-derived glutamate into the TCA cycle (Deberardinis et al., 2008b). We find supportive evidence for this phenotype in a greater M+0 glutamate fractional enrichment from the [U-¹³C] glucose cells (figure 5.4d).

5.2.3 [U-¹³C]glutamine results of cells labeled with DNA dyes or sorted by FUCCI

As tcaSIM does not incorporate a labeled input at the level of alpha-ketoglutarate, only an analysis of the raw fractional enrichment data is available for the [U-¹³C]glutamine labeling experiments. These results total 10 sorts, incorporating labeling data from 20 minutes to 2 hours from DNA dye sorts and various FUCCI vectors (G1 vector, SG2M vector, or cells harboring both). In these labeling experiments the general hypothesis of the project is validated and compliments the glucose labeling data of 5.2.2 (figure 5.5). The m+0 species are universally lower in SG2M implying more glutamine carbon feeding the TCA cycle in general in SG2M relative to G1. This is specifically seen in the first pass species of the m+5 in glutamate and the m+4 in citrate. Additionally, the smaller labeled isotopologues in the intermediates suggest higher rates of glutamine carbon cycling in SG2M.

5.2.4 Metabolomics results of cells sorted by Hoechst

To further examine metabolic alterations in the cell cycle, a targeted metabolomics pilot was conducted in k562 cells sorted by Hoechst into G1 vs SG2M populations (figure 5.6). The results are of three sorts on separate days. As this was attempted as a screen to uncover what would likely be the most robust and interesting pathway related to cell cycle stage, strict criteria were used to prioritize metabolite alterations. Specifically, we used three criteria to assess each metabolite. To be considered candidates for future study, we applied three criteria – significant alterations according to at least two methods from raw signal, TIC, and mg protein, and achieving a false discovery rate of less than 0.05. Five metabolites passed the criteria, with all of them having logical connections to the cell cycle. Aconitate levels increased in SG2M, further supporting changes in central metabolism, the hypothesis of the project. S-lactoylglutathione was the most striking change, interesting in that it is a waste product of glycolysis so this data is in support of the glucose labeling data. UMP is a nucleotide so this helps validate the idea of the project, that potentially nucleotide biosynthesis is upregulated in S phase as the pools of this nucleotide are larger. S-adenosylhomocysteine is involved in one carbon metabolism, which is required for DNA synthesis. Finally, and most interesting to me, phosphocreatine levels actually decreased in sg2m relative to g1. Why this is the case is speculative, perhaps interesting in the connection between phosphocreatine and glycolysis in “fast twitch” muscle. Striated skeletal muscle comes in two general forms, slow “aerobic” twitch muscle fibers that rely more on oxidative phosphorylation, and fast “anaerobic” twitch muscle fibers that rely more on glycolysis. Phosphocreatine is known in this system to be an important sink of phosphate donors during the rapid demand for ATP during fast twitch muscle contraction. The levels of phosphocreatine may be falling in SG2M relative to G1 due to an increased need for rapid ATP replenishment, perhaps also explaining the increase in glycolytic rate.

5.3 Methods

5.3.1 Creating Fucci vector stably infected cell lines

The pRetroX-G1-Red Vector and pRetroX-SG2M-Cyan Vector were purchased from Clontech. The plasmids were transfected into supercompetent E.coli cells, with the plasmids re-purified. HEK-293T cells were transfected with the vectors, and the virus containing media was collected and used to infect k562 cells. Positive infectants were selected by sorting either positive populations or clones via flow cytometry.

5.3.2 Sorting cells by DNA content

Cells were incubated with the Vybrant DyeCycle™ Violet stain per manufacturer's instructions. For Hoechst stains, cells were concentrated at 9×10^6 cells per ml in RPMI medium with 10% serum, and incubated with 10 micromolar Hoechst for 30 minutes. Cells were sorted at 8000 events per second for the Hoechst experiments. Cells were collected in 2x Leibovitz's solution with 20% serum, which after the sort was diluted 1:1 with sheath fluid to 1x Leibovitz's and 10% serum. Sorted populations were spun down and resuspended in ^{13}C labeling medium.

5.3.3 Sorting cells by the Fucci reporter system

Cells were concentrated to a similar density as Hoechst sorts in the same media, and sorted at a similar speed. The AmCyan laser was used to sort cells expressing the SG2M vector, and the mCherry laser was used to sort cells expressing the G1 vector.

5.3.4 Cell culture and metabolic experiments

K562 cells were grown in RPMI media with 2mM glutamine added, with 10% fetal bovine serum and a mixture of penicillin streptomycin antibiotics. For metabolic experiments, the relevant ^{13}C tracer was replaced in media lacking the metabolite, and dialyzed serum lacking low molecular weight metabolites was used in place of complete serum. For $[\text{U-}^{13}\text{C}]$ glucose experiments, 5mM glucose was used. For $[\text{U-}^{13}\text{C}]$ glutamine experiments, 2mM glutamine was used. Labeling experiments spanned a timeframe of 20 minutes to two hours.

5.4 Discussion

5.4.1 A unique form of data on the general concept of glutamine metabolism and cell proliferation

The mechanistic justifications and phenomenological evidence for the importance of glutamine metabolism in cancer metabolism or cell proliferation are numerous and do not need more reciting (DeBerardinis et al., 2008a; DeBerardinis et al., 2007; Deberardinis et al., 2008b; Hensley and DeBerardinis, 2015; Hensley et al., 2013; Rajagopalan and DeBerardinis, 2011). However, specific to this project, two

concepts are worth mentioning. First, is the idea of a dependence of glutamine for nucleotide synthesis in S-phase. This has been shown in Kras driven fibroblasts, as glutamine withdrawal induced apoptosis in S phase that could be rescued with the addition of nucleotides (Gaglio et al., 2009). Second, glutamine metabolism plays an important role in the xCT transporter to exchange glutamate for cystine which is converted to cysteine, the rate limiting metabolite in glutathione biosynthesis. As there are numerous reports of a redox control of cell cycle progression, this could also be relevant to the observed phenotype in k562 cell cycle stages (Bloom, 1997; Srivastava et al., 2014).

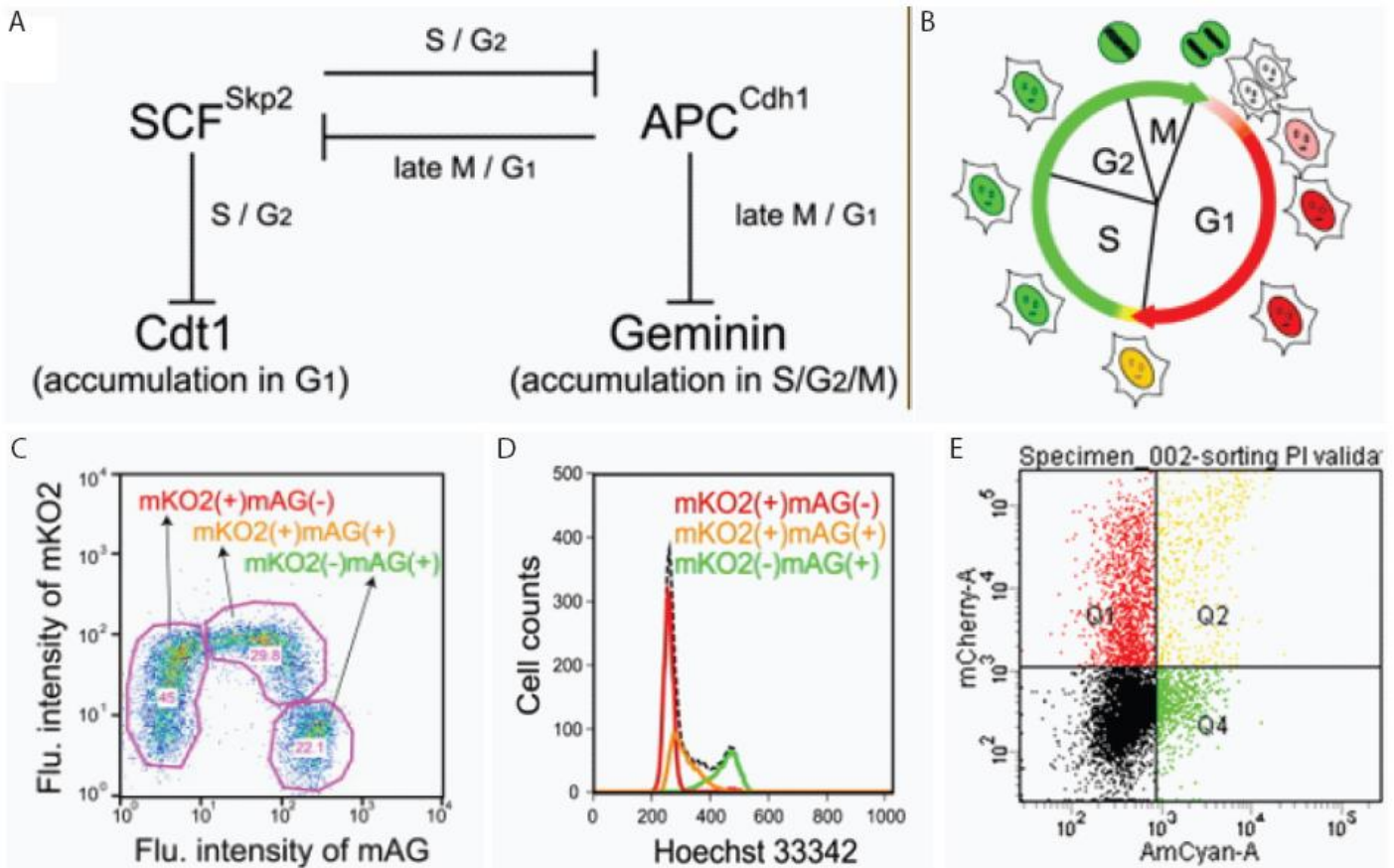


Figure 5.1: Description of the FUCCI cell cycle stage reporter system.

(A) Interaction diagram for the reporter proteins, Cdt1 and Geminin, of the FUCCI reporter system. SCF and APC are both ubiquitin ligases that reciprocally inhibit each other, leading to cyclic oscillations in their activities. Geminin is a substrate of the APC, active in late M/G1, whereas Cdt1 is a substrate for SCF which is active in S/G2. Consequently, Cdt1 protein levels accumulate in G1, whereas Geminin levels accumulate in S/G2/M. Figure reproduced from Sakaue-Sawano, Kurokawa et. Al. 2008.

(B) Schematic and validating experimental data (C) and (D) of the FUCCI system. mKO2-hCdt1, shown in red, is a reporter construct labeling G1 cells, whereas mAG-hGem, shown in green, is a reporter construct labeling G2/M cells (depicted at top and validated by DNA content using transfected HeLa cells Hoechst stained at middle and bottom). Figure A-D reproduced from Sakaue-Sawano, Kurokawa et. Al. 2008.

(E) K562 cells, which were used for metabolic assays, infected with both reporters.

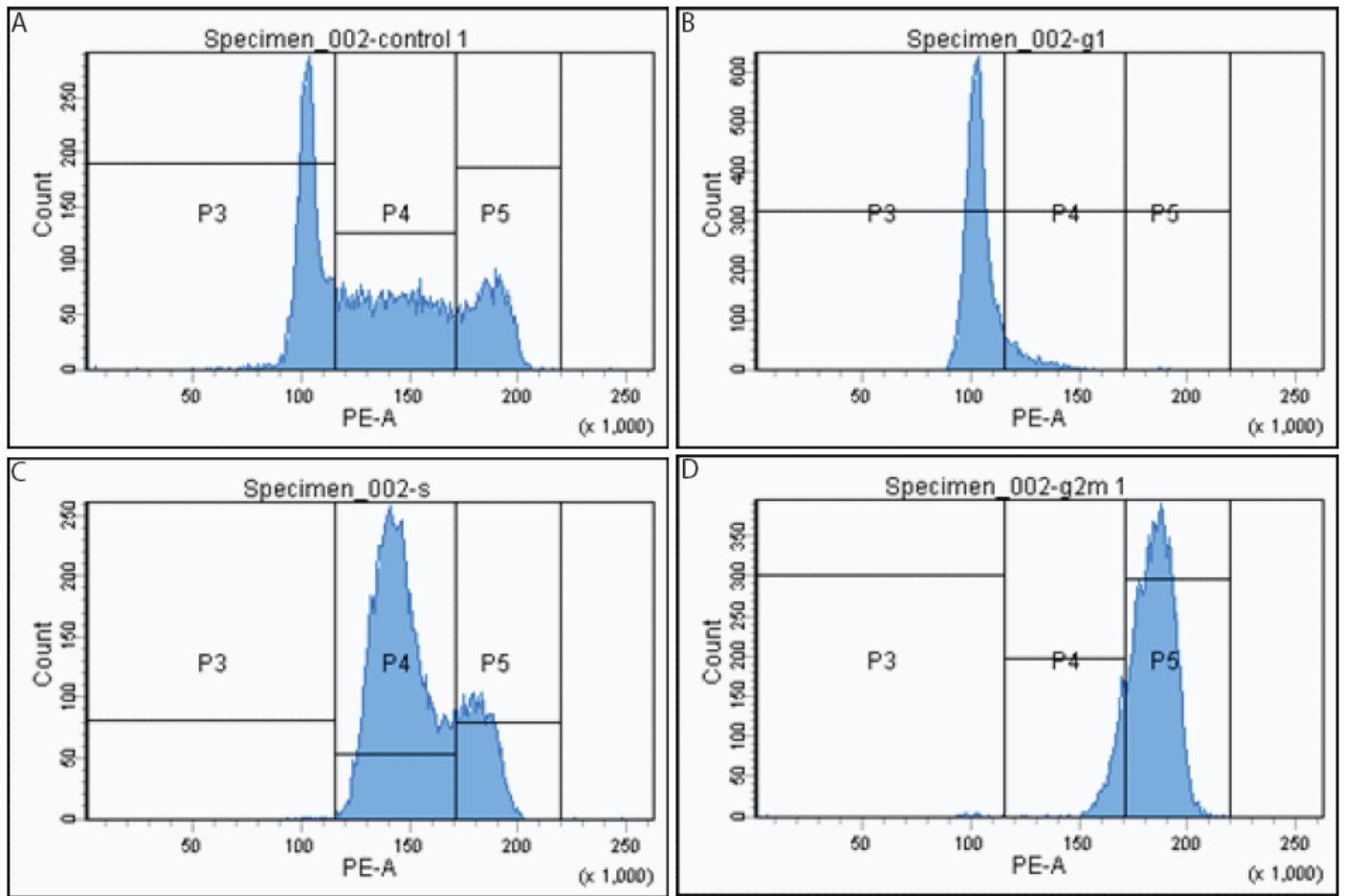


Figure 5.2: Example of sorting cells by Hoechst dye

- (A) Example of the original population before sorting. The gates P3, P4, and P5 correspond to sorting cells by G1 (1n DNA content), S (between 1n and 2n DNA content), and G2/M phase (2n DNA content).
- (B) Resulting cells sorted by the P3 (G1) gate.
- (C) Resulting cells sorted by the P4 (S) gate.
- (D) Resulting cells sorted by the P5 (G2/M) gate.

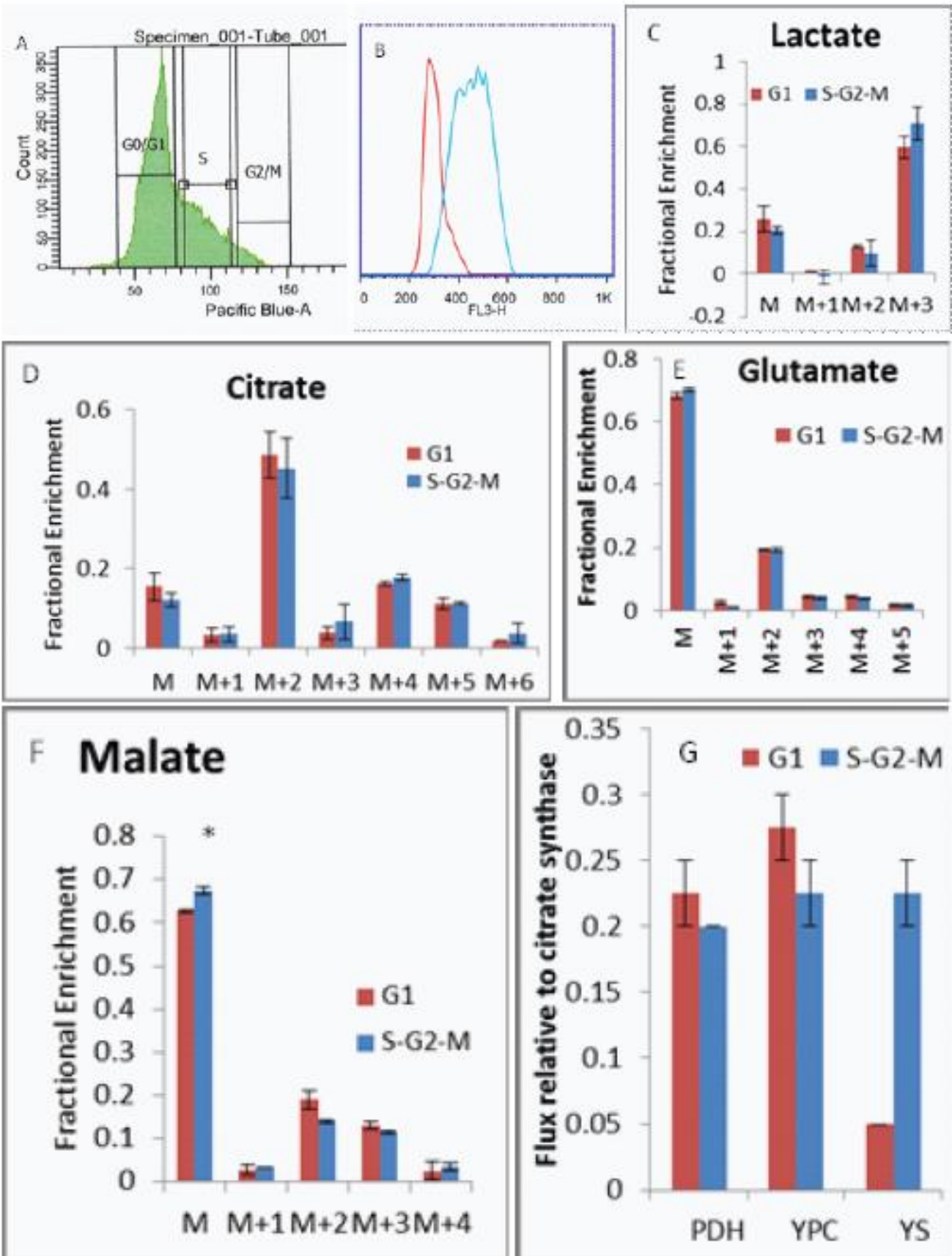


Figure 5.3: Pilot of sorting K562 cells stained with Vybrant DNA dye followed by a 2 hour [U-¹³C] glucose label.

(A) Shown are results of staining the dye and assessing signal in an unsorted population. Cells were sorted into two groups – g0/g1 named “g1”, and non-g1 incorporating the S and G2/M gates, called “S-G2-M.”

(B) Results of cell populations sorted as described in (A), validated with a separate dye, propidium iodide of fixed cells.

(C) Lactate fractional enrichment results.

(D) Citrate fractional enrichment results.

(E) Glutamate fractional enrichment results.

(F) Malate fractional enrichment results.

(G) Results of modeling the data with tcaSIM as described in chapter 2.

* = $p < 0.05$ by student's unpaired t test.

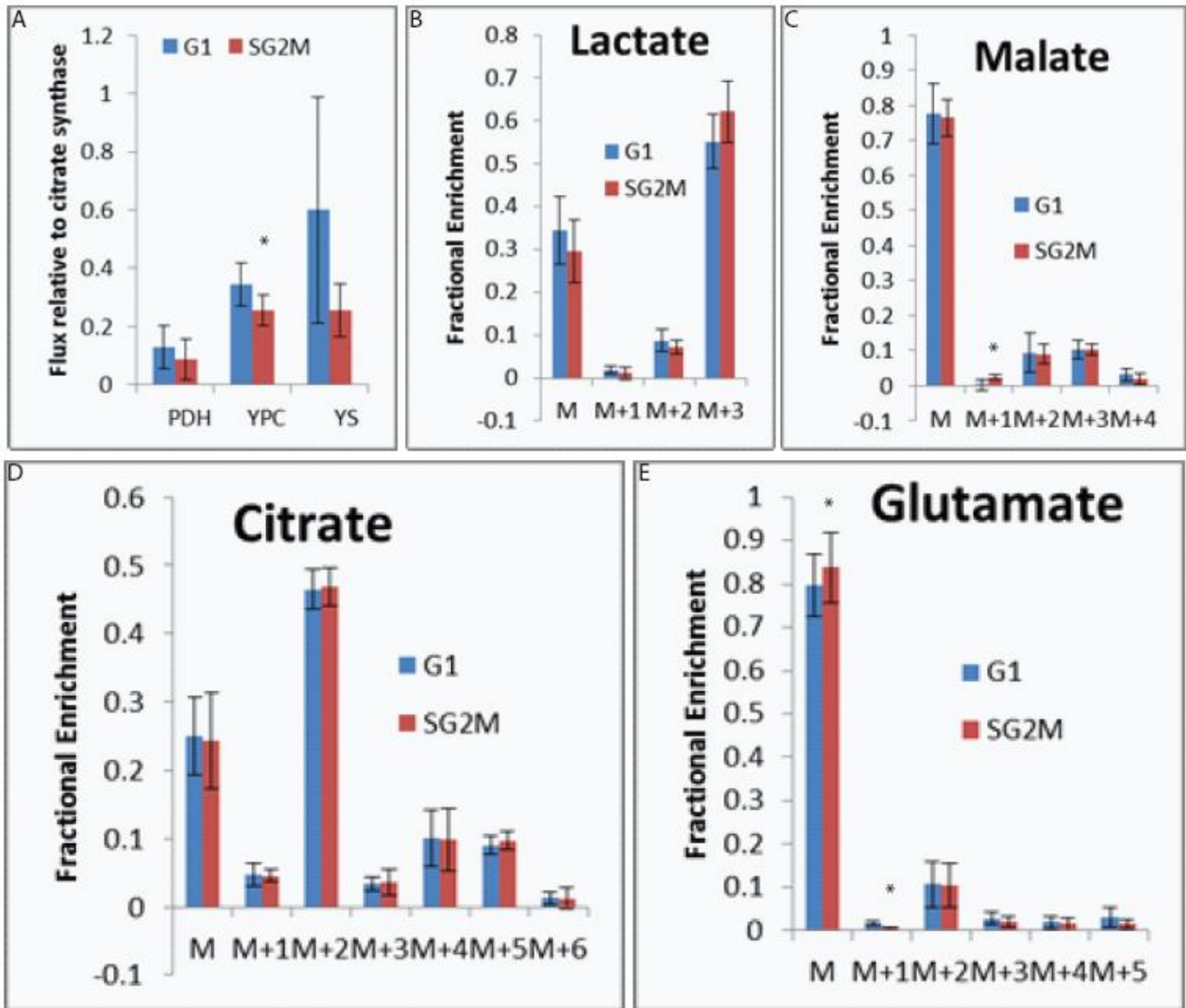


Figure 5.4: Aggregate results of [U-¹³C]glucose labeling experiments in G1 vs SG2M sorted K562 cells stained with DNA dyes.

- (A) Aggregate tcaSIM modeling results.
 - (B) Aggregate lactate fractional enrichment results.
 - (C) Aggregate citrate fractional enrichment results.
 - (D) Aggregate glutamate fractional enrichment results.
 - (E) Aggregate malate fractional enrichment results.
- * = p<0.05 by student's paired t test.

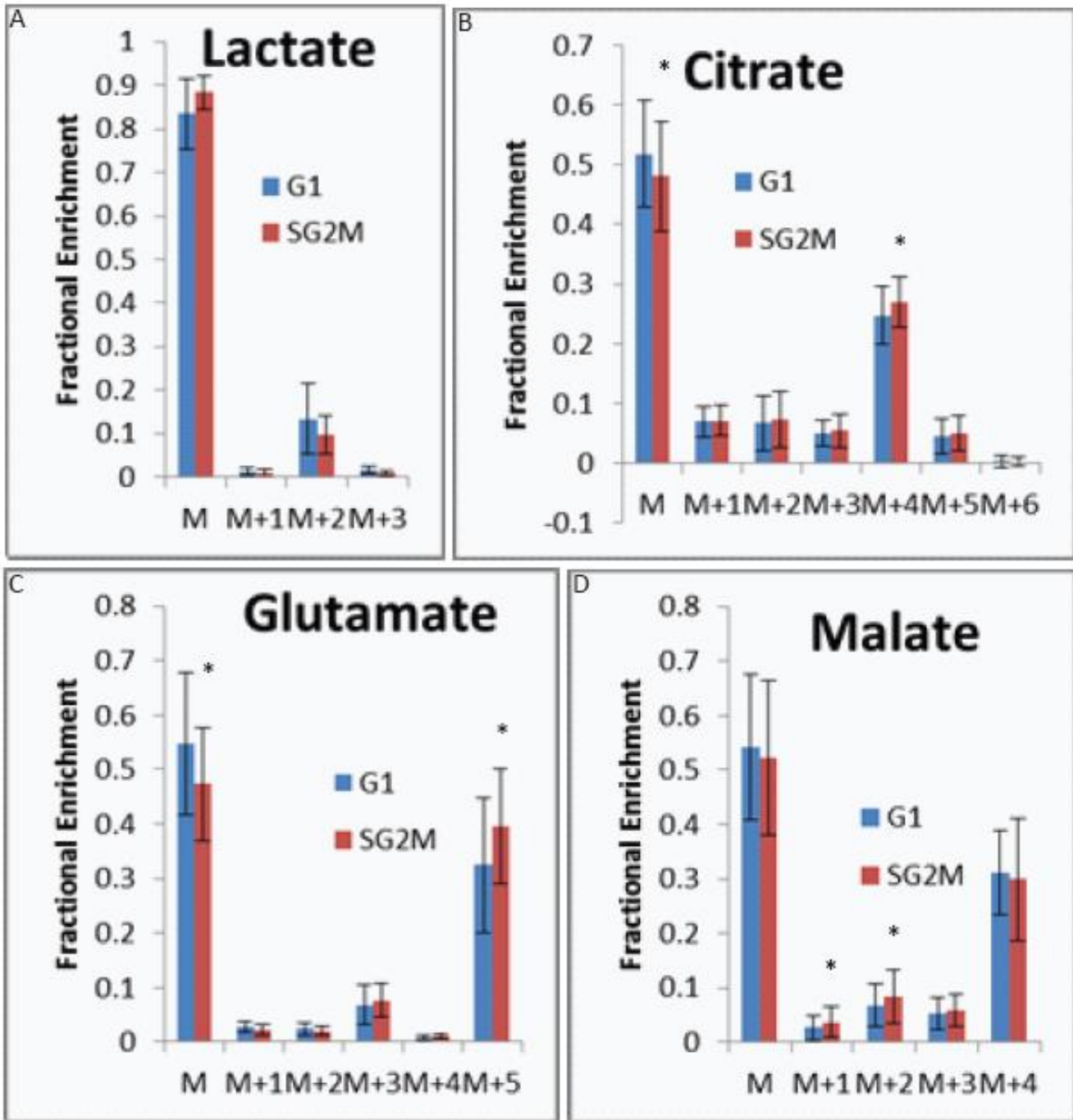


Figure 5.5: Aggregate results of [U-¹³C]glutamine labeling experiments in G1 vs SG2M sorted K562 cells stained with DNA dyes or expressing various combinations of FUCCI reporters.

- (A) Aggregate lactate fractional enrichment results.
- (B) Aggregate citrate fractional enrichment results.
- (C) Aggregate glutamate fractional enrichment results.
- (D) Aggregate malate fractional enrichment results.

* = $p < 0.05$ by student's paired t test.

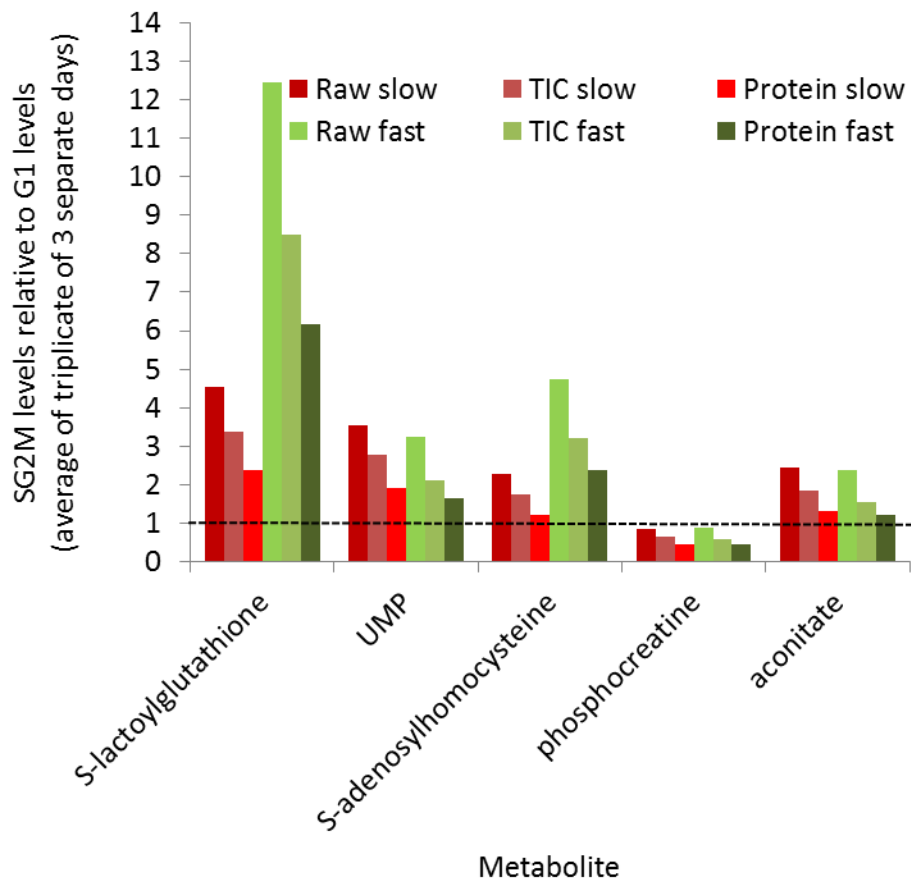


Figure 5.6: Results of a metabolomics pilot of k562 cells sorted into G1 and SG2M populations with Hoechst dye. N = 3 sorts on separate days, for two conditions fast and slow sorts, for a total of 6 separate sorts. All metabolites shown pass criteria of being significant ($p < 0.05$ by student's t test) in the raw data and by one method of normalization (protein or total ion current). Additionally, all metabolites pass a false discovery rate of less than 0.05.

CHAPTER 6: SUMMARY AND FUTURE DIRECTIONS

We have made progress in three areas of understanding the metabolism of primary human tumors *in vivo*. First, we have made progress in the analysis of *in vivo* tumor metabolism. Second, we have made progress in uncovering the connections between the tumor microenvironment and metabolism. Third, we have provided proof of principle of a novel experimental workflow to begin to understand the cellular origins of whole tumor metabolic phenotypes.

6.1.1 Progress in the analysis of primary human tumor metabolism *in vivo*

Prior to these studies, there were two general classes of the modern literature on ^{13}C glucose metabolism of primary human tumors *in vivo*. The first class consisted of qualitative assessment of tumor metabolism from both GC/MS and NMR data (Fan et al., 2009; Sellers et al., 2015). The second class consisted of more rigorous analysis of NMR data (Maher et al., 2012).

We have developed a conceptual framework to more rigorously analyze GC/MS data. First, by utilizing patient-matched normalization, we were able to account for the heterogeneity in tracer exposure and patient-specific tissue of origin metabolism. This significantly reduced the number of patients necessary to establish significant differences between tumor and lung, and to begin to establish correlations to other aspects of tumor biology. This is not trivial given the cost of the infusions and the labor-intensive process in incorporating each new patient into the trial. Second, we have significantly extended the scope of the

qualitative GC/MS analysis to incorporate the concepts of multiple turns ($m+1s$) and the upstream source of labeling when multiple sources converge on an input (in our case, extracellularly imported lactate and intracellularly generated 3PG from glycolysis converging on the pyruvate that is utilized by the TCA cycle). The latter concept additionally introduces the issue of whole body metabolism during *in vivo* tracer stable isotope tracer experiments. This concept, crucial to the interpretation of the data, was absent from the previous literature, specifically in the interpretation of NSCLC patient tumor metabolism (Sellers et al., 2015). Third, we have developed a workflow to cross validate GC/MS and NMR phenotypes by correlation. This combines the precision of NMR positional information with the breadth of GC/MS data, both in the increased available number of metabolites to sample and the wealth of information present in the underlying patterns of isotopologues. This wealth of information in GC/MS isotopologues underlies our fourth novel achievement, modeling the GC/MS data of primary human tumor metabolism. As stated previously, this avoids pitfalls and more precisely defines true changes in metabolism in the area of focus vs. perturbations in other areas of the system.

6.1.2 Future directions in the analysis of primary human tumor metabolism in vivo

Administration of the tracer:

One critique that has been made of bolus administration of ^{13}C is the issue of where to sample along the evolution of the bolus. Specifically, sampling on the downward slope of the enrichment curve of the tracer in the plasma can potentially cause misinterpretation of the tissue enrichment data. What can look like

an enhancement of a metabolic activity can actually reflect reduced washout from an upstream metabolite being less enriched as the tracer enrichment is dropping. We demonstrate that this is unlikely a concern with our phenotypes of interest of first pass oxidative and non-oxidative glucose metabolism through the data of patient 3. Additionally, in all seven patients administered a bolus followed by a continuous infusion, the fractional enrichment of [U-¹³C]glucose in the plasma after bolus administration was never higher than subsequent timepoints during the infusion. This demonstrates that a significant rise and fall of enrichment in our ten minute “bolus” administration is highly improbable. However, to further safeguard against a bolus effect we could potentially decrease the rate of our initial “bolus” infusion.

A separate administration issue is the variable levels of ¹³C enrichment in the plasma. Some factors likely contributing to this variability are unavoidable, such as differences in whole body glucose metabolism between patients (e.g. patients with pre-existing or iatrogenic diabetes). However, one factor that could potentially be easily improved is the dose of tracer we administer to each patient. Currently, we are using a standard dose of 8 gram bolus followed by 8 grams per hour. There may be less variability in plasma ¹³C enrichment levels between patients if dosing amounts are calculated by each individual patient by total body weight, total body volume, resting blood glucose concentration, or a mixture of these parameters. To address this concern in variability of glucose delivered between patients, I have calculated the area under the curve of total [U-¹³C] delivered per infusion, by combining the fractional enrichment and plasma glucose concentration curves. There is a weak, insignificant trend ($R^2 = 0.19$) that the more glucose delivered, the less the tumor fractional enrichment relative to patient matched lung. This does not appear to be a major driver of the phenotype.

In vivo measurements vs. extracted tissue fragment measurements:

Practical aspects of the experimental workflow in the operating room complicate the final interpretation of the results. Due to the nature of the lobectomy, a period ensues between potential compromise of the lung microenvironment and freezing in liquid nitrogen. Ultimately, the goal is to assay tumor metabolism non-invasively *in vivo*. This would provide kinetic information of multiple sampled data points throughout the experiment to move closer to actual metabolic rate calculation and fluxes, and remove concerns of artifacts induced from tissue extraction. One exciting developing method is ^1H - ^{13}C magnetic resonance spectroscopy *in vivo*. Currently, the method suffers from sensitivity issues and greater peak overlay than ^{13}C NMR, yet proof of principle for *in vivo* ^{13}C metabolite tracer infusions with subsequent analysis of the TCA cycle has been demonstrated (De Graaf, 2013). An alternative area of active research at UTSW is the use of hyperpolarized ^{13}C tracers to analyze metabolism *in vivo*. This method is much more sensitive with clearer separated peaks than ^1H - ^{13}C magnetic resonance spectroscopy. However, drawbacks include the need to be able to hyperpolarize the substrate, the extremely short period of time to assay metabolism before the metabolite loses hyperpolarization (minutes), and the current need to infuse supra-physiologic levels of hyperpolarized substrate for detection. This short half-life of the hyperpolarized state of the metabolite is problematic when one wants to look farther downstream of a nutrient, such as the entry of glucose-derived carbon into the TCA cycle. Nonetheless, proof of principle has been established that hyperpolarized pyruvate can be used to assess the rate of the pyruvate dehydrogenase reaction in cell culture, with hopes of taking this methodology *in vivo* (Nelson *et al.*, 2013) (Yang *et al.*, 2014). Since mouse studies are much more amenable to experimental manipulation to validate phenotypes such as invasive sampling for nutrient extraction rates and

immediate extraction of tissue, a future project at UTSW could entail a comparison between hyperpolarization and traditional ^{13}C infusion methods in a mouse tumor model.

Deciphering the origin of pyruvate-derived TCA cycle label:

One possible explanation for the observation that the lactate enrichment is higher than the 3PG is a combination of the enhanced glycolysis of the tumor and a possible bolus effect. Specifically, it is possible that the fractional enrichments in glycolytic intermediates such as 3PG are much higher at the beginning of the experiment and begin to fall, with lactate lagging behind at the end of the pathway. As discussed in chapter 2, the available evidence does not support a bolus effect in our infusions. However, if present, a bolus effect could lead to two possible outcomes. First, the metabolized lactate could be generated in the tumor. An enhancement of glycolysis earlier during the infusion, followed by a drop in the glycolytic rate, could lead to a buildup of lactate and a drop in glycolytic intermediates later into the infusion. This leads to a provocative speculation that perhaps enhanced glycolysis in tumors is beneficial to maximize the efficiency of trapping carbon from a compromised perfusion. A second possibility is that the lactate could be generated but not metabolized. To analyze bolus effects, in vivo ^1H - ^{13}C magnetic resonance spectroscopy could analyze the evolution of signal of metabolites like lactate over time. If it plateaus early and then declines or stays roughly the same, this would be suspicious of a bolus effect. Similarly, if a similar phenotype is seen in the glutamate enrichment it would be suspicious for a bolus effect. However, if both slowly rise over time, this would strongly argue against a bolus effect.

Co-infusions of carefully chosen tracers can distinguish extracellular lactate from intracellular glycolysis derived pyruvate as TCA cycle substrate choice. This concept has been successfully utilized to distinguish acetate vs. pyruvate's contribution to the acetyl-CoA pool feeding the TCA cycle (Mashimo et al., 2014). Essentially, the [2-¹³C] lactate used in the mice studies could be co-infused with the [U-¹³C] glucose, and all of the above questions could be revisited by analyzing the 4,5 doublet by NMR. If the predominant lactate signal in a tissue was M+1, this would imply more import than intracellular generation. The modeling could be run, and assessed whether a better fit was achieved with the M+1 or M+3 lactate signal, or a mixture of the two. As tcaSIM allows a stepwise function between the two scenarios, best fits of how much each species contributes to the overall signal could be generated.

6.2.1 Progress in uncovering the connection between the tumor microenvironment and metabolism

We have discovered that perfusion, as assessed by the surrogate marker of DCE-MRI contrast enhancement, is significantly correlated to the tumor ¹³C signal in TCA cycle intermediates in the NSCLC patient [U-¹³C]glucose infusions. However, as noted, there is an alternative explanation to this phenotype. The correlation could be due to the growth of aggressive clones within a given tumor or in comparing various tumors. Specifically, oncogene driven reprogramming of cellular metabolism and proliferation could lead to areas of densely packed clones that prohibit significant entry of contrast agent.

6.2.2 Future directions in uncovering the connection between the tumor microenvironment and metabolism

To ascertain the most likely scenario, we have two routes of investigation. We can continue to draw correlations between the oncogenotype, ^{13}C signal, and contrast enhancement. Either the three will continue to correlate, or one factor will become clearly more significantly correlated to ^{13}C signal than the other. However, as a significant fraction of oncogenic drivers remain to be discovered in NSCLC, this may not be conclusive. Perturbations of tumor perfusion in mouse models of NSCLC and observation of the presence or absence of changes in ^{13}C would provide convincing data on the robustness to tumor biology in general of the correlation between contrast enhancement and ^{13}C signal. I had conducted pilot experiments on the 1.5T Aspect MRI to test whether I could reproduce similar correlations between ^{13}C signal in TCA cycle intermediates and contrast enhancement in mouse xenograft models of NSCLC tumors. The only attempt made was to generate similar data on whole tumor ROI contrast enhancement and ^{13}C signal in A549 cell line xenografts compared to A549 xenografts engineered to re-express the tumor suppressor LKB1. These experiments were difficult to interpret in that unlike the patient tumor data, the qualitative analysis of first pass m+2 metabolism and modeling results contradicted each other. I am more inclined to believe the modeling results given their congruence with other results in the lab specifically focused on LKB1's contribution to ^{13}C labeling across a large panel of NSCLC cell lines.

However, this leads to the issue that the modeling gave the opposite results as the human studies, in that contrast enhancement was now directly correlated to PDH flux relative to citrate synthase in this pilot series in mouse xenografts. There are several caveats associated with the interpretation of this pilot. First, over-expressing a tumor suppressor may not be equivalent to assessing the natural influence of the oncogenotype on metabolism. Second, are studies of small differences in perfusion of rapidly growing tumors

in the highly hypoxic mouse flank a good enough model for the much better perfused spontaneously formed human tumor in the lung?

I would rather repeat this pilot with various cell lines injected into the mouse lung (this method has been successfully conducted by James Kim's lab). This would be asking a similar question in a more relevant model to the human studies. Additionally, Rolf Brekken's lab has characterized the microvessel density of a panel of NSCLC cell lines grown as flank xenografts in mice, of which glucose consumption rates *in vitro* have been characterized by a graduate student in our lab. Supporting the general hypothesis of the human studies, the *in vitro* glucose consumption rate was shown to have an inverse correlation to the *in vivo* microvessel density (n=12, $r^2=0.3279$) in this NSCLC cell line panel.

The most direct experiments would be to alter perfusion in a paired series of mice bearing flank xenografts of an identical cell line. Ideally, the pilot series above would yield lines with either high or low contrast enhancement in a good range of separation. Furthermore, it would be ideal if *in vitro* glucose consumption results were correlated to the *in vivo* ^{13}C signal in TCA cycle intermediates from $[\text{U-}^{13}\text{C}]$ glucose infusions. Regardless if the correlation holds up, I would move forward with cell lines of high contrast enhancement injected into contralateral flanks to cell lines of low contrast enhancement. The mice would be segregated into three groups: control, increased perfusion, and decreased perfusion.

However, how to acutely and specifically alter tumor perfusion is not straightforward. Many agents that alter perfusion can simultaneously alter tumor metabolism (Gallagher and Tallant, 2004; Jordan and Sonveaux, 2012). VEGF signaling has been shown to crosstalk to signaling pathways in tumor cells known to reprogram metabolism (EGFR, AKT/PI3K)(Goel and Mercurio, 2013). A direct solution to alter perfusion was developed in rats bearing tumors in fat pads of the inguinal cleft. Tumors grown in this area are supplied by a

single epigastric artery and drained by a single epigastric vein. Blood from donor mice have been demonstrated in this method to be used as an infusate through a catheter in the saphenous artery (Tozer et al., 1994). The infusion rate of rat donor blood containing [^{13}C] tracer could be infused into the saphenous artery at various rates to mimic various levels of perfusion. This could be validated by DCE-MRI on the 1.5T Aspect by adding gadovist to the infusate and measuring the dynamics of the infusion. If our model is correct, once at steady state, tumors with lower perfusion rates should demonstrate less contrast enhancement, and higher ^{13}C signal in TCA cycle intermediates from a [$\text{U-}^{13}\text{C}$]glucose infusion.

While ideal in terms of controlled experimentation, the setup above is technically demanding. A practical test of the model would be to infuse [$\text{U-}^{13}\text{C}$]glucose in the tail vein as in previous infusions in mice, with or without addition of a beta-oxidation inhibitor. Our hypothesis is that acetyl-CoA from fatty acid oxidation may be inhibiting PDH flux in better perfused regions of the tumor. This draws upon the concept of the Randle cycle whereby fatty acid oxidation inhibits pyruvate dehydrogenase activity (Hue and Taegtmeyer, 2009). This would assess the first portion of the logic of the substrate diffusion model, of substrate competition within tumors, before moving to the complexity of altering perfusion.

6.3 Progress and future directions in studying intratumor metabolic heterogeneity at the cellular level

The general proof of principle has been established that sorting individual populations of cancer cells can yield information into the metabolic program of subpopulations. Next, this concept should be utilized to study a mixed population in culture of fibroblasts and cancer cells. This would help validate the method and move the method closer to being able to account for intratumor cell type heterogeneity. Afterwards, this

method could be used to assay a mixed injection of fibroblasts and cancer cells in a mouse xenograft to discern where the majority of the glucose oxidative signal arises. Finally, the two projects can be combined, to assay the heterogeneity in cell of origin and microenvironment in primary human tumors. Fresh tissue fragments from the OR could be transported to the lab and disaggregated. The fibroblasts, immune cells and cancer cells could be sorted and subsequently analyzed for ^{13}C readout in TCA cycle intermediates. Additionally, to truly study the question of the metabolic activities upon cellular transformation, lung epithelial cells could be compared to the adenocarcinoma cells of a patient NSCLC tumor.

BIBLIOGRAPHY

- Barnes, S.L., Whisenant, J.G., Loveless, M.E., and Yankeelov, T.E. (2012). Practical dynamic contrast enhanced MRI in small animal models of cancer: data acquisition, data analysis, and interpretation. *Pharmaceutics* 4, 442-478.
- Birsoy, K., Possemato, R., Lorbeer, F.K., Bayraktar, E.C., Thiru, P., Yucel, B., Wang, T., Chen, W.W., Clish, C.B., and Sabatini, D.M. (2014). Metabolic determinants of cancer cell sensitivity to glucose limitation and biguanides. *Nature* 508, 108-112.
- Bloom, A.Y.a.E.T. (1997). Control of Cell Cycle Progression in Human Natural Killer Cells Through Redox Regulation of Expression and Phosphorylation of Retinoblastoma Gene Product Protein. *Blood* 89, 4092-4099.
- Buescher, J.M., Antoniewicz, M.R., Boros, L.G., Burgess, S.C., Brunengraber, H., Clish, C.B., DeBerardinis, R.J., Feron, O., Frezza, C., Ghesquiere, B., *et al.* (2015). A roadmap for interpreting C metabolite labeling patterns from cells. *Current opinion in biotechnology* 34, 189-201.
- Burk, D., and Schade, A.L. (1956). On respiratory impairment in cancer cells. *Science* 124, 270-272.
- Cheng, T., Sudderth, J., Yang, C., Mullen, A.R., Jin, E.S., Matés, J.M., and DeBerardinis, R.J. (2011). Pyruvate carboxylase is required for glutamine-independent growth of tumor cells. *Proceedings of the National Academy of Sciences* 108, 8674-8679.
- Chih-Feng, C., Ling-Wei, H., Chun-Chung, L., Chen-Chang, L., Hsu-Huei, W., Yuan-Hsiung, T., and Ho-Ling, L. (2012). In vivo correlation between semi-quantitative hemodynamic parameters and Ktrans derived from DCE-MRI of brain tumors. *International Journal of Imaging Systems and Technology* 22, 132-136.
- Churchill, J.R., and Studzinski, G.P. (1970). Thymidine as synchronizing agent. III. Persistence of cell cycle patterns of phosphatase activities and elevation of nuclease activity during inhibition of dna synthesis. *Journal of Cellular Physiology* 75, 297-303.
- Coleman, C.N., Mitchell, J.B., and Camphausen, K. (2002). Tumor hypoxia: chicken, egg, or a piece of the farm? *Journal of clinical oncology : official journal of the American Society of Clinical Oncology* 20, 610-615.
- Colombo, S.L., Palacios-Callender, M., Frakich, N., Carcamo, S., Kovacs, I., Tudzarova, S., and Moncada, S. (2011). Molecular basis for the differential use of glucose and glutamine in cell proliferation as revealed by synchronized HeLa cells. *Proceedings of the National Academy of Sciences* 108, 21069-21074.
- Commisso, C., Davidson, S.M., Soydaner-Azeloglu, R.G., Parker, S.J., Kamphorst, J.J., Hackett, S., Grabocka, E., Nofal, M., Drebin, J.A., Thompson, C.B., *et al.* (2013). Macropinocytosis of protein is an amino acid supply route in Ras-transformed cells. *Nature* 497, 633-637.
- Cooper, S. (2004). Rejoinder: whole-culture synchronization cannot, and does not, synchronize cells. *Trends in Biotechnology* 22, 274-276.
- Curi, R., Newsholme, P., and Newsholme, E.A. (1988). Metabolism of pyruvate by isolated rat mesenteric lymphocytes, lymphocyte mitochondria and isolated mouse macrophages. *Biochem J* 250, 383-388.
- Davidson, S.M., and Vander Heiden, M.G. (2012). METabolic adaptations in the tumor MYCenvironment. *Cell Metab* 15, 131-133.
- Dawson, D.M., Goodfriend, T.L., and Kaplan, N.O. (1964). LACTIC DEHYDROGENASES: FUNCTIONS OF THE TWO TYPES RATES OF SYNTHESIS OF THE TWO MAJOR FORMS CAN BE CORRELATED WITH METABOLIC DIFFERENTIATION. *Science* 143, 929-933.
- De Graaf, R.A. (2013). In vivo NMR spectroscopy: principles and techniques (John Wiley & Sons).
- DeBerardinis, R.J., Lum, J.J., Hatzivassiliou, G., and Thompson, C.B. (2008a). The Biology of Cancer: Metabolic Reprogramming Fuels Cell Growth and Proliferation. *Cell Metabolism* 7, 11-20.

DeBerardinis, R.J., Mancuso, A., Daikhin, E., Nissim, I., Yudkoff, M., Wehrli, S., and Thompson, C.B. (2007). Beyond aerobic glycolysis: Transformed cells can engage in glutamine metabolism that exceeds the requirement for protein and nucleotide synthesis. *Proceedings of the National Academy of Sciences* 104, 19345-19350.

Deberardinis, R.J., Sayed, N., Ditsworth, D., and Thompson, C.B. (2008b). Brick by brick: metabolism and tumor cell growth. *Curr Opin Genet Dev* 18, 54-61.

Derdak, Z., Mark, N.M., Beldi, G., Robson, S.C., Wands, J.R., and Baffy, G. (2008). The Mitochondrial Uncoupling Protein-2 Promotes Chemoresistance in Cancer Cells. *Cancer research* 68, 2813-2819.

Dierckx, R.A., and Van de Wiele, C. (2008). FDG uptake, a surrogate of tumour hypoxia? *European journal of nuclear medicine and molecular imaging* 35, 1544-1549.

Doherty, J.R., and Cleveland, J.L. (2013). Targeting lactate metabolism for cancer therapeutics. *The Journal of clinical investigation* 123, 3685-3692.

Fan, T.W., Lane, A.N., Higashi, R.M., Farag, M.A., Gao, H., Bousamra, M., and Miller, D.M. (2009). Altered regulation of metabolic pathways in human lung cancer discerned by (13)C stable isotope-resolved metabolomics (SIRM). *Molecular cancer* 8, 41.

Favaro, E., Bensaad, K., Chong, M.G., Tennant, D.A., Ferguson, D.J., Snell, C., Steers, G., Turley, H., Li, J.L., Gunther, U.L., *et al.* (2012). Glucose utilization via glycogen phosphorylase sustains proliferation and prevents premature senescence in cancer cells. *Cell Metab* 16, 751-764.

Feizi, A., and Bordel, S. (2013). Metabolic and protein interaction sub-networks controlling the proliferation rate of cancer cells and their impact on patient survival. *Sci Rep* 3.

Fletcher, J.W., Djulbegovic, B., Soares, H.P., Siegel, B.A., Lowe, V.J., Lyman, G.H., Coleman, R.E., Wahl, R., Paschold, J.C., Avril, N., *et al.* (2008). Recommendations on the Use of 18F-FDG PET in Oncology. *Journal of Nuclear Medicine* 49, 480-508.

Gaglio, D., Soldati, C., Vanoni, M., Alberghina, L., and Chiaradonna, F. (2009). Glutamine deprivation induces abortive s-phase rescued by deoxyribonucleotides in k-ras transformed fibroblasts. *PloS one* 4, e4715.

Galbraith, S.M., Lodge, M.A., Taylor, N.J., Rustin, G.J., Bentzen, S., Stirling, J.J., and Padhani, A.R. (2002). Reproducibility of dynamic contrast-enhanced MRI in human muscle and tumours: comparison of quantitative and semi-quantitative analysis. *NMR Biomed* 15, 132-142.

Gallagher, P.E., and Tallant, E.A. (2004). Inhibition of human lung cancer cell growth by angiotensin-(1-7). *Carcinogenesis* 25, 2045-2052.

Gameiro, P.A., Laviolette, L.A., Kelleher, J.K., Iliopoulos, O., and Stephanopoulos, G. (2013). Cofactor balance by nicotinamide nucleotide transhydrogenase (NNT) coordinates reductive carboxylation and glucose catabolism in the tricarboxylic acid (TCA) cycle. *J Biol Chem* 288, 12967-12977.

Gatenby, R.A., and Gillies, R.J. (2004). Why do cancers have high aerobic glycolysis? *Nat Rev Cancer* 4, 891-899.

Goel, H.L., and Mercurio, A.M. (2013). VEGF targets the tumour cell. *Nature reviews Cancer* 13, 871-882.

Grassian, A.R., Metallo, C.M., Coloff, J.L., Stephanopoulos, G., and Brugge, J.S. (2011). Erk regulation of pyruvate dehydrogenase flux through PDK4 modulates cell proliferation. *Genes Dev* 25, 1716-1733.

Guillaumond, F., Leca, J., Olivares, O., Lavaut, M.-N., Vidal, N., Berthezène, P., Dusetti, N.J., Loncle, C., Calvo, E., Turrini, O., *et al.* (2013). Strengthened glycolysis under hypoxia supports tumor symbiosis and hexosamine biosynthesis in pancreatic adenocarcinoma. *Proceedings of the National Academy of Sciences* 110, 3919-3924.

Halestrap, A.P., and Price, N.T. (1999). The proton-linked monocarboxylate transporter (MCT) family: structure, function and regulation. *Biochem J* 343 Pt 2, 281-299.

Hensley, C.T., and DeBerardinis, R.J. (2015). In vivo analysis of lung cancer metabolism: nothing like the real thing. *The Journal of clinical investigation* 125, 495-497.

Hensley, C.T., Wasti, A.T., and DeBerardinis, R.J. (2013). Glutamine and cancer: cell biology, physiology, and clinical opportunities. *The Journal of clinical investigation* 123, 3678-3684.

Higashi, K., Clavo, A.C., and Wahl, R.L. (1993). Does FDG uptake measure proliferative activity of human cancer cells? In vitro comparison with DNA flow cytometry and tritiated thymidine uptake. *Journal of nuclear medicine : official publication, Society of Nuclear Medicine* 34, 414-419.

Higashi, K., Ueda, Y., Sakurai, A., Wang, X.M., Xu, L., Murakami, M., Seki, H., Oguchi, M., Taki, S., Nambu, Y., *et al.* (2000). Correlation of Glut-1 glucose transporter expression with. *European journal of nuclear medicine* 27, 1778-1785.

Hiller, K., Metallo, C.M., Kelleher, J.K., and Stephanopoulos, G. (2010). Nontargeted elucidation of metabolic pathways using stable-isotope tracers and mass spectrometry. *Analytical chemistry* 82, 6621-6628.

Hirayama, A., Kami, K., Sugimoto, M., Sugawara, M., Toki, N., Onozuka, H., Kinoshita, T., Saito, N., Ochiai, A., Tomita, M., *et al.* (2009). Quantitative Metabolome Profiling of Colon and Stomach Cancer Microenvironment by Capillary Electrophoresis Time-of-Flight Mass Spectrometry. *Cancer research* 69, 4918-4925.

Hori, S., Nishiumi, S., Kobayashi, K., Shinohara, M., Hatakeyama, Y., Kotani, Y., Hatano, N., Maniwa, Y., Nishio, W., Bamba, T., *et al.* (2011). A metabolomic approach to lung cancer. *Lung cancer (Amsterdam, Netherlands)* 74, 284-292.

Hu, J., Locasale, J.W., Bielas, J.H., O'Sullivan, J., Sheahan, K., Cantley, L.C., Vander Heiden, M.G., and Vitkup, D. (2013). Heterogeneity of tumor-induced gene expression changes in the human metabolic network. *Nature biotechnology* 31, 522-529.

Huang, T., Civelek, A.C., Li, J., Jiang, H., Ng, C.K., Postel, G.C., Shen, B., and Li, X.F. (2012). Tumor microenvironment-dependent 18F-FDG, 18F-fluorothymidine, and 18F-misonidazole uptake: a pilot study in mouse models of human non-small cell lung cancer. *Journal of nuclear medicine : official publication, Society of Nuclear Medicine* 53, 1262-1268.

Hue, L., and Taegtmeyer, H. (2009). The Randle cycle revisited: a new head for an old hat. *Am J Physiol Endocrinol Metab* 297, E578-591.

Jackson, A., Li, K.L., and Zhu, X. (2014). Semi-Quantitative Parameter Analysis of DCE-MRI Revisited: Monte-Carlo Simulation, Clinical Comparisons, and Clinical Validation of Measurement Errors in Patients with Type 2 Neurofibromatosis. *PloS one* 9.

Jordan, B.F., and Sonveaux, P. (2012). Targeting tumor perfusion and oxygenation to improve the outcome of anticancer therapy. *Frontiers in pharmacology* 3, 94.

Karlsson, H., DePierre, J.W., and Nassberger, L. (1997). Energy levels in resting and mitogen-stimulated human lymphocytes during treatment with FK506 or cyclosporin A in vitro. *Biochim Biophys Acta* 1319, 301-310.

Kennedy, K.M., and Dewhirst, M.W. (2010). Tumor metabolism of lactate: the influence and therapeutic potential for MCT and CD147 regulation. *Future oncology (London, England)* 6, 127-148.

Kim, J.-w., and Dang, C.V. (2006). Cancer's Molecular Sweet Tooth and the Warburg Effect. *Cancer research* 66, 8927-8930.

Koh, D.M., and Collins, D.J. (2007). Diffusion-weighted MRI in the body: applications and challenges in oncology. *AJR American journal of roentgenology* 188, 1622-1635.

Kuhajda, F.P. (2000). Fatty-acid synthase and human cancer: new perspectives on its role in tumor biology. *Nutrition* 16, 202-208.

Kung, H.N., Marks, J.R., and Chi, J.T. (2011). Glutamine synthetase is a genetic determinant of cell type-specific glutamine independence in breast epithelia. *PLoS genetics* 7, e1002229.

Le, A., Lane, A.N., Hamaker, M., Bose, S., Gouw, A., Barbi, J., Tsukamoto, T., Rojas, C.J., Slusher, B.S., Zhang, H., *et al.* (2012). Glucose-independent glutamine metabolism via TCA cycling for proliferation and survival in B cells. *Cell Metab* 15, 110-121.

Lemons, J.M., Feng, X.J., Bennett, B.D., Legesse-Miller, A., Johnson, E.L., Raitman, I., Pollina, E.A., Rabitz, H.A., Rabinowitz, J.D., and Collier, H.A. (2010). Quiescent fibroblasts exhibit high metabolic activity. *PLoS Biol* 8, e1000514.

Levine, A.J., and Puzio-Kuter, A.M. (2010). The Control of the Metabolic Switch in Cancers by Oncogenes and Tumor Suppressor Genes. *Science* 330, 1340-1344.

Maher, E.A., Marin-Valencia, I., Bachoo, R.M., Mashimo, T., Raisanen, J., Hatanpaa, K.J., Jindal, A., Jeffrey, F.M., Choi, C., Madden, C., *et al.* (2012). Metabolism of [U-13C]glucose in human brain tumors in vivo. *NMR in Biomedicine* 25, 1234-1244.

Marin-Valencia, I., Yang, C., Mashimo, T., Cho, S., Baek, H., Yang, X.-L., Rajagopalan, Kartik N., Maddie, M., Vemireddy, V., Zhao, Z., *et al.* (2012). Analysis of Tumor Metabolism Reveals Mitochondrial Glucose Oxidation in Genetically Diverse Human Glioblastomas in the Mouse Brain In Vivo. *Cell Metabolism* 15, 827-837.

Mashimo, T., Pichumani, K., Vemireddy, V., Hatanpaa, K.J., Singh, D.K., Sirasanagandla, S., Nannepaga, S., Piccirillo, S.G., Kovacs, Z., Foong, C., *et al.* (2014). Acetate is a bioenergetic substrate for human glioblastoma and brain metastases. *Cell* 159, 1603-1614.

McClelland, M.L., Adler, A.S., Deming, L., Cosino, E., Lee, L., Blackwood, E.M., Solon, M., Tao, J., Li, L., Shames, D., *et al.* (2013). Lactate dehydrogenase B is required for the growth of KRAS-dependent lung adenocarcinomas. *Clinical cancer research : an official journal of the American Association for Cancer Research* 19, 773-784.

McKnight, S.L. (2010). On Getting There from Here. *Science* 330, 1338-1339.

Metallo, C.M., Gameiro, P.A., Bell, E.L., Mattaini, K.R., Yang, J., Hiller, K., Jewell, C.M., Johnson, Z.R., Irvine, D.J., Guarente, L., *et al.* (2012). Reductive glutamine metabolism by IDH1 mediates lipogenesis under hypoxia. *Nature* 481, 380-384.

Mitchison, J.M. (1971). *The Biology of the Cell Cycle* (Cambridge University Press).

Mitra, K., Wunder, C., Roysam, B., Lin, G., and Lippincott-Schwartz, J. (2009). A hyperfused mitochondrial state achieved at G1-S regulates cyclin E buildup and entry into S phase. *Proceedings of the National Academy of Sciences of the United States of America* 106, 11960-11965.

Morrish, F., Isern, N., Sadilek, M., Jeffrey, M., and Hockenbery, D.M. (2009). c-Myc activates multiple metabolic networks to generate substrates for cell-cycle entry. *Oncogene* 28, 2485-2491.

Nelson, S.J., Kurhanewicz, J., Vigneron, D.B., Larson, P.E., Harzstark, A.L., Ferrone, M., van Criekinge, M., Chang, J.W., Bok, R., Park, I., *et al.* (2013). Metabolic imaging of patients with prostate cancer using hyperpolarized [1-(1)3C]pyruvate. *Sci Transl Med* 5, 198ra108.

Ng, C.S., Raunig, D.L., Jackson, E.F., Ashton, E.A., Kelcz, F., Kim, K.B., Kurzrock, R., and McShane, T.M. (2010). Reproducibility of perfusion parameters in dynamic contrast-enhanced MRI of lung and liver tumors:

effect on estimates of patient sample size in clinical trials and on individual patient responses. *AJR American journal of roentgenology* 194, W134-140.

Pavlidis, S., Whitaker-Menezes, D., Castello-Cros, R., Flomenberg, N., Witkiewicz, A.K., Frank, P.G., Casimiro, M.C., Wang, C., Fortina, P., Addya, S., *et al.* (2009). The reverse Warburg effect: aerobic glycolysis in cancer associated fibroblasts and the tumor stroma. *Cell cycle (Georgetown, Tex)* 8, 3984-4001.

Racker, E., Resnick, R.J., and Feldman, R. (1985). Glycolysis and methylaminoisobutyrate uptake in rat-1 cells transfected with ras or myc oncogenes. *Proceedings of the National Academy of Sciences of the United States of America* 82, 3535-3538.

Rajagopalan, K.N., and DeBerardinis, R.J. (2011). Role of Glutamine in Cancer: Therapeutic and Imaging Implications. *Journal of Nuclear Medicine* 52, 1005-1008.

Reitzer, L.J., Wice, B.M., and Kennell, D. (1979). Evidence that glutamine, not sugar, is the major energy source for cultured HeLa cells. *The Journal of biological chemistry* 254, 2669-2676.

Sakaue-Sawano, A., Kurokawa, H., Morimura, T., Hanyu, A., Hama, H., Osawa, H., Kashiwagi, S., Fukami, K., Miyata, T., Miyoshi, H., *et al.* (2008). Visualizing Spatiotemporal Dynamics of Multicellular Cell-Cycle Progression. *Cell* 132, 487-498.

Salem, C., El-Alfy, M., and Leblond, C.P. (1998). Changes in the rate of RNA synthesis during the cell cycle. *Anat Rec* 250, 6-12.

Schell, J.C., Olson, K.A., Jiang, L., Hawkins, A.J., Van Vranken, J.G., Xie, J., Egnatchik, R.A., Earl, E.G., DeBerardinis, R.J., and Rutter, J. (2014). A role for the mitochondrial pyruvate carrier as a repressor of the Warburg effect and colon cancer cell growth. *Mol Cell* 56, 400-413.

Schieke, S.M., McCoy, J.P., Jr., and Finkel, T. (2008). Coordination of mitochondrial bioenergetics with G1 phase cell cycle progression. *Cell cycle (Georgetown, Tex)* 7, 1782-1787.

Sellers, K., Fox, M.P., Bousamra, M., 2nd, Slone, S.P., Higashi, R.M., Miller, D.M., Wang, Y., Yan, J., Yuneva, M.O., Deshpande, R., *et al.* (2015). Pyruvate carboxylase is critical for non-small-cell lung cancer proliferation. *The Journal of clinical investigation* 125, 687-698.

Skog, S., and Tribukait, B. (1985). Discontinuous RNA and protein synthesis and accumulation during cell cycle of Ehrlich ascites tumour cells. *Exp Cell Res* 159, 510-518.

Sonveaux, P., Vegran, F., Schroeder, T., Wergin, M.C., Verrax, J., Rabbani, Z.N., De Saedeleer, C.J., Kennedy, K.M., Diepart, C., Jordan, B.F., *et al.* (2008). Targeting lactate-fueled respiration selectively kills hypoxic tumor cells in mice. *The Journal of clinical investigation* 118, 3930-3942.

Srivastava, N., Kollipara, R.K., Singh, D.K., Sudderth, J., Hu, Z., Nguyen, H., Wang, S., Humphries, C.G., Carstens, R., Huffman, K.E., *et al.* (2014). Inhibition of cancer cell proliferation by PPARgamma is mediated by a metabolic switch that increases reactive oxygen species levels. *Cell Metab* 20, 650-661.

Tozer, G.M., Shaffi, K.M., Prise, V.E., and Cunningham, V.J. (1994). Characterisation of tumour blood flow using a 'tissue-isolated' preparation. *British journal of cancer* 70, 1040-1046.

Tu, B.P., Mohler, R.E., Liu, J.C., Dombek, K.M., Young, E.T., Synovec, R.E., and McKnight, S.L. (2007). Cyclic changes in metabolic state during the life of a yeast cell. *Proceedings of the National Academy of Sciences* 104, 16886-16891.

Urasaki, Y., Heath, L., and Xu, C.W. (2012). Coupling of glucose deprivation with impaired histone H2B monoubiquitination in tumors. *PloS one* 7, e36775.

van Baardwijk, A., Doms, C., van Suylen, R.J., Verbeken, E., Hochstenbag, M., Dehing-Oberije, C., Rupa, D., Pastorekova, S., Stroobants, S., Buell, U., *et al.* (2007). The maximum uptake of (18)F-deoxyglucose on

positron emission tomography scan correlates with survival, hypoxia inducible factor-1alpha and GLUT-1 in non-small cell lung cancer. *European journal of cancer (Oxford, England : 1990)* *43*, 1392-1398.

Vander Heiden, M.G., Cantley, L.C., and Thompson, C.B. (2009). Understanding the Warburg Effect: The Metabolic Requirements of Cell Proliferation. *Science* *324*, 1029-1033.

Vesselle, H., Schmidt, R.A., Pugsley, J.M., Li, M., Kohlmyer, S.G., Vallires, E., and Wood, D.E. (2000). Lung cancer proliferation correlates with [F-18]fluorodeoxyglucose uptake by positron emission tomography. *Clinical cancer research : an official journal of the American Association for Cancer Research* *6*, 3837-3844.

Walch, A., Rauser, S., Deininger, S.O., and Hofler, H. (2008). MALDI imaging mass spectrometry for direct tissue analysis: a new frontier for molecular histology. *Histochem Cell Biol* *130*, 421-434.

Warburg, O. (1925). The Metabolism of Carcinoma Cells. *The Journal of Cancer Research* *9*, 148-163.

Warburg, O. (1956a). On respiratory impairment in cancer cells. *Science* *124*, 269-270.

Warburg, O. (1956b). On the origin of cancer cells. *Science* *123*, 309-314.

Weinhouse, S. (1955). Oxidative metabolism of neoplastic tissues. *Advances in cancer research* *3*, 269-325.

Weinhouse, S. (1956). On respiratory impairment in cancer cells. *Science* *124*, 267-269.

Wise, D.R., Ward, P.S., Shay, J.E., Cross, J.R., Gruber, J.J., Sachdeva, U.M., Platt, J.M., DeMatteo, R.G., Simon, M.C., and Thompson, C.B. (2011). Hypoxia promotes isocitrate dehydrogenase-dependent carboxylation of alpha-ketoglutarate to citrate to support cell growth and viability. *Proceedings of the National Academy of Sciences of the United States of America* *108*, 19611-19616.

Xie, H., Hanai, J., Ren, J.G., Kats, L., Burgess, K., Bhargava, P., Signoretti, S., Billiard, J., Duffy, K.J., Grant, A., *et al.* (2014). Targeting lactate dehydrogenase--a inhibits tumorigenesis and tumor progression in mouse models of lung cancer and impacts tumor-initiating cells. *Cell Metab* *19*, 795-809.

Yang, C., Harrison, C., Jin, E.S., Chuang, D.T., Sherry, A.D., Malloy, C.R., Merritt, M.E., and DeBerardinis, R.J. (2014). Simultaneous steady-state and dynamic ¹³C NMR can differentiate alternative routes of pyruvate metabolism in living cancer cells. *J Biol Chem* *289*, 6212-6224.

Yankeelov, T.E., and Gore, J.C. (2009). Dynamic Contrast Enhanced Magnetic Resonance Imaging in Oncology: Theory, Data Acquisition, Analysis, and Examples. *Current medical imaging reviews* *3*, 91-107.

Yano, K., Ohoshima, S., Shimizu, Y., Moriguchi, T., and Katayama, H. (1996). Evaluation of glycogen level in human lung carcinoma tissues by an infrared spectroscopic method. *Cancer letters* *110*, 29-34.

Ying, H., Kimmelman, A.C., Lyssiotis, C.A., Hua, S., Chu, G.C., Fletcher-Sananikone, E., Locasale, J.W., Son, J., Zhang, H., Coloff, J.L., *et al.* (2012). Oncogenic Kras maintains pancreatic tumors through regulation of anabolic glucose metabolism. *Cell* *149*, 656-670.

Yun, J., Rago, C., Cheong, I., Pagliarini, R., Angenendt, P., Rajagopalan, H., Schmidt, K., Willson, J.K., Markowitz, S., Zhou, S., *et al.* (2009). Glucose deprivation contributes to the development of KRAS pathway mutations in tumor cells. *Science* *325*, 1555-1559.

Yuneva, M.O., Fan, T.W., Allen, T.D., Higashi, R.M., Ferraris, D.V., Tsukamoto, T., Mates, J.M., Alonso, F.J., Wang, C., Seo, Y., *et al.* (2012). The metabolic profile of tumors depends on both the responsible genetic lesion and tissue type. *Cell Metab* *15*, 157-170.

Zahra, M.A., Tan, L.T., Priest, A.N., Graves, M.J., Arends, M., Crawford, R.A., Brenton, J.D., Lomas, D.J., and Sala, E. (2009). Semiquantitative and quantitative dynamic contrast-enhanced magnetic resonance imaging measurements predict radiation response in cervix cancer. *International journal of radiation oncology, biology, physics* *74*, 766-773.

Zhang, J., Chen, L., Chen, Y., Wang, W., Cheng, L., Zhou, X., and Wang, J. (2014a). Tumor vascularity and glucose metabolism correlated in adenocarcinoma, but not in squamous cell carcinoma of the lung. *PloS one* 9, e91649.

Zhang, J., Fan, J., Venneti, S., Cross, J.R., Takagi, T., Bhinder, B., Djaballah, H., Kanai, M., Cheng, E.H., Judkins, A.R., *et al.* (2014b). Asparagine plays a critical role in regulating cellular adaptation to glutamine depletion. *Mol Cell* 56, 205-218.

Zois, C.E., Favaro, E., and Harris, A.L. (2014). Glycogen metabolism in cancer. *Biochemical pharmacology*.

Zu, X.L., and Guppy, M. (2004). Cancer metabolism: facts, fantasy, and fiction. *Biochemical and biophysical research communications* 313, 459-465.